
Università Campus Bio-Medico di Roma

School of Engineering

PhD Course in Biomedical Engineering

(XXVII - 2012/2014)

# Interfacing the peripheral nervous system: towards the development of a bidirectional neural communication

Francesco Maria Petrini

**Coordinator**

Prof. Giulio Iannello

**Supervisor**

Prof. Silvestro Micera

**Co-Supervisors**

Prof. Loredana Zollo,

Stanisa Raspopovic, phd

June 2015

# Interfacing the peripheral nervous system: towards the development of a bidirectional neural communication

A thesis presented by

Francesco Maria Petrini

in partial fulfillments of the requirements of the degree of

Doctor of Philosophy

in Biomedical Engineering

**Coordinator**

Prof. Giulio Iannello

**Supervisor**

Prof. Silvestro Micera

**Co-supervisors**

Prof. Loredana Zollo,

Stanisa Raspopovic, phd

June 2015

# Table of contents

Chapter 1 Introduction ..... 9

Chapter 2 The peripheral nervous system: essential considerations ..... 18

Chapter 3 Prediction of hand force and velocity from human alpha motoneurons recordings ..... 47

Chapter 4 Restoring natural sensory feedback in real-time bidirectional hand prostheses ..... 93

Chapter 5 Sensory substitution in amputees: intraneural versus transcutaneous nerve stimulation for the bidirectional prosthetic control ..... 126

Chapter 6 Conclusions and perspectives ..... 147

Chapter 7 Bibliography ..... 151

# Abstract

The human hand executes incredibly sophisticated tasks as the result of the synergistic interplay between motor and sensory functionalities. The hand loss is a life changing physiological and psychological trauma, which degrades significantly every day activities of people. The ideal prosthesis should restore sensory and motor capabilities to amputees. Current available devices, however, provide users with a restricted gamma of movements and without sensory feedback and, as a consequence, are often abandoned.

In the last 20 years, the fascinating possibility to access the human peripheral nervous system, for the development of natural and effortless man-machine interfaces, has been proposed.

However, presently, there is a gap between the proofs-of-concept that have been shown and reliable and efficient assistive bidirectional devices. Main reason for it is a limited basic understanding both about: i) the nature of the efferent peripheral signals that could be used as the signal triggering the actuation of a neuroprosthesis, and ii) about the effects of the afferent neural stimulation, and the way to use it in a sophisticated manner.

Present thesis is aiming to advance the basic knowledge and to introduce novel findings into the bidirectional neuroprosthesis implementation. Indeed it presents novel strategies for decoding subjects' voluntary motor intention from efferent fibers firing recordings, and for restoring sensory feedback in amputees by stimulating the afferent fibers in optimal way to transmit the effective sensory feedback to the brain. The design of these algorithms has been inspired by the natural mechanisms by which the peripheral nervous system drives hand movements and the physiological sensations coming from interaction with objects and their manipulation.

# Chapter 1 Introduction

When a person undergoes a limb amputation, it faces staggering emotional and financial lifestyle changes. The amputee requires a prosthetic device and services that become a life-long event.

There are 1.9 million amputees in the USA, whose 500.000 lost partially or completely the arm. Moreover, 185.000 new amputations are performed each year, increasing the opportunities for prosthesis providers (www.amputee-coalition.org). Approximately 14% are executed on upper limbs (http://www.centeropcare.com). The exact number of people with the same problem, worldwide, is difficult to ascertain, as many countries do not keep records of the number of people with limb amputation. However, in the developed countries, that have a lifestyle similar to the United States one, the number of amputees can be estimated starting from the presented incidence and prevalence. In the European Union, for example, a total number of 3 million along with 290 thousands new amputees/year would be counted. Over these, 40 thousands would be upper limb amputees.

Since the first prosthesis was developed after World War I (Schlesinger, 1919), several solutions have been proposed to amputees in order to restore the sophisticated functionalities the human hand is capable of. Passive, body powered and myoelectric prostheses are currently commercially available (Micera et al., 2010).

Hand passive (cosmetic) prostheses have no functionality and are bio-mimetically designed to give the amputees an artificial limb that is an esthetic replacement of the missing one.

Active body-powered devices drive their motion by exploiting the energy produced by remnant joint movements. Myoelectric prostheses, finally, translate the superficial electrical activity of muscles (superficial

electromyogram, sEMG) recorded over the arm or the forearm in motor actuations (i.e., prosthesis movements).

Among those possibilities, myolectric prostheses are, presently, the most promising toward a complete restoration of the motor hand functionalities. They, indeed, use the sEMG which contains the user motor intention sent from the brain to muscles. For this reason, those devices may result more intuitive to control for the user, with respect to the body-powered ones.

However, the abandonment rates of current available myoelectric prostheses (such as those sold from established corporations as Ottobock, Touchbionics or RSL-Steeper, among the others) in favour of the body-powered or cosmetic ones are still very high (Biddiss et al., 2007). The main reasons of this tendency have to be searched, other than in the high weight, in the incapacity of reliably restoring fine motor control functionalities (limited dexterity) and in the complete absence of restored sensory feedback (Biddis et al., 2007).

Indeed, current prostheses allow amputees only 1 or 2 degrees of freedom (hand open/close and pronosupination) controlled by homologous or non homologous strategies. By homologous strategy it is meant that a muscle contraction, executed by the amputee, drives a prosthetic movement that corresponds to the one that would have been produced by the contraction itself. Those degrees of freedom are not enough for replying to the needs of most of the amputees, i.e. household maintenance (car repairs, shovelling snow, gardening, electrical work), or hobbies (playing an instrument, riding a bike). Moreover, these prostheses, not providing any kind of sensory feedback, constrain the user to continuously visually monitor the task they execute.

Finally, the lack of those functionalities may also be the cause of the low level of embodiment (i.e. the prosthesis is perceived as a foreign body) reported by amputees (Botvinick and Cohen, 1998; Armel and Ramachandran, 2003; Ehrsson et al., 2004; Tsakiris and Haggard, 2005; Longo et al., 2008; Moseley et al., 2008).

On the robotic side, current prostheses potentially offer dexterity comparable with the human hand one (Farina et al., 2014). Muscle interfacing with its inherent limitations, hence, is the cause of the incapability of restoring fine motor control.

In particular, sEMG signal, despite the main advantage of being easy to pick up, is affected by several factors that make its recording not stable over time. In particular, known issues are sensitivity to electrode repositioning (which is inherent for the superficial electrode recordings), changes in electrode-skin impedance (e.g., because of sweating), relative movement of the muscle with respect to the electrodes, posture of the arm, muscles cross-talk, among others (Jian et al., 2013, Young et al., 2011, Scheme et al., 2010, Merletti et al., 2010, Farina et al., 2010). Because of these reasons, extensive research is presently conducted for developing a reliable muscle-machine interface, focusing both on improving the hardware for communicating with the body (i.e. recording) and the algorithms for decoding hand motion parameters from sEMG to drive the prosthesis (Micera et al., 2010).Regarding decoding algorithms, 3 main approaches have been developed in the last years (Farina et al., 2010, Fougner et al., 2012): (i) pattern recognition, (ii) mapping EMG into simultaneous and proportional control signals, (iii) direct extraction of the neural code from the surface EMG.

Pattern recognition consists of remapping recorded forearm muscles sEMG in a features space where the different user's intended movements can be discriminated by an artificial classifier. By this approach, a high number of movements can be predicted and transferred to the hand prosthesis, robustly to the factors abovementioned (Englehart et al., 1999, Englehart and Hudgins, 2003, Hargrove et al., 2010). However, two obstacles still avoid its transfer to clinical use (Jiang et al., 2012b): (1) an eventual classification error leads to an unwanted movement and (2) the prediction of a high number of degrees of freedom (DoFs) is achieved with unnatural strategies (e.g. the activity of a specific muscle is used for

starting a movement different with respect to that in which it is naturally involved).

Pattern recognition does not allow the user to control (as it should be in physiologic conditions) the range of prosthesis movement. Giving the user this capability is the goal of implementing a mapping of EMG signal features into the continuous control signals. The rationale behind this approach is the existing relation between muscle electrical activity and force generated, and force generated and kinematics produced by hand movement. Vital for the success of this decoding algorithm is the calibration of mapping parameters. This has to be conducted relying on measures of the healthy hand muscles, which are showed to be correlated with the controlateral side in case of bimanual tasks (Muceli et al., 2010, Nielsen et al., 2011, Jiang et al., 2012a). Several attempts have been executed on healthy subjects and amputees, without translation to the prosthesis control tasks (e.g. Jiang et al., 2009). Recently, though, healthy humans have proportionally controlled, with encouraging results, several DoFs of a prosthetic hand (Gijsberts et al., 2014, Fougner et al., 2014). In definitive, clinical tests with amputees controlling a prosthesis using this approach have not yet been conducted.

The extraction of alpha motoneurons drive to muscles (i.e. the spiking activity) from sEMG recordings has recently become a matter of study (Xu et al., 2001, De Luca et al., 2006, Holobar et al., 2007). This methodology, however, is at its early stage. There has not been, indeed, demonstration of its feasibility in a full online system, mainly because of the computational complexity of the algorithm.

In summary, these sophisticated sEMG-based strategies still do not allow amputees to control naturally all the prosthesis DoFs. In particular, independent homologous control of the thumb has never been obtained until recently. Indeed, in 2014, such an achievement has been accomplished by Pasquina et al. (2014). Their team implanted 6 IMES (implantable myoelectric sensors, Weir et al., 2009) in the forearm muscles of an amputee for more than 6 months showing stable

simultaneous and proportional control of wrist pronation/supination, hand opening/closing, and thumb abduction/adduction. The ongoing clinical study is FDA approved.

Intramuscular recordings are a very promising tool for future prostheses control, not being highly affected by the aforementioned factors harming sEMG. However, Pasquina et al. (2014), made only a report about the first 6 months of experiments and did not provide any measure of the functional performances obtained by means of the system. Hence, sensitivity to movement of the muscles with respect to the electrodes, or to posture of the arm have to be evaluated.

The mentioned approaches, being homologous, envision the availability of remnant forearm muscles to enrol in the movements that have to be controlled with the prosthesis, avoiding, hence, applicability on higher level amputees (above the elbow).

To solve this problem, in 2007, Todd Kuiken (Kuiken et al., 2004) developed a revolutionary surgical method called Targeted Muscle Reinnervation (TMR). The remnant nerves of amputees with shoulder disarticulation were redirected over the big muscles of the chest. After re-growth period, sEMG signals from these muscles could be recorded chronically, allowing the patients homologous control over several arm DoFs. An advantage of recording muscles electrical activity over the chest with respect to the forearm is the possibility to increase the distance between targeted recording sites and then to diminish crosstalk. This guarantees a higher number of decoded DoFs with respect to those from forearm muscles. An unexpected effect of the surgery was a restored tactile sensation elicited by mechanical skin solicitation (Kuiken et al., 2007). Because of this property, the team tried to implement a bidirectional prosthesis (Kim et al., 2010), i.e. a device that, other than the movement control, could elicit homologous sensations over the parts of the phantom hand interacting with external objects. In particular, the mechanical stimuli provided over the chest were driven by the readout of prosthesis sensors. However, since the superficial electromyogram, used

as a control signal, was recorded from the same body region that had to be mechanically stimulated to provide feedback, real-time bidirectional control was difficult to achieve.

TMR has been recently used on a person with transhumeral amputation just above the elbow (Yao et al., 2015). The sensory and motor nerves have been redirected to different arm muscles, so to differentiate the locations where the sEMGs were recorded and where the sensations were elicited. The subject was able to control a robotic grip and perceive the force exerted over a grasped object.

In conclusion TMR seems currently a very promising solution for high level amputees for both motor and sensory functionalities restoration.

A very interesting approach for decoding in real-time kinematic and dynamic parameters of the human hand motion relies on ultrasound (US) imaging (Castellini and Passig, 2011; Zhou and Zheng, 2012; Guo et al., 2013; Sierra González and Castellini, 2013). Two great limitations are the bulkiness of the current available technology and the high sensitivity to US probe shift with respect to the skin. Now, even if the second issue could be solved with sophisticated image processing algorithms (Sierra González and Castellini, 2013), the low portability of the hardware seems to be, at present, a problem with no immediate solution.

Another fascinating possibility that has been explored in the last decade is interfacing of the peripheral nerves, instead of muscles, with neural electrodes (Navarro et al., 2005). The rationale behind this is that the neural pathways between periphery and the brain are anatomically still present post-amputation (Mercier et al., 2006, Reilly et al., 2006).

In particular, from motor nerve recordings should be possible to reliably extract a huge amount of information (kinematics and dynamics of the hand movements) for controlling homogonously and effortless a prosthetic device. The electroneurogram (ENG), indeed, is potentially a reliable source of information, being less affected by changes in the interface between recording system and source of signal, during different conditions with respect to superficial and invasive EMG recordings.

On the other side, activation of afferent fibers (by means of electrical stimulation) should elicit simple or complex natural sensations in amputees. Indeed, in this way, the link between skin, muscle, tendon and joint mechanoreceptors on one end and the brain on the other, should be restored.

Dhillon et al., (2004) demonstrated that the neural pathways from periphery to brain are not only anatomically but also functionally still present. They implanted longitudinal intrafascicular electrodes (LIFEs) in median and ulnar nerves of 8 amputees. They recorded motor related ENG and elicited proprioceptive and tactile sensations over the phantom hand. The intensity of evoked sensations was modulable by the intensity or frequency of the stimulation.

Successively (Dhillon and Horch, 2005) have demonstrated that the motor-related ENG recorded by one electrode channel was exploitable for the control of 1 DoF (open/close) of a gripper.

Few years later, another two groups in Asia and Europe did further investigations with a similar interfacing technology. Jia et al, in 2007, implanted median, radial and ulnar nerves of an amputee with LIFEs and showed that the motor-related ENG activity recorded in the radial nerve was strong enough to drive the extension of the fingers of an artificial hand. Micera and Rossini et al., 2010, (Rossini et al., 2010) showed that an amputee implanted in the median and ulnar nerves, with tfLIFEs, was able to control multiple grasps (pinch, ulnar, power grasps) of a prosthesis. Posterior off-line analysis showed that the 3 DoFs (plus rest) could be discriminated with overall accuracy of 85% (Micera et al., 2011). The afferent nerves of the amputee were stimulated to elicit sensations. Results similar to those reported by Dhillon et al. (2004) were obtained. In particular, tactile but no proprioceptive sensations were reported.

However, despite it was demonstrated that motor related recordings could be used for on-off control of prosthesis, it has been never shown that the high amount of kinematic or kinetic information conveyed through the peripheral nerves can be actually extracted.

Moreover, nevertheless there is the evidence that nerve stimulation can be used as tool for restoring natural sensory feedback in amputees, it has never been proved that such an approach can be successfully integrated, clearly distinguished and exploited by amputees in the closed-loop control of a bidirectional prosthesis.

In conclusion, peripheral nerve interfacing is, presently, still at level of proof of the concept.

On the other side, sensory feedback can be restored to amputees also by means of non- invasive techniques. Mechanical stimulation (i.e. vibration) of the skin over the forearm (or eventually the arm) has been driven by tactile and proprioceptive angular information from a robotic hand (Cipriani et al., 2012). This approach, however, requires a training (eventually long), from the amputees in order to learn the sensory feedback code (i.e. how the prosthesis information are traduced into mechanical stimulation modulation) which is not homologous.

A captivating way to restore sensory feedback to amputees is the electrical stimulation of the human upper peripheral nerves by means of electrodes placed on the skin (Transcutaneous Electrical Nerve Stimulation, TENS). Indeed, by this kind of stimulation, tactile sensations can be elicited over the phantom hand of an amputee (Szeto and Saunders, 1982). TENS causes an activation of most of the sensory fibers simultaneously (low selectivity) (Kuhn et al., 2010) but it should not require training for the patient because sensations that evoke are naturally located over the phantom hand. To the best of our knowledge, there are no commercial products or research publications that propose a bidirectional prosthesis in which the sensory feedback is restored by means of TENS.

This work therefore rises from the necessity of developing more natural-like prostheses than those presently available.

To achieve this goal, as objectives of the present thesis, we aimed at verifying whether:

i. It is possible to reliably extract complex motor related information from peripheral efferent nerves recordings

ii. It is possible to integrate peripheral nerves stimulation to elicit natural, clear and exploitable sensations in the closed-loop control of a bidirectional prosthesis

iii. It is possible to integrate transcutaneous superficial nerve stimulation for restoring homologous sensory feedback in the closed-loop control of a bidirectional prosthesis.

These questions are addressed in chapters 3, 4 and 5, respectively. The content of these chapters reproduces manuscripts that I co-authored, published or in preparation. As such, these chapters are organized as self-contained manuscripts and may repeat some of the information already introduced in other parts of this thesis. I hope the reader will share my view that this repetition is acceptable and does not detract from the presentation of the thesis.

In Chapter 2 a dissertation about the peripheral nervous system is inserted together with the technology currently available for interfacing it. In chapter 6 the achievements obtained in this work are summarized, their relevance is discussed and further investigations are proposed.

# Chapter 2 The peripheral nervous system: essential considerations

The peripheral nervous system (PNS) is constituted by nerves and ganglia exiting the brain and the spinal cord (central nervous system, CNS). Its function is to provide a link between the CNS, organs and extremities (e.g. arms and legs) and to convey sensory and motor information. In particular, instructions are transferred from the CNS to muscles and glands (motor division of the PNS) and sensory information from peripheral receptors (e.g. muscle spindles, golgi tendon organs and skin mechanoreceptors) to the CNS (sensory division).

The peripheral nervous system is divided into the autonomic and somatic nervous systems. Nerves and ganglia of the latter communicate with voluntary muscles and skin receptors while those of the former determine the functions of internal organs (e.g. heart or liver).

Ganglia are groups of cell bodies that are located just outside the spinal cord. Peripheral nerves are constituted by neurons axons. They are classified in cranial nerves, which emerge from the brain and the brainstem and spinal nerves, i.e. those exiting the spinal cord. In particular, the latter exits from two locations (Fig. 2.1): those belonging to the motor division come out from the ventral portion of the spinal cord (ventral root) while those of the sensory division from the dorsal one (dorsal root).

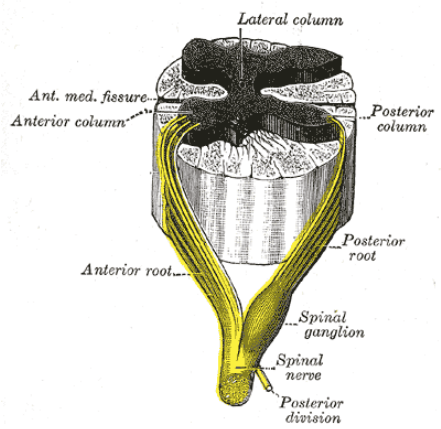


**Fig. 2.1.** Dorsal and Ventral roots. Picture extracted from Gray's Anatomy.

***Nerve Anatomy***

Each nerve is covered by a sheath of connective tissue named epineurium, which envelopes the fascicles, bundles of nerve fibers enclosed in another connective formation, the perineurium. Nerve fibers are constituted by a neuron axon, covered by Schwann's, (eventually) myelin sheaths and a connective matrix that folds all these structures, the endonerium. Nerves are bundled along with vessels to satisfy their high requirement of energy. The described nerve structure is drawn and pictured in Fig. 2.2A and 1.2B respectively.

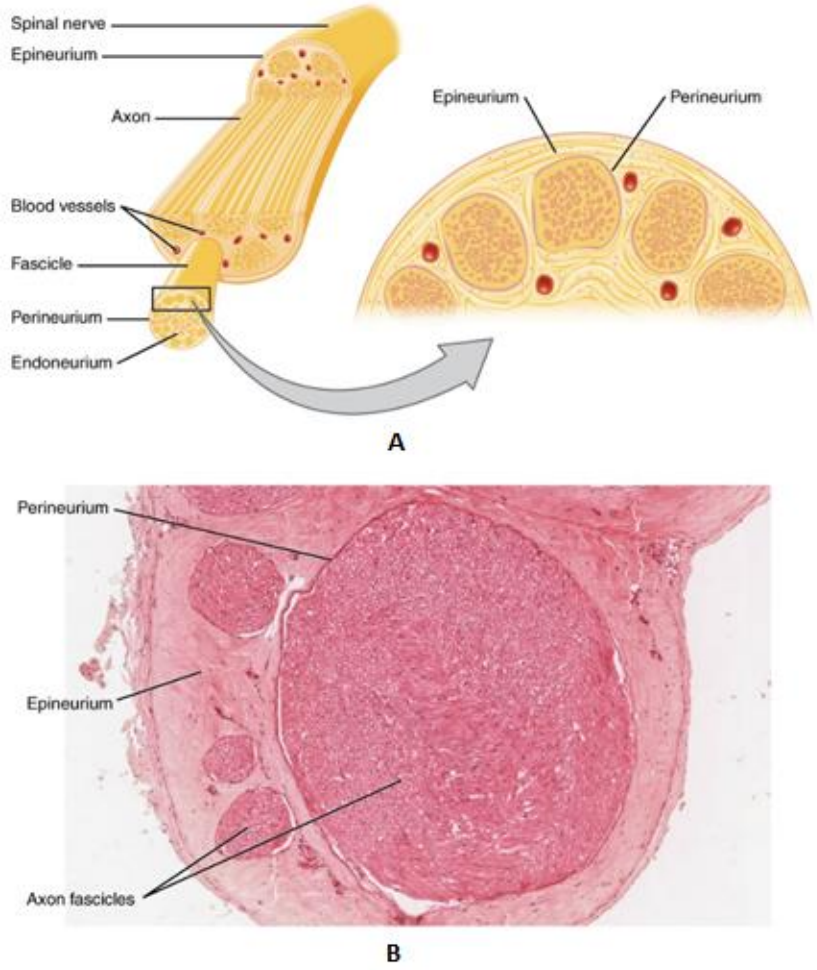


**Fig. 2.2.** (A) Schematic of a nerve structure. (B) Microscopy of a nerve section. Extracted and readapted from OpenStax College - Anatomy & Physiology, Connexions Web site. http://cnx.org/content/col11496/1.6/, Jun 19, 2013.

Nerve fibers are called afferent if belonging to sensory division, efferent to motor division and autonomic if being part of the autonomic system. The size of fibers and nerves is variable among people and within the single person.

There are three types (A, B, C) of nerve fibers clustered with respect to their diameter size. Those of the group A are myelinated, have the largest diameter and the highest conduction velocity. They, in turn, are classified

in alpha (afferent or efferent fibers), beta (afferent or efferent fibers), gamma (efferent fibers) and delta fibers (afferent fibers), according to their diameter size. Nerve fibers in group B are myelinated with smaller diameter than group B ones. They are the preganglionic fibers of the autonomic nervous system and have a low conduction velocity. The C group fibers are unmyelinated, have the smallest diameter and low conduction velocity. These fibers include the postganglionic ones in the autonomic nervous system and those at the dorsal roots bringing information about nociception (pain), temperature, touch, pressure and itch. In Table 2.1 are reported conduction velocity and diameter size of the somatic sensory and motor fibers.

**Table 2.1.** Classification, geometric properties and conduction velocity of the peripheral nerve fibers belonging to groups A, C.

| Classification | Diameter | Myelin | Conduction velocity | Associated sensory receptors |
|---|---|---|---|---|
| Aα | 13-20 µm | Yes | 80–120 m/s | Responsible for proprioception |
| Aα | 13-20 µm | Yes | 80–120 m/s | Golgi tendon organ |
| Aβ | 6-12 µm | Yes | 33–75 m/s | Secondary receptors of muscle spindle<br>All cutaneous mechanoreceptors<br>Free nerve endings of touch and pressure |
| Aδ | 1-5 µm | Thin | 3–30 m/s | Nociceptors of neospinothalamic tract<br>Cold thermoreceptors |
| C | 0.2-1.5 µm | No | 0.5-2.0 m/s | Nociceptors of paleospinothalamic tract<br>Warmth receptors |
| Aα | 13-20 µm | Yes | 80–120 m/s | Extrafusal muscle fibers |
| Aγ | 5-8 µm | Yes | 4–24 m/s | Intrafusal muscle fibers |

***Nerve Physiology***

The nerves transport digital information coded by action potentials (or spikes). A spike is defined as a fast change (1 to 3 ms) of the trans-

membrane voltage of the neuron due mostly to the flow of $Na^+$ and $K^+$ ions through ionic channels (within the membrane itself) (Fig. 2.3).

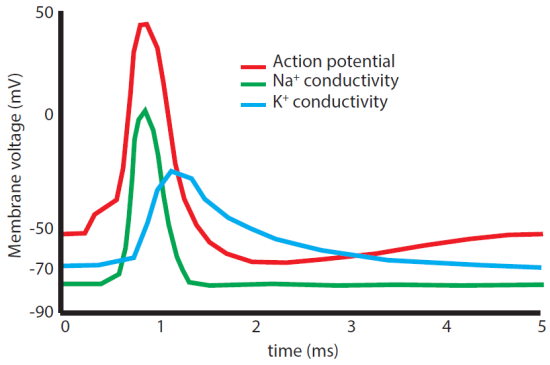


**Fig. 2.3.** Action Potential and its generation. Based on (Hodgkin and Huxley, 1952). Patch clamp of a squid giant axon.

The spike is generated in the soma or in the axon of a neuron and then transmitted along the axon itself.

The action potential propagation occurs because of the ions flow along the axon. In particular, once the $Na^+$ ions, that generated the action potential itself, are into the axon, they flow along the internal membrane (Nernst-Planck equation) and activate ionic channels. If they are activated in a sufficiently high number, a new action potential is generated.

Axons enfolded with sheaths of myelin propagate quicker the action potential. In that case, indeed, ionic channels are disposed only in correspondence of membrane portions where there is no myelin (nodes of Ranvier). Moreover, the membrane tracts between two nodes of Ranvier have higher impedance (than axons with no myelin). This causes the action potential to jump from one node of Ranvier to another without ions

leakage in between (saltatory propagation, Tasaki, 1939, Huxley et al., 1949), and, thus, increases the velocity of propagation.

The generation of an action potential has been modeled in 1952 by Hodgkin and Huxley (Hodgkin and Huxley, 1952 a), while its conduction was modeled starting from cable equations of Lord Kalvin, and was formalized by (Helmholtz, H. 1850) and excellently described in (Scott, 1975).

In the peripheral nervous system, spikes can be physiologically generated in a neuron only thanks to the input from other cells or sensory receptors. The connection between two cells is called synapse. The one sending the action potential is called presynaptic, while the other postsynaptic.

Artificially, among many other ways, the spikes can be elicited also by means of extracellular electrical stimulation (Rattay et al., 1986). This is very relevant to the scope of the present thesis.

***Motor system***

*Alpha Motoneurons*

The content of this section is extracted and reformulated, from a recent and exhaustive review on the motor system, written by Heckman and Enoka in 2012 (Heckman and Enoka, 2012).

The motoneuron and the muscle fibers that it innervates, with the latter referred to as the muscle unit, constitute the motor unit. The motor unit provides the primary output for the CNS, converting sensory (from mechanoreceptors) and descending neural inputs into forces to generate

movement. Individual muscles comprise a population of motor units that controls the force exerted during a contraction. The motoneurons of the population are located in relatively close proximity in either the ventral horn of the spinal cord or the brain stem.

Motor units are classified differently according to the evaluation principles. However, the most common and old categorization, that has been proposed, is the one of Burke and colleagues. According to it, 3 types of motor units are differentiated by determining the profile of an unfused tetanus and then measuring the rate of decline in tetanic force to a prescribed protocol of electrical stimulation. The interstimulus interval for the unfused tetanus is set at 1.25×contraction time of the motor unit twitch, and produced a profile that either did or did not increase monotonically during the tetanus; a profile that did not increase monotonically was described as exhibiting sag. Those units displaying sag were classified as fast-twitch (type F) motor units, whereas those with no sag were considered to be slow twitch (type S). The type F units were then subjected to 6 min of intermittent electrical stimulation (40 Hz for 330 ms, once per second) and the rate of decline in peak tetanic force was used to distinguish motor units that were either fast-to-fatigue (type FF) or fatigue-resistant (type FR). The properties of muscle fibers and motor units are, however, not so discrete, as demonstrated successively.

Furthermore, type S motor units are smaller (in terms of number of muscle fibers innervated by its motoneuron) but their population is more numerous than the type FF one (Fig. 2.4A).

It is interesting to notice that motor unit properties correlate with motor neuron ones. In fact, S motor units, compared to F ones, have smaller motoneurons in terms of axon and body (dendrites included).

Since the pioneering work of Adrian and Bronk, it has been known that the force exerted by a muscle depends on the number of motor units recruited into action and the rates at which these motor units discharge action potentials.

In particular, motor units are recruited in an orderly sequence from those with smaller force (S) to those with higher force (FF) (Henneman's or size principle). The phenomenon is due to difference in motoneuron resistance to inputs from the CNS and the sensory systems. Type S motoneurons have higher resistance (being smaller in size) compared to type FF ones, hence, have more significant variation of membrane potential to the same ionic current. The consequences on the force exerted by the muscles are pictured in Fig. 2.4B. Finally, the relative contribution of a recruited motor unit to a given action depends on the rate at which it discharges action potentials (rate coding). The observed rates for the same motor unit depend on the task being performed.

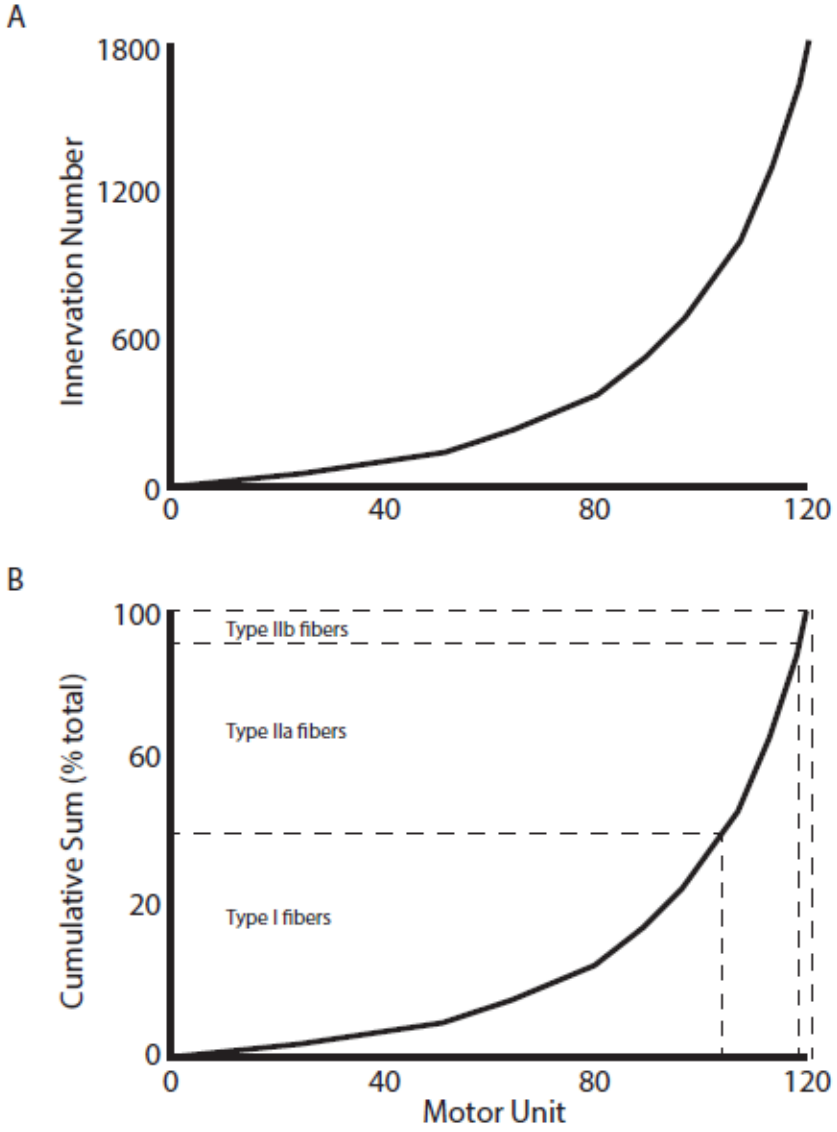


**Fig. 2.4.** Proportions of motor units in the first dorsal interosseous muscle that innervate the different muscle fiber types. (A) The distribution of innervation numbers for the 120 motor units. (B) The number of motor units that innervate the different fiber types. Extracted from (Enoka and Fuglevand, 2001).

*Gamma motoneurons*

Gamma motoneurons exits, as alpha ones, the ventral roots of the spinal cord. They are smaller than alpha motoneurons and are involved in

determining the level of tension of muscular fibers within the muscle spindles (see Sensory System subsection).

*Beta motoneurons*

Beta motoneurons exits the ventral roots of the spinal cord and have smaller diameter than alpha ones. They innervate both intrafusal (within muscle spindles) and extrafusal muscle fibers.

***Sensory system***

Sensory fibers bring several types of information from receptors that are in the periphery via the spinal cord to the brain, allowing humans to perceive exteroreceptive, interoceptive and proprioceptive sensations (respectively, stimuli coming from outside and inside of the body, and related to the position of the body in the space). These fibers (primary afferents) have the soma in the ganglia just outside the spinal cord and make synaptic connection with the secondary afferents in the dorsal roots.
In the following sections exteroceptive and proprioceptive sensations will be treated.

*Exteroceptive sensations*

The content of this subsection is based on three recent reviews (Gardner, 2010, Johansson and Flanagan, 2009, and Abraira and Ginty, 2013).
Tactile and nociceptive sensations are coded peripherally by mechanoreceptors that are in the skin. Low and high thresholds mechanoreceptors react respectively to the former and the latter stimuli.

Low threshold mechanoreceptors are classified as Ab, Ad or C (Table 2.2). In the glabrous skin are Pacinian corpuscles, Ruffini endings, Meissner corpuscles, and Merkel discs (Fig. 2.5), while in the hairy skin are longitudinal and circumferential lanceolate endings. High threshold mechanoreceptors can be Ab, Ad or C (Table 2.2) and present free nerve endings both in the hairy and glabrous skin (Fig. 2.5).

**Table 2.2.** A Comparison of Cutaneous Mechanoreceptor Subtypes. Extracted from (Abraira and Ginty, 2013)

| Physiological subtype | Associated fiber (conduction velocity[1]) | Skin type | End organ/ending type | Location | Optimal Stimulus[4] | Response properties |
|---|---|---|---|---|---|---|
| SAI-LTMR | Aβ (16-96m/s) | Glabrous | Merkel cell | Basal Layer of epidermis | Indentation |  |
| | | Hairy | Merkel cell (touch dome) | Around Guard hair follicles | | |
| SAII-LTMR | Aβ (20-100m/s) | Glabrous | Ruffini[2] | Dermis[3] | Stretch |  |
| | | Hairy | unclear | unclear | | |
| RAI-LTMR | Aβ (26-91m/s) | Glabrous | Meissner corpuscle | Dermal papillae | Skin movement |  |
| | | Hairy | Longitudinal lanceolate ending | Guard/Awl-Auchene hair follicles | Hair follicle deflection | |
| RAII-LTMR | Aβ (30-90m/s) | Glabrous | Pacinian corpuscle | Deep dermis | Vibration |  |
| Aδ-LTMR | Aδ (5-30m/s) | Hairy | Longitudinal lanceolate ending | Awl-Auchene/ Zigzag hair follicles | Hair follicle deflection |  |
| C-LTMR | C (0.2-2m/s) | Hairy | Longitudinal lanceolate ending | Awl-Auchene/ Zigzag hair follicles | Hair follicle deflection |  |
| HTMR | Aβ/Aδ/C (0.5-100m/s) | Glabrous Hairy | Free nerve ending | Epidermis/Dermis | Noxious mechanical |  |

1 Conduction velocities can vary across species.

2 Though SAII-LTMR responses have been observed in both glabrous skin of humans and hairy skin of mice, they have only been postulated to arise from Ruffini endings, though direct evidence to support this idea is lacking.

3 Although SAII-like responses are present in the mouse, Ruffini endings or Ruffini-like structures have not been identified in rodents.

4 The stimulus described is the optimal stimulus known to elicit the response properties depicted in the last column of this table. However, it is probable, and often times documented, that multiple physiological subtypes can be recruited with any one particular tactile stimulus. For example, indentation of hair skin is likely to activate not

only SAI-LTMRs associated with guard hairs but also longitudinal lanceolate endings of the Ab-, Ad-, and C-LTMR type.

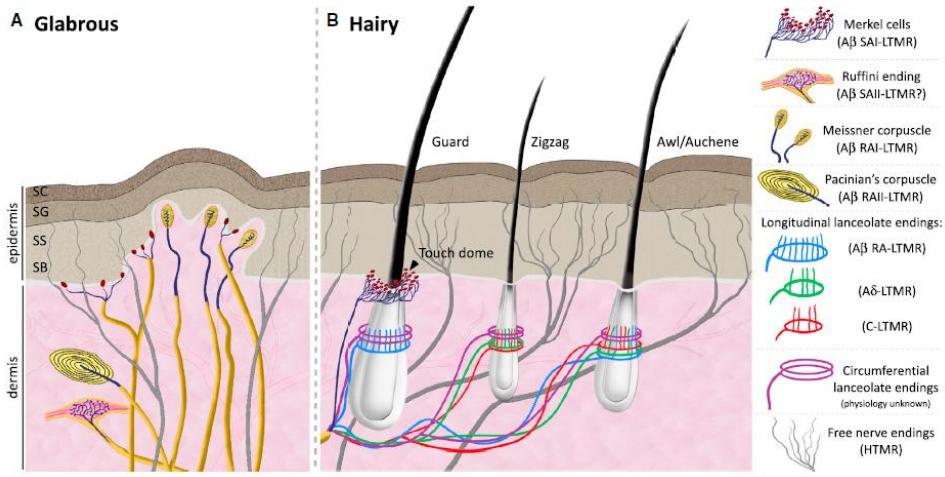


**Fig. 2.5.** The Organization of Cutaneous Mechanoreceptors in Skin. Innocuous touch information is processed by both glabrous hairless (A) and hairy (B) skin. Abbreviations: SA, slowly adapting; RA, rapidly adapting; LTMR, low-threshold mechanoreceptor; HTMR, high-threshold mechanoreceptor; SC, stratum corneum; SG, stratum granulosum; SS, stratum spinosum; SB, stratum basalis. Extracted from (Abraira and Ginty, 2013).

In the following text, glabrous skin low threshold mechanoreceptors will be presented, being the organs responsible for tactile sensations elicited mainly in the human hand palm.

Each hand has approximately 150 000 mechanoreceptors connected to 30 000 primary afferent fibers. In the fingertip (where the density is the highest) there are 2500 receptors/cm$^2$ innervated by 250-300 fibres.

RAI (Rapidly Adapting, type I) and SAI (Slowly Adapting, type I) afferent fibers terminate superficially in the skin with respectively Meissner and Merkel endings. The former reply to dynamic skin deformation of 1-10 Hz

frequency range while the latter respond to skin indentation and static stimuli with a firing activity proportional to the intensity of the stimulus.

Individual Meissner corpuscle and Merkel disc receptors are smaller than a fingerprint ridge, however, since each RAI and SAI fiber innervates 15-20 corpuscles, their receptive field can extend even to more than a single finger.

RAII (Rapidly Adapting, type II) and SAII (Slowly Adapting, type II) fibers, on the other side, reply respectively to high frequency (10-300 Hz) dynamic perturbation on the skin (e.g. vibration), and skin stretches. They terminate, orderly, in Pacini and Ruffini-like endings. Each of these fibers innervate one single mechanoreceptor.

Type I fibers are more numerous than type II ones (Fig. 2.6). In particular the former range between 30 and 140 fibers/cm$^2$ (respectively in hand palm and fingers) while the latter are less than 30 fibers/cm$^2$.

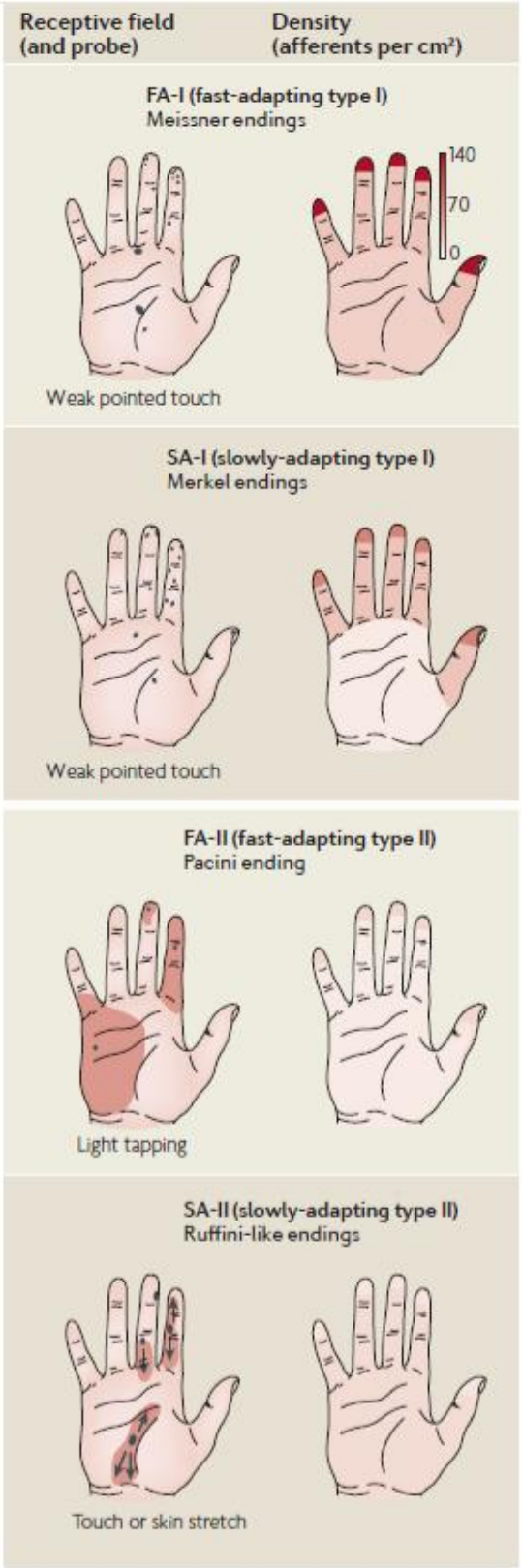


**Fig. 2.6.** Mechanoreceptors distribution in the hand. Readapted from (Johansson and Flanagan, 2009).

It is important to notice that mechanoreceptors reply most specifically to a particular stimulus but they are not completely insensitive to others. Moreover, since naturally a mechanical stimulus is a complex combination of simple ones, often, different afferent fibers discharge at the same time (with their own pattern) in reply to an external solicitation.

We report, hereafter, some examples of afferent pool activation in different tasks that are going to clarify the characteristics of mechanoreceptors:

**1. pick and place task:** when the hand squeezes (phase I) an object to lift it up (phase II) and place it back (phase III), the loads exerted perpendicularly and orthogonally to the skin increase (phase I) to a plateau (phase II) and decrease back (phase III). In the first phase all the afferent fibers increase their discharging activity, in the second one SAI and SAII maintain their firing proportionally to the perpendicular and orthogonal loads respectively, in the third one all the fibers are again all active. RA fibers present an increase in their discharging activity during the discontinuities (contact with the object and its release). Fig. 2.7. summarizes the process.

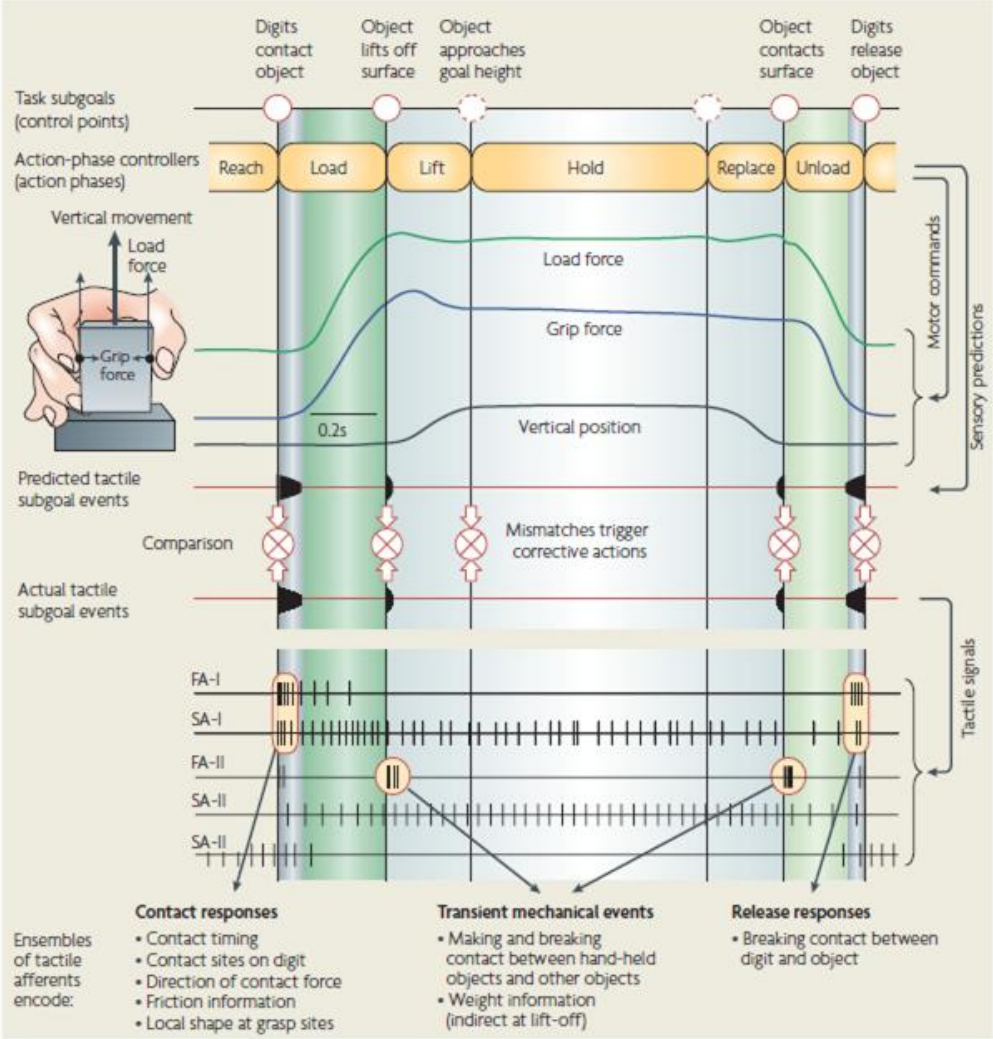


**Fig. 2.7.** Sensorimotor contro point in a prototypic manipulation task. Extracted from (Johansson and Flanagan, 2009).

**2. stimulus of increasing intensity.** In the pick and place task, the activity of individual types of afferent fibers in response to the specific mechanical stimuli has been showed. In reality, not the single fiber but a population of them is recruited in the solicited areas of the skin. The intensity of the stimulus (e.g. orthogonal to the skin) would have been coded, in this case, by both an increase in the number of fibers recruited and their firing activity. (Muniak et al., 2007)

**3. texture recognition.** SAI, RAI and RAII afferents are involved in this task. Both spatial (firing rate proportional to the distance between surface discontinuities) and temporal coding (a specific firing temporal pattern codes for a particular surface). In particular the spatial coding is dominant for surfaces with discontinuities coarser than 1 mm (and is expressed mostly by SAI fibers) while the temporal coding is dominant for discontinuities less coarse than 1 mm (expressed mostly by RAI and II). (Weber et al., 2013)

**4. object movement on the skin.** When an object runs over the skin, this is stretched, thus, different areas are solicited. In this case, dynamic activation of SAI and RAII fibers innervating different areas occurs along with SAII discharge following skin stretches. (Pei and and Bensmaia, 2014).

*Proprioceptive sensations*

The content of this section is based on (Pearson, 2001) and (Proske and Gandevia, 2012).

The term *proprioception* was passed down to us by Sherrington. He stated, "In muscular receptivity we see the body itself acting as a stimulus to its own receptors—the proprioceptors."

Proprioceptive fibers send to CNS and PNS (motoneurons in particular) information about muscle activity. There are three types of proprioceptive fibers: Ia, Ib, II. Ia and II fibers have their endings in the muscle spindles (Fig. 2.8) which are organs that embed muscle fibers (named for this reason intrafusal) in parallel with extrafusal ones (in opposition to

intrafusal ones). The word "fusal" comes from the Latin nomenclature for muscle spindle, which is "fusus neuromuscularis". Ib fibers have their endings in the Golgi tendon organs (Fig. 2.9), which are wrapped in the tendons connecting muscle fibers to bones.

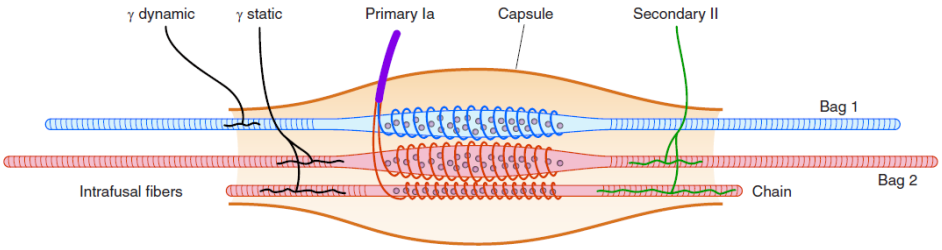


**Fig. 2.8.** Diagrammatic representation of the mammalian muscle spindle. The intrafusal fibers include the large nuclear bag 1 and bag 2 fibers together with the smaller nuclear chain fibers. Ends of the bag fibers extend beyond the capsule while chain fibers lie within the limits of the capsule. Large, group Ia afferent fibers terminate as primary endings, making spiral terminations around the nucleated portions of all three intrafusal fiber types. Smaller, group II afferent fibers terminate as secondary endings, lying to one side of the primary endings and supplying bag 2 and chain fibers. Gamma dynamic (g dynamic) fusimotor fibers innervate bag 1 fibers, while gamma static (g static) fusimotor fibers innervate bag 2 and chain fibers. Extracted from (Proske and Gandevia, 2012).

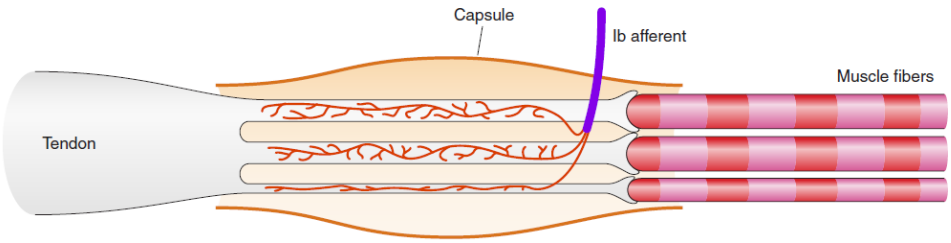


**Fig. 2.9.** Diagrammatic representation of the mammalian Golgi tendon organ. The Group Ib axon penetrates the receptor capsule and branches, each branch terminating on a tendon strand that is attached to a muscle fiber. A typical tendon organ has 10 or more muscle fibers attached to it, each fiber belonging to a different motor unit. Contraction of a motor unit supplying a tendon organ stretches the tendon strand to which its muscle

fiber is attached, generating activity in the Ib axon. Extracted from (Proske and Gandevia, 2012).

Ia afferents have a discharging activity that is proportional to muscle fibers velocity, contraction and length (dynamic fibers). IIa ones, on the other side, code for the length of muscles (but with a smaller velocity-sensitive component, static fibers). Gamma motoneurons make synaptic connection with intrafusal muscle fibers to contract them and enhance the spiking activity of the fusal afferents.

Ib fibers send information about the tension produced by the muscle fibers connected to their endings.

In definitive, the overall activity of Ia, II and Ib fibers brings to the CNS information about the whole muscle length, the velocity and the force of its contraction.

Proprioceptors are particularly important for the control of muscles contraction and coordination. They, indeed, make synapses with interneurons in the spinal cord that excite or inhibit motoneurons of the same (homologous) or other (heterologous) muscles.

In particular some simple circuits are note, such as the autogenic and reciprocal inhibition reflexes (Hultborn, 2006, Jankowska, 1992, Jankowska, 2013a, Jankowska, 2013b). In the former, an Ib fiber sends inhibitory postsynaptic potentials (IPSP) to a motoneuron of the homologous muscle. In the reciprocal inhibition reflex, on the other side, Ia and II fibers cause an excitatory postsynaptic potential (EPSP) to a motoneuron of the homologous muscle and, in the meantime, an IPSP to a

motoneuron of the heterologous muscle. This reflex coordinates the activity of antagonist muscles or muscle groups belonging to two sides of the body (such as legs muscles).

***Motor and sensory system physiology modeling***

Computational models describing the relation between alpha motoneurons pool recruitment and discharge rate and force produced by the corresponding innervated muscle have been developed along the years (Fuglevand et al., 1993, Lowery and Erim, 2005, Dideriksen et al., 2011, Contessa and De Luca 2013, Heckman and Binder 1991), under the condition of isometric contraction.

Computational models that predict the spiking activity of many different classes of cutaneous and muscle afferents in response to external stimuli on the skin are available (Mileusnic et al., 2006, Mileusnic and Loeb, 2006, Sripati et al., 2006).

***Nerves of the hand***

Median, ulnar and radial are the nerves of the hand. In particular, the median nerve receives input from skin mechanoreceptors of the first three fingers, part of the fourth one and the underlying portions of the palm (Fig. 2.10.); the ulnar nerve from the fifth finger, part of the fourth one and the underlying palm (Fig. 2.10.); the radial from the dorsal of the hand (Fig. 2.10).

Motoneurons folded in the three nerves innervate the muscles that are reported in Table 2.3. Briefly, the median nerve controls the flexors of the

first three fingers and wrist and the pronators of the wrist, the ulnar one the flexors of the fourth and fifth fingers and the wrist and the supinator of the wrist, while the radial the extensors.

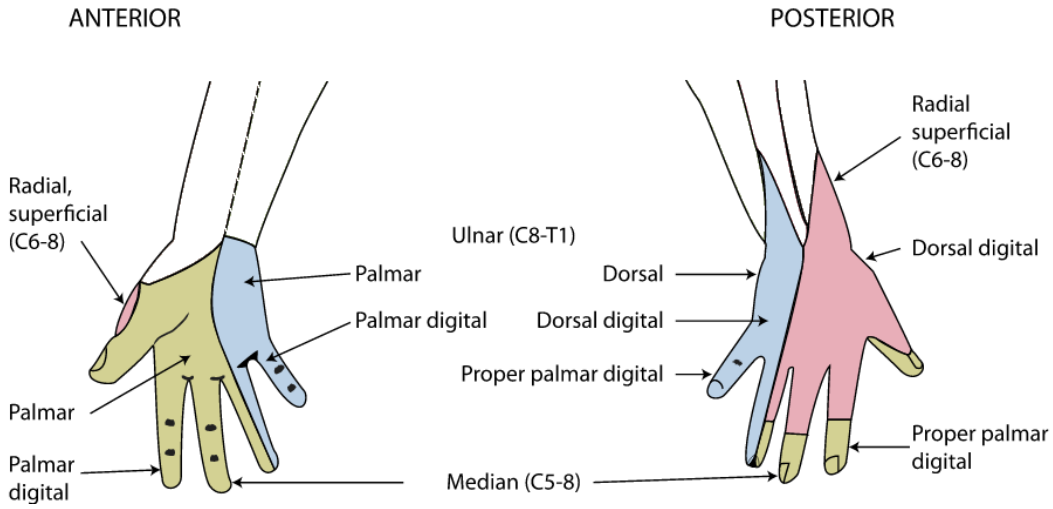


**Fig. 2.10.** Innervation of cutaneous mechanoreceptors.

**Table 2.3.** Innervation of hand muscles.

| Nerve | Muscles |
|---|---|
| radial | Extensors: **carpi radialis longus** and **brevis**, **digitorum**, **digiti minimi**, **carpi ulnaris**, **pollicis longus** and **brevis**, and **indicis**. Other: **abductor pollicis longus**, supinator |
| median | Flexors: **carpi radialis**, **pollicis longus**, **digitorum profundus** (half), **superficialis**, |

| | |
|---|---|
| | and **pollicis brevis** (superficial head). Other: **palmaris longus**. **abductor pollicis brevis**, **opponens pollicis**, and first and second **lumbricals**, pronator teres, pronator quadratus muscle. |
| ulnar | **Flexor carpi ulnaris**, **flexor digitorum profundus** (half), **palmaris brevis**, **flexor digiti minimi**, **abductor digiti minimi**, **opponens digiti minimi**, **adductor pollicis**, **flexor pollicis brevis** (deep head), **palmar** and **dorsal interossei**, and third and fourth **lumbricals**. |

***Peripheral nerve interfaces***

Several peripheral nerve interfaces have been developed up to present (Navarro et al. 2005, Schultz and Kuiken, 2012).

They are classified according to their design, level of invasiveness and selectivity (Fig. 2.11) which refers to the capacity to record from or stimulate a target number of fibers (a mathematical definition of selectivity has been provided by Raspopovic et al., 2011).

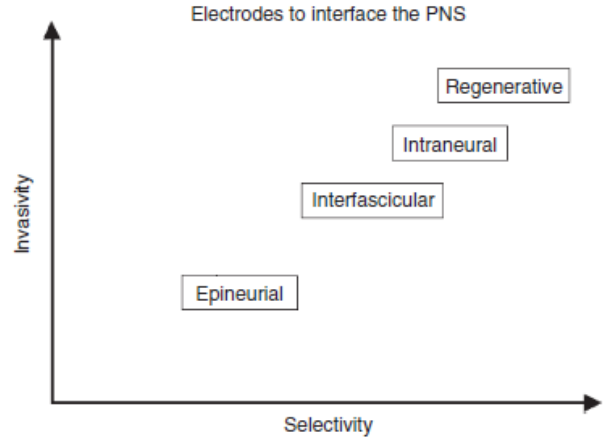


**Fig. 2.11.** The different types of electrodes applied to interface peripheral nerves classified regarding invasivness and selectivity. This represents a general classification, despite that selectivity actually depends on the type of nerve and anatomical and physiological considerations for each particular application. Extracted and readapted from (Navarro et al., 2005).

Epineural electrodes are disposed around the epineurium of the nerve. There are mainly of two types: cuff and FINE electrodes.

- cuff electrodes (Fig. 2.12) were firstly proposed by (Naples et al., 1990). They are composed by an insulating tubular sheath on which stripes of conductive material are printed. The electrode is wrapped around the nerve.

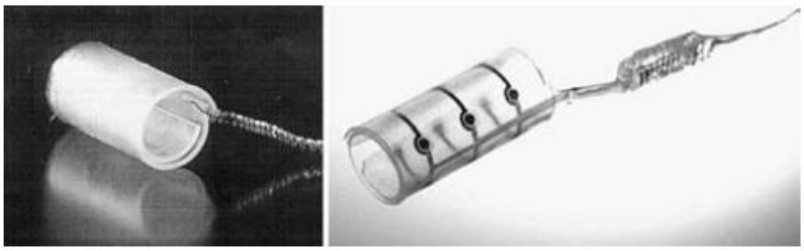

**Fig. 2.12.** Examples of cuff electrode made on silicone and hybrid silicone-polyimide cuff electrode (from IBMT). Extracted from (Navarro et al., 2005).

- FINE (flat interface nerve electrode) electrodes (Fig. 2.13, Tyler and Durand, 2002) present the same design of cuff electrodes with the difference that the external cylindrical tube is replaced by a rectangular one, which has the purpose of reshaping the nerve and making more accessible also the inner fascicles. As a consequence, FINE electrodes have higher selectivity than cuffs.

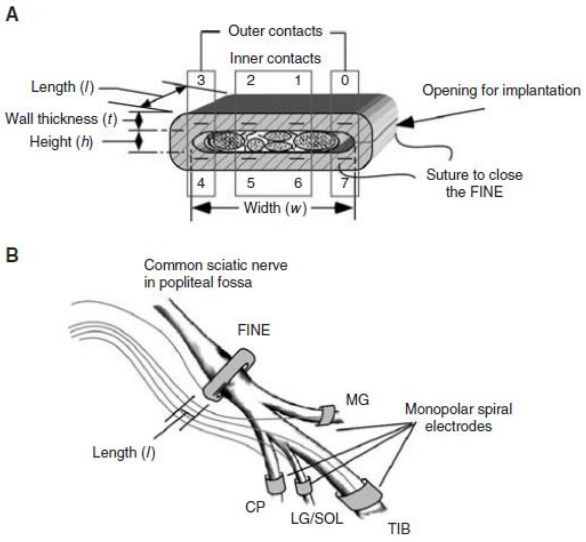


**Fig. 2.13.** Flat-interface nerve electrode (FINE) electrode design and implant location. (A) Schematic cross-section of a FINE on a plurifascicular nerve. (B) Location of the experimental electrodes on the sciatic nerve (from Tyler and Durand, 2002, with permission). CP, common peroneal; LG/SOL, lateral gastrocnemius/soleus; MG, medial gastrocnemius; TIB, tibial. Extracted from (Navarro et al., 2005).

Intraneural electrodes are implanted within the nerve fascicles. The most-known designs are LIFE and TIME electrodes.

- LIFE (longitudinal intrafascicular electrodes) electrodes (Fig. 2.14) are wires of conductive materials covered by insulating component (Malagodi et al., 1989). The recording/stimulating active sites derive from

portions of the device bared of the insulation. Variations of this design have been proposed along the years. One of these is the tfLIFE (thin film LIFE, Hoffmann and Kock, 2005) which is developed on a micropatterned polyimide substrate filament, folded in half so that each side has four active recording sites.

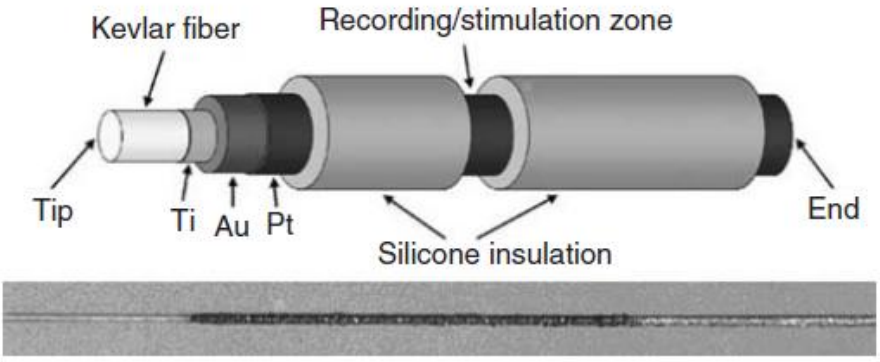


**Fig. 2.14.** Schematic representation of a polymer-based intrafascicular electrode (polyLIFE). The polyLIFE consists of a Kevlar fiber, metallized with titanium (Ti), gold (Au), and platinum (Pt) and insulated with silicone. The recording/stimulation zone consists of approximately 1 mm non-insulated portion of the metallized fiber. At the bottom panel, micrograph of the recording/stimulating zone of a LIFE made from metallized Kevlar fiber. In the center is the recording/stimulating region where platinum black has been deposited. Extracted from (Navarro et al., 2005).

- TIME (transversal intrafascicular multipolar electrode, Boretius et al., 2010) electrodes are an upgraded version of LIFEs. They have similar structure but are implanted transversally in the nerve.

Penetrating microelectrodes:

- MEA (Multi Electrodes Array) electrodes are constituted by an array of conductive sites shaped as needles which are transversally inserted in the nerve. Different versions have been independently developed by different

research groups or corporations. For instance, at University of Utah, silicon-glass technology has been used to produce 3D arrays of 128 electrodes with constant or varying height from 250 to 600 mm (Fig. 2.15).

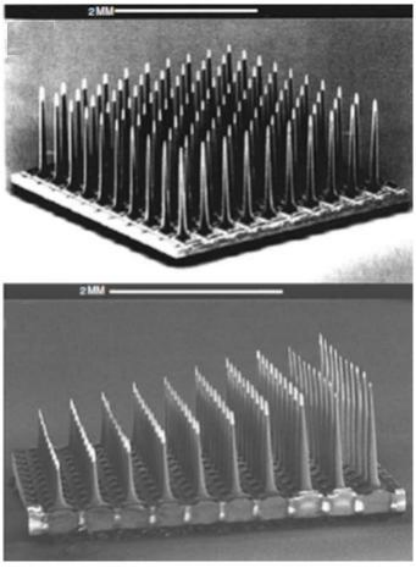


**Fig. 2.15.** Penetrating electrodes developed at the University of Michigan (up) (from Neuronexus Inc.) and at the University of Utah (down). Extracted from (Navarro et al., 2005).

- Microneurography electrodes are shaped as needles and inserted percutaneously in the nerve. Their placement in the nerve is executed for a limited amount of time (not chronically).
- Interfascicular electrodes are a hybrid technology that combines intraneural and cuff electrodes (Fig. 2.16).

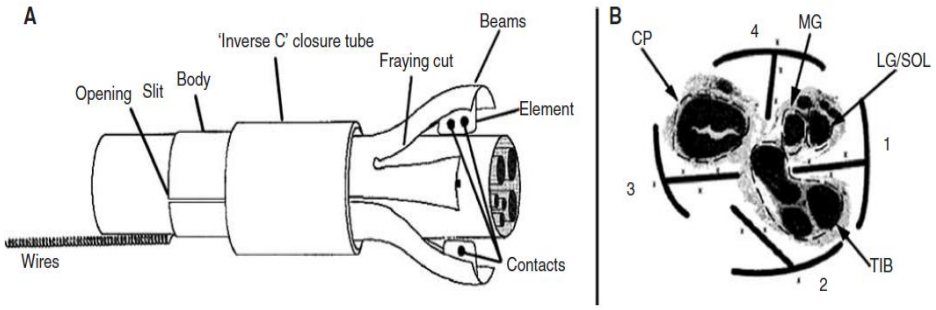


**Fig. 2.16.** (A) Schematic representation of a slowly penetrating interfascicular nerve electrode. Each element is slowly urged into the epineurium by a small force applied by the beams. The center of the electrode is closed with a second tube around the center. Two interfascicular contacts are located on one side of each penetrating element. (B) Cross-section of an implanted nerve. The four elements penetrated within the nerve separating the nerve into three compartments. Tibial (TIB), lateral gastrocnemius/soleus (LG/SOL), medial gastrocnemius (MG), and common peroneal (CP) fascicles are indicated. Extracted from (Navarro et al., 2005).

Regenerative electrodes are constituted by an array of holes in which conductive material is placed. They exploit the capacity of axons to re-grow after a lesion. For their implant, a portion of the nerve is cut and, then, between the two resulting nerve stumps the electrode is placed. The nerve fibers regenerate within the electrode holes (Fig. 2.17).

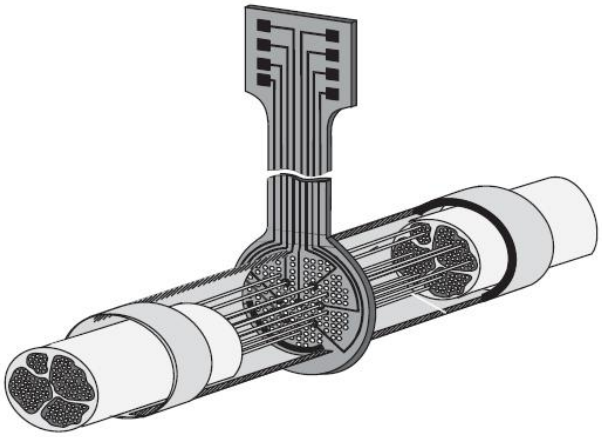

**Fig. 2.17.** Schematic concept of a regenerative electrode. Nerve fibers of a sectioned nerve grow through the holes of the electrode encased in a guidance tube.

All of presented electrodes could be potentially used both for recording and stimulation, with different performances and possible usages.

# Chapter 3 Prediction of hand force and velocity from human alpha motoneurons recordings

The content of this chapter has been included in Petrini, F.M., Mazzoni, A.**, Rigosa, J.**, Giambattistelli, F., Granata, G., Guglielmelli, E., Zollo, L., Capogrosso, M., Raspopovic, S.*&, Micera, S.*&, "Prediction of hand force and velocity from human alpha motoneuron recordings", Neuron, 2015, (in preparation).

**SUMMARY**

Peripheral neural interfaces could enable a natural and effortless control of dexterous hand prostheses. However, it is unclear how and to what extent efferent nerves recordings can be exploited for motor prediction. To address this very important issue, we developed a novel method to acquire alpha motoneurons activity in the human nerves during voluntary hand movements. In these recordings, we identified alpha motoraxons spiking features that correlate with grasping force and movement velocity. These properties were then used to design a decoding algorithm, which successfully estimates the dynamics of the hand from efferent neural signals.

Finally, we developed a model of proprioceptive reflex pathway which showed that sensory feedbacks have a secondary role in determining the firing of alpha motoneurons during voluntary hand control, supporting the

transferability of our results to amputees, which lack the afferent return to the brain.

**INTRODUCTION**

The development of a device capable to restore full motor functionalities of the human hand in amputees is still a challenge (Micera et al., 2010, Farina et al., 2014). Despite the existence of several dexterous and biomimetic prostheses (Ottobock, TouchBionics, RSLSteeper), their control is unnatural, unintuitive and limited to one or two degrees of freedom. This is mainly due to limitations in extracting the motor intention from the body and in particular from muscles (Farina et al., 2014, Merletti et al., 2010), which are presently used as source of signal for driving the prosthesis movement. Such limitations are due to the instability of the recording condition during motor tasks (mutual distance between muscular fibers and electrodes, Merletti et al., 2010).

A fascinating and promising solution to these issues is represented by peripheral nerve interfaces (Navarro et al., 2005, Shultz et al., 2012). Indeed, the neural pathways between the brain and the remnant peripheral nerves have been shown to be anatomically (Mercier et al., 2006, Reilly et al., 2006) and functionally (Dhillon et al., 2004) intact, even after many years from the amputation. Furthermore, Dhillon and Horch (Dhillon and Horch, 2005) showed that motor related activity can be recorded from the remnant nerves of people with transradial amputation through longitudinal electrodes, and used for controlling 1 degree of freedom of a prosthesis. More recently Micera's group (Rossini et al., 2010,

Micera et al., 2011) enabled an amputee to drive, in similar experimental conditions, three different grasps of a robotic hand. However, there is still no evidence that information related to the intended grasping force, or the kinematics of the hand can be extracted from peripheral nerve data. These features are essential for the intuitive and effortless control of the prosthetic device. Moreover, demonstrating such possibility would provide a clear justification for preferring nerve over muscle interfaces.

Therefore, the aim of the present work was to investigate and characterize the properties of human alpha motoraxons discharge during voluntary hand movements, providing, then, the basis for the design of innovative control strategies for electroneurogram (ENG)-driven prostheses. To achieve this goal, we developed a novel procedure to record alpha motoraxons electrical activity in human subjects during voluntary hand movements. This method relies on the combined use of microneurography (Gandevia and Hales., 1997) and peripheral nerve ultrasound (Curry and Timothy, 2011). We showed that the firing of efferent fibers presents features that correlate with hand grasping force and movement velocity. Then, a decoding algorithm was implemented to predict kinematic and dynamic parameters of the hand motion from alpha motoraxons recordings.

Finally, we wanted to evaluate whether these results could be transferred to the case of human amputees, which have damaged proprioceptive reflex pathways and, hence, different alpha motoneurons firing behavior (Gandevia et al., 1990). In order to conduct this investigation, we developed a computational model integrating alpha motoneurons with

central nervous system (CNS) commands and muscle activities, and force and movement dependent feedbacks brought by proprioceptive fibers.

## RESULTS

### *Recording alpha motoneurons activity in human subjects during hand movements*

In order to record human alpha motoneurons activity, we developed and applied a novel microneurography procedure on six healthy volunteers (four males, two females).

First, each of them was comfortably positioned on a chair with the right arm placed on a support over a table (Fig. 3.1A). Second, a neurologist identified the median nerve site using nerve ultrasound imaging (Fig. 3.1B, bottom) and guided the insertion of the microneurographic active electrode, through the skin above the elbow (Fig. 3.1B, top), into the nerve itself. Finally, another neurologist individuated the correct and final placement for the electrode using a qualitative procedure. In particular, we hypothesized the recorded signals were generated by motoraxons if they were (i) correlated with active hand movements executed by the participant (prerogative of efferent but also proprioceptive fibers), (ii) negligible when a mechanical stimulus was applied over the belly or the tendons of the hand muscles innervated by the median nerve (Table S1), event that causes proprioceptive fibers to discharge (Bergenheim et al., 1996).

The superficial electromyogram (sEMG, Fig. 3.S1) of the hand muscles innervated by the median nerve (Table 3.S1), the motion velocity and the

hand grasping force were simultaneously acquired. The subjects were asked to perform two tasks: unloaded fingers flexion/grasps (Table 3.S2) repeated at three different velocities driven by a GUI (*velocity task*, Fig. 3.1C and Fig. 3.S1) and three types of grasp (pinch, tridigital, cylindrical one) at increasing force over a pressure sensor (*force task*, Fig. 3.1D and Fig. 3.S1). Finally, the recorded multi-unit activity was processed off-line to extract single-unit spikes. The neural recordings of three out of six subjects were analyzed since they presented a signal to noise ratio higher than 2 in all the tasks.

We confirmed that the neural and muscular fibers discharges were highly correlated (Fig. 3.2A, B) in all the subjects. As expected from the anatomy of the neuromuscular system, it was always possible to identify a specific muscle (or a small group of neighbor muscles) which activity was optimally correlated with the ENG signal. This muscle was the finger flexor for Sub. 1, the group of thumb intrinsic muscles of for Sub. 2, and the flexor pollicis longus for Sub. 3. For the last subject, in particular, since the correlation of the ENG signal with two muscles was very similar, we selected the one reported, relying on the guidance provided by the neurologist.

Single units were extracted (6, 6, and 4 units for subjects 1, 2 and 3 respectively, Fig. 3.2.C) using a custom implementation of the method proposed by (Citi et al., 2008). Their average firing rate during voluntary hand movements was 12.7±1.5 Hz for Sub. 1, 13.7±2.8 Hz for Sub. 2 and 12.27±0.04 Hz for Sub. 3 (Fig. 3.2D).

These findings are coherent with the physiological discharge of alpha motoneurons (Enoka and Fuglevand, 2001). In addition to this, we observed no activity when participants were at rest (1.3±0.14 Hz, 0.94±0.45 Hz, 1.6±0.5 Hz, Fig. 3.2D). The absence of a significant baseline activity excludes the possibility that the signal may have come from autonomic fibers or beta and gamma motoneurons. Moreover, the recorded ENG signals anticipated the sEMG ones (Fig. 3.2E, F). Absence of baseline and anticipation of sEMG corroborate the hypothesis of alpha motoneurons acquisition and reject the eventuality of other type of fibers activity recording.

***Force modulation***

Remarkably, alpha motoneuron firing pattern during force task was very repeatable across subjects and trials, no matters the grasp type nor the force exerted by the subject. In particular (Fig. 3.3A, blue), the motoneurons firing presented a steep rise, correspondent to the moment in which the participants were squeezing the sensor to reach the required force, followed by a stable discharge level, when the subjects were maintaining the desired pressure. In both these phases, the neural activity showed a quasi-linear increment with the lower values of applied force (Fig. 3.3B-F). Instead, for higher levels of force, slowly increasing firing rates were observed until saturation (Fig. 3.3 B-F).

We modeled this behavior (Fig. 3.3C, E, red), as follows:

$$FR(f) = \frac{B}{C+e^{-f/D}} - A; \qquad (1)$$

where $f$ and $FR$ are respectively the normalized force and the normalized firing rate of the alpha motoneurons. A, B and C determine the saturation

value ($\frac{B}{C} - A$), while D represents the saturation speed. These parameters have no unity of measure. The best fitting was given by A=0.45, B=1.26, C=1.85, D=0.23, ($R^2$=0.78, p<0.01) in the case of the stable level of firing, and A=0.48, B=0.36, C=0.3, D=0.34, ($R^2$=0.78, p<0.01) for the peaks.

In conclusion, these results indicate that alpha motoneurons are adaptive cells and that they saturate over certain level of excitation (i.e., the force desired from the CNS). The saturation level is higher but is faster to obtain during force reaching than during holding (respectively, $\frac{B}{C} - A$ = 0.23 and 0.72, D=0.23 and 0.34).

***Alpha motoneurons maximum firing does not correlate with movement velocity***

While motoneurons maximum firing presented a strong correlation with force, unexpectedly we found that such behavior was not maintained when the velocity of voluntary hand flexions/grasps was changed (*velocity task*). In this case, instead, motoneurons firing rate presented a similar normalized range (i.e., the same peak, since minimum firing rate is null) independently of movement velocity (Fig. 3.4A, second raw). These results were consistently reproduced in all the 3 subjects (Fig. 3.4B). We noticed instead that the motion speed was linearly correlated with the normalized firing rate slopes ($R^2$=0.77, p<0.01, Fig. 3.4C) with specific values for each velocity (0.1 ± 0.05, 0.19 ± 0.13, 0.27 ± 0.16, p<0.01, Fig. 3.4D). It is important to notice that the results are obtained by the analysis of the portions of the recorded neural activity in which the subjects were executing a flexion. Finally, we observed that the discharging activity

during fingers extension was not negligible, suggesting a synergy of the flexor muscles in such task, with the antagonist ones.

***Decoding of force and velocity***

After verifying that kinematic and dynamic information about voluntary hand movements are readily available from motoneurons activity (see previous section), we then investigated whether the information could be used for prosthesis control to predict grasping forces and muscle contraction velocities from ENG data with a resolution of 100 ms.

In particular, we defined a feature set to decode forces and another to decode velocities (Table 3.S5). Hence, the exponential of the average motoneurons firing rate (AFR) was used to detect forces while the first time derivative of AFR was used to detect velocities (Fig. 3.5A, B, green and blue). The other features were computed in order to identify subjects' rest and activity in the AFR (Fig. 3.5A, B, all colors but green and blue).

Rest was decoded with high performance in both cases (mean accuracy 88%, Fig. 3.5C), as expected considered the absence of baseline in alpha motoneurons firing.

Four different forces were discriminated with reasonable accuracy (47.5%, confusion matrix, Fig. 3.5C, top, with respect to 36% empirical chance level), which became higher in the case of three classes separation (60% with respect to 47% empirical chance level, Fig. 3.5C, bottom). The velocity decoder, on the other side, registered a sufficient score in distinguishing three clusters (46.3%, confusion matrix, Fig. 3.5C, top, with respect to 48% empirical chance level) while obtained acceptable performance in the case of two folds (68% with respect to 66% empirical

chance level, Fig. 3.5C, bottom). It is important to notice that decoding performances exceeding empirical chance levels are statistically relevant (□=0.05, Combrisson and Jerbi, 2015). These results show the potential of ENG recordings to provide necessary information for the natural control of prostheses even with few recorded units as in this study.

***Interplay of supraspinal and peripheral control signals on efferent activity***

In order to investigate the impact of supraspinal and peripheral inputs onto the generation of the observed dynamic behavior of alpha motoneurons, we developed a simplified model of the neuromuscular system (Fig. 3.S2). In particular, we wanted to understand to which extent alpha motoneurons firing could change in absence of proprioceptive feedbacks during voluntary hand movements, to assess the transferability of our findings to people with damages to such sensory pathways. To reach this goal, we implemented two types of feedbacks, one dependent on fingers movement (specifically, the product of position and velocity) and muscles force, similar to those brought to alpha motoneurons by Ia, II, Ib afferent fibers (Maltenfort et al., 2003, Mileusnic and Loeb, 2006). We named them respectively movement (MF) and force (FF) feedback, and we set excitatory the former while inhibitory the latter (Jankowska, 2013b), both acting on alpha motoneurons activity. Alpha efferent fibers were modeled by adaptive regular spiking neurons as in (Izhikevich et al., 2003), whose firing was driven by a noisy CNS input, together with the afferent feedbacks afore described. We hypothesized such CNS contribution to be proportional to the desired muscle force as in

(Fuglevand et al., 1993, Contessa and De Luca, 2013). Finally, we hypothesized that the contribution of movement feedback was negligible during the force task, being the fingers quasi-steady.

The weights modulating the amplitude of the feedbacks on the motoneurons and characterizing the relationship between motoneurons firing rate and muscle force were tuned on our experimental efferent recordings (Fig. 3.S3). The model, remarkably, reproduced qualitatively the natural dynamics of alpha motoneurons observed during the *force* (an initial peak, followed by a stable level of firing, compare Fig. 3.3A and Fig. 3.6A, blue) and *velocity* (independency of the motoneurons maximum firing rate on the motion velocity, and presence of residual motoneurons activity during the extension phase of the motion, compare Fig. 3.4A,B and 7A,B, red) *tasks*. Moreover, the model was able to fit with high accuracy the relationship of the firing rate peak and the plateau firing with the force ($R^2$=0.96 and $R^2$=0.98 respectively, Fig. 3.6D,E, blue). Also, the linear correlation between the movement velocity and the firing rate slope were predicted with high accuracy ($R^2$=0.99, Fig. 3.7C, red).

Then, we removed from this validated model, the feedbacks. Remarkably, the model captured the natural dynamics of alpha motoneurons observed during the *force task* even without sensory contribution (green in Fig. 3.6). In particular, when looking at the underlying dynamics (Fig. 3.6D, E), the experimental results were accurately reproduced by the sole adaptive neurons ($R^2$=0.975, average from Fig. 3.6D, E). As expected, though, we discovered that the saturating effects resulted to be stronger (saturation value 0.49/0.65 respectively for with/without inhibition) and closer to

experimental findings (saturation value 0.22) in presence of inhibitory force feedback. These results indicate, on one side, that weak adaptation is sufficient to reproduce in a qualitative and quantitative way the observed dynamics, on the other side, suggest that, during hand movement control, inhibitory force related feedbacks lower, and hence smooth the activity of alpha motoneurons which may favor a more accurate exertion of grasping forces.

Analogously, the alpha motoneurons firing dynamic identified in the *velocity task* was reproduced when the movement feedback was null, simply by the adaptive properties of the cells (force feedback missing), and when the force feedback was inhibitory (compare Fig. 3.7A and S3 with Figure 4A, and Fig. 3.7A with S3). In particular, the independency of the maximal neurons discharge from the motion velocity (Fig. 3.7B) and its linear correlation with the firing slope (Fig. 3.7C) were replicated. Nonetheless the prediction accuracy of the model was higher when the excitatory movement feedback was implemented. Indeed, in the efferent activity recorded within each velocity task we noticed a surprisingly smooth decrease of firing rate associated to the change in direction of the movement from extension to flexion: in Fig. 3.4A, firing rate does not come back to baseline right after the peak. Interestingly, this was emulated more precisely by an excitatory movement feedback as effect of the feedback delay (Fig. 3.7D). These findings corroborates the hypothesis that the role of movement feedback during hand motor control might be limited to helping the CNS in the fine orchestration of couples of antagonists (such as flexor and extensors).

Finally, in order to verify the hypothesis of an inhibitory force and of an excitatory movement feedback, we tested the predicting capabilities of the model when such feedbacks had opposite sign. We calibrated, as previously illustrated, the weights regulating the influence of the feedbacks on motoneurons discharge by means of the experimental recordings (Fig. 3.S4). The excitatory force feedback produced extreme fluctuations in alpha motoneurons firing as visible in the outshoot in Fig. 3.6C, making these results far from our observations ($R^2$=0.73, average from Fig. 3.6D, E). We also found that the hypothesis of an inhibitory movement feedback has to be discarded. This, indeed, would have drastically suppressed alpha motoneurons firings (Fig. 3.7A, first row) not allowing the development of the muscular force necessary to execute movements with highest speed.

Moreover, in order to test the assumption that the CNS provides motoneurons with an input related to the desired muscle force, we run a falsification test consisting in replacing the force proportional drive with an input proportional to velocity, as in the second experimental task. We found that the modeled firings completely mismatched the experimental observations (Fig. 3.7E, F), confirming our hypothesis. In conclusion, the presented results showed that, during voluntary hand movements, the firing of alpha motoneurons is mostly conditioned by intrinsic properties of such cells than by the feedback brought by proprioceptive fibers.

**DISCUSSION**

In the present study, we reported the first successful recording, characterization and modeling of alpha motoneurons axons firings from the median nerve of healthy humans during volitional hand motor tasks, in physiological conditions, by exploiting a novel hybrid ecography/microneurography technique. Up to now, indeed, few groups (Freyschuss and Knutsson, 1971, Gandevia et al., 1990) have convincingly acquired the electrical activity of human alpha motoneuron peripheral axons. However, in these cases the afferent fibers were anesthetized, and this is likely to change motoneurons discharge during voluntary motion (Gandevia et al., 1990). Ribot et al. (Ribot et al., 1986) instead used microneurographic techniques to acquire efferent activity from the peroneal nerve (located in the lower limb) of 16 healthy subjects. They placed the electrode in a portion of the nerve in which electrical stimulation caused muscular twitch and no firing activity could be recorded in response to mechanical stimuli that activates tactile or proprioceptive receptors. However, they did not validate these assumption with a quantitative analysis of the recorded signal.

Our procedure was reliable for different experimental conditions and did not require surgery or anesthesia. The precise placement of the active electrode in the nerve, obtained with the aid of ultrasound imaging, avoided extensive stimulation of the subjects, which is instead required in a common session of microneurography (Gandevia and Hales, 1997). Moreover, we validated with off-line analysis of the ENG recordings the hypothesis of efferent acquisition. Also, even if the pioneering studies of Sir Sunderland on the anatomy of the human peripheral nerves

(Sunderland, 1945, Sunderland, 1978) suggested an accentuated mixture of afferent and efferent fibers within the single fascicles, more recent studies (Jabaley, 1980, Hallin, 1990) are sponsoring the opposite idea that fibers of equal nature are confined in the same portion of the fascicle. This strongly supports the feasibility of pure multi-unit (motor) recording in the human median nerves.

The technique, however, presents some limitations that have to be taken into account in order to reproduce it. In particular, the quality of the signal recorded relied strongly on the skills of the neurologist. The microneurographic session was limited in duration, due to the subject's compliance, and electrode's placement stability. This constrained the maximal number of trials repetitions to be relatively low. Finally, with different insertions it was impossible to place the needle tip within comparable fibers populations.

Only one channel could be acquired per time, hence, promising results obtained with the current procedure could be enhanced, if it would be possible to perform simultaneous recordings from different fascicles, i.e., with a multi-channel electrode. That is also an indication for the design of the devices for recording to be used in the future. Because of these limitations, the overall procedure results poorly efficient in terms of successful human recordings compared with the number of acquisition performed. Indeed, six subjects participated to the protocol, but a good quality signal was acquired, throughout all the required motor tasks, only from half of them.

Notwithstanding these limitations, this recording method allowed us to characterize quantitatively the relationship between motoneurons firing rate and hand motion parameters such as force exerted and velocity of execution. In particular, in tasks in which the subject was asked to exert and hold a specific level of force over an object, we showed that the motoneurons firing rate presents a first steep rise followed by a plateau. Both these phases were correlated with the exerted level of force, until the occurrence of saturation. This happened not only during force holding, in agreement with previous results (Monster and Chan, 1977), but also during force application. More specifically, we observed that the maximum tension produced by motor units is not only determined by the contractile properties of muscle fibers but is also bounded by the behavior of motoneurons whose firing rate does not exceed a certain saturation level limiting in this way the muscle contraction into sustainable limits.

Interestingly, we also found that the discharge of motoneurons does not vary in terms of maximal activation during movements executed at different velocities. Instead, the firing rate grows steadily in time with a slope linearly proportional to the velocity of motion. This result was unexpected because we were driven by the hypothesis that the CNS controls directly different tasks, acting on the main variable involved (which, in our case, were the force and the velocity), (Stein, 1974).

Moreover, we showed that our findings of motoneurons behavior could potentially lead to a real-time control of motion speed and grasping force. Our results are direct evidence that more information, exploitable for the direct control of neuroprosthetic devices, is available in peripheral nerves

recordings with respect to what previously shown on ENG signals decoding (Micera et al. 2010, Rossini et al 2010, Micera et al., 2011, Dhillon et al., 2005, Jia et al., 2007). In fact, starting from only a targeted single-channel recording, we achieved a neural-based decoding of movement parameters such as force and velocity, which was not previously shown. Translating this result to the control of artificial limbs represents an important breakthrough for the neuroprosthetics field. In the next future multi-channel recordings should be also used to disentangle whether a bigger amount of information could be extracted in order to exploit the potential of this approach.

Finally, starting from these experimental data, we developed and calibrated a novel computational model for brief muscle contractions, which enabled us to understand the underlying mechanisms involved during the studied tasks. In particular, we remarkably showed that the features observed in alpha motoneurons discharge are explained by modeling them as adaptive regularly spiking cells (Izhikevich, 2003) under the assumption that supraspinal inputs are proportional to the target force, even in the absence of feedback. Crucially, this was true also for the second task in which the movement was performed at fixed velocity. Remarkably, this has been recently confirmed also experimentally by (Funglevand et al., 2015) during ramp force exertion tasks with EMG recordings. Such result supports the hypothesis that the outcomes of our analysis are valid and transferrable also to the case of people with damages to peripheral afferent pathways, as it is for amputees. Such achievement additionally reinforces the idea of using nerve interfaces for

prostheses control. Furthermore, it promotes the possibility to test new developed control strategies on healthy subjects, before conducting a surgery on an amputee for implanting neural electrodes. In this scenario, the availability of a stable multichannel microneurography electrode becomes of paramount importance in order to obtain experimental conditions almost matching the ones achievable with chronically implanted intraneural electrodes.

Importantly, our model, combined with the observed experimental data, can provide a better comprehension of the mechanisms underlying voluntary hand motor control. In particular, when simulating motoneurons activity during static force varying tasks we discovered that its saturation (Fig. 3.3C) is enhanced by an inhibitory force feedback (Fig. 3.6D). A single motoneuron receives from proprioceptive fibers the information that other efferent fibers have been recruited and stabilizes its spiking activity toward a plateau. Its maximal contribution, indeed, is not anymore required. This enforces the idea that the proprioceptive force-related feedback, acting on the neuronal pool in charge of controlling hand muscles, enables a very precise (and therefore fatigueless) exertion of grasping force. Interestingly we observed that in case of excitatory force feedback the neuromuscular system becomes highly unstable (Fig. 3.6 C,D,E) and does not allow any kind of fine force control.

By simulating motoneurons activity during dynamic fixed-velocity tasks we found that the excitatory movement-related feedback justifies the discharging activity of motoneurons during the early extension phase of the velocity task (Fig. 3.7A, D) which presence was not expected (since

flexor muscles are not involved in it). This supports the concept that movement related feedback serves to regulate the interaction between antagonist muscles in order to obtain fine fingers movements. Therefore, we have confirmed (Jankowska, 2013b) that, even if multiple factors (from periphery) condition the activity of motoneurons, the overall effect on them is inhibitory in the case of force related feedback and excitatory in the case of movement related feedback from muscles. It is interesting to notice that, while, in the lower limb, feedback is pivotal for alternating flexors and extensor activity to continue locomotion (even without a drive from higher levels of the CNS, i.e. automatic motion, Edgerton et al., 2008), in the upper limb, feedback seems to have a smaller impact in determining the motoneurons firing activity. Still, the feedback-driven modulations might play a determinant role in smoothing muscles contraction to exert movements in a more precise way, or when unexpected adaptations have to be performed. It is interesting to notice the analogy with other sensory modalities as touch. The brain, indeed, plans accurately the movement to exert and relies on information of contact with objects to assess its prediction and eventually modify its actuation (Flanagan et al., 2006).

Regarding high level signals to alpha motoneurons, we verified the plausibility of the hypothesis that the tension exerted by the muscles is proportional to the CNS drive. Indeed, only a supraspinal output proportional to the target force (and not to the velocity) can drive the fingers at different velocities during the execution of the same movement (compare Fig. 3.7A and Fig. 3.7E). This finding proposes a solution to the scientific debate about the strategy of motion control that the CNS exploits

(Stein, 1974). Indeed, this validation is coherent with the hypothesis that the CNS drives muscular activation always through a force-dependent mechanism rather than implementing different control strategies according to the specific motor task.

Other than the biologically sound model we implemented for the single motoneurons (Izhikevich, 2003), very peculiar in our work is the feedback representation. First, we considered an unsupervised feedback. In previous papers (Lowery and Erim, 2005, Dideriksen et al., 2011, Contessa and De Luca 2013) the feedback was generated as a function of the difference between the prescribed target force and the actual force generated, but it was unclear how this difference was computed. In our model this was generated automatically by the interaction between motoneurons and peripheral afferents originating the different feedbacks so the model did not require extra assumptions. Second, we implemented at the same time force feedback and, for the first time to the best of our knowledge, movement feedback.

Our model still presents some limitations that should be overcome in future developments. In particular, we did not directly implement recruitment dynamics, and we had then to introduce a phenomenological relationship between firing rate and force (Equation 2). This is due to the fact that we wanted to simulate a number of neurons comparable to that of the recorded axons in order to closely match neurophysiologic results. Moreover, our model did not take into account time-dependent dynamics modulation due to fatigue since our experimental data involved short-lasting forces. For the sake of simplicity we did not include the

contribution of gamma motoneurons. Moreover, the proprioceptive feedback from antagonist or contralateral muscles (Jankowska, 2013b) as well as the presynaptic inhibition on afferent fibers (Fink et al., 2014) are not explicit, even if taken into account by calibrating the free parameters of the model by the experimental recordings. Finally, we did not take into account the change of tension due to muscle length and velocity of contraction (Gordon et al., 1966, Wilkie, 1949).

In conclusion, this work made a concrete step toward the understanding of how the nervous system controls force and velocity of hand movements, and consequently toward the development of future bidirectional prosthetic devices (Raspopovic et al., 2014, Tan et. al 2014), based on a physiologically plausible neural control.

## EXPERIMENTAL PROCEDURES

### *Microneurography and nerve ultrasound*

The procedure applied to record from human median nerve was approved by the ethical committee of the Campus Bio-Medico University and all the subjects signed the informed consent.

The combination of ultrasound imaging and microneurographic fibers qualitative exploration is described in continuation. Two FHC UNP40GAS electrodes (diameter 250μm, length 40 mm, Fig. 3.1B, top), shaped as needles, were used. One of them was placed in the median nerve at the elbow level (active electrode), while the other (reference) was placed through the skin, 3 cm away from the active one. A neurologist inserted the active needle through the skin with the help of an Esaote MyLab

70XVG, equipped with a 14-18 MHz probe. He first positioned the probe over the skin (2 cm above the elbow) and then inserted the active needle orthogonally with respect to the ultrasound probe. This provided a visual feedback (Fig. 3.1B) to the neurologist, who confirmed when the electrode was placed inside the nerve. Then, another neurologist had to locate the tip of the active electrode in proximity of efferent fibers. To reach this goal she used a procedure designed by our team that is modified from the common standards used in microneurography (Gandevia and Hales, 1997). The subject was asked to actively open and close the hand. The neurologist, in the meanwhile, moved the electrode until a signal correlated with subject's movement was recorded. Then, she verified that the ENG did not correlate with any of the following conditions: i) tactile stimuli of the hand skin; ii) palpation of the arm and hand muscles belly and tendons; iii) passive moving of the fingers. These conditions were devised in order to exclude the acquisition from proprioceptive, tactile, and autonomic fibers. Indeed, the latter do not fire synchronously with skeletal muscles contraction, tactile fibers are excluded by condition i), while the proprioceptive cells by ii) and iii), since they should fire in correspondence of the muscular and joint movements and/or their solicitation (Bergenheim et al., 1999). The overall procedure may last up to 1 hour.

***Data recording***

The sEMG signals were recorded in a differential configuration with two Wet Ag/AgCl electrodes (SpesMedica) placed over the belly of the muscles

and referred to a ground represented by a metal strip placed over the biceps (Fig. 3.1B, top). The signals were amplified by a factor $10^4$ and filtered in the band 100-1000 Hz by a GRASS qp511. The differential microneurographic signal was referred to the mentioned ground, amplified by a factor $10^5$ and filtered in the band 300-3000 Hz (Gandevia et al., 1997) by a GRASS p511. All these signals were recorded at a sampling rate of 10000 Hz with a 16-bits data acquisition (DAQ) board (National Instruments PCI-6251), installed on a personal computer (PC) running a custom program written in Labview that handled the recording. In order to help the microneurographer to execute the research for the efferent fibers firing activity, the envelope of the microneurographic signal was showed in the real-time and a thresholded version of it was sent to a speaker.

***Motion tasks***

Each subject was asked to execute three types of task: i) grasping, ii) velocity and iii) force tasks. More in particular they consisted in:

i) Different grasps/movements among those reported in Table 3.S2 without holding objects. This task was required to identify a subset of motions with which the recorded ENG was correlated.

ii) Different grasps/movements, chosen from the subset selected in i), without holding objects executed at three different velocities, driven by a cursor (Fig. 3.1C) that runs at 17, 26 and 47 degree/s. Every movement was repeated 3 times for each velocity. Between two repetitions, subjects

had a rest of 2 s. An example of task repetition can be seen in Fig. 3.1C and Fig. 3.S1.

iii) Pinch, tridigital, and cylindrical grasps exerted at different forces over a deformable sphere (diameter of 6.3 cm) connected through a catheter to a pressure sensor (Taffoni et al., 2013). A GUI indicated to the subjects the type of grasp, the level of force requested and that they were exerting (Fig. 3.1D). Four different force levels (corresponding to 1, 2, 4, and 6 kPa) were demanded, three times each. Between two repetitions, subjects rested for 2s. An example of task execution can be seen in Fig. 3.1D.

The number of repetitions of different movements was constrained by the multitude of tests to be performed during one experimental session, which is time-limited by microneurography setup preparation time, recording stability (Vallbo et al., 2004) and subject compliance (they had to stay very steady, holding a fixed position, conditions easily inducing fatigue).

***Off-line data processing***

In order to extract single cell activities, the microneurographic signals were spike-sorted (Lewicki, 1998, Quiroga et al., 2004) with the following steps. The signal was first wavelet denoised and sorted with a custom version of (Citi et al., 2008). Neurons firing rate (FR) was computed by counting the number of spikes occurring in a not overlapping sliding window of 100 ms (Cunningham et al., 2009). This was then smoothed with a 2 Hz non-causal low-pass filter.

The envelope of the sEMG signal was used for the following analysis. It was computed by removing the mean of the signal and by non-causal low-

pass filtering with a cut-off frequency of 2 Hz. Firing rate and sEMG signal were processed with a causal filter in order to avoid the creation of any temporal shift between them.

***Firing rate behavior analysis***

*Subjects' inclusion*

For this analysis only subjects with a signal to noise ratio higher than 2 have been considered (3 out of 6). This has been computed as quotient between the maxima detected in portions of the signal where the subjects were performing a muscular activation and where they were resting.

*EMG selection*

The muscle with the sEMG most correlated (Spearman index) with the ENG in both the velocity and force tasks was selected for the subsequent analysis. The selection details are described in Table 3.S4.

*ENG versus sEMG: temporal causality analysis*

The recordings from the *force task* were used for this analysis since the noise was much lower than in the *velocity task* (~6 vs ~2). FRs and sEMGs were normalized with respect to their maximum in the task (Table 3.S3). Then, for each motion repetition, the delay between the 50% of the maxima of sEMG and ENG activities were calculated and analyzed (Fig. 3.2A). The trials in which the distortion caused by noise produced a mutual temporal shift between sEMG and ENG higher than 100 ms were discarded (considered as not physiological, Macefield et al., 1996)

*Force, velocity analysis*

For the force task, FRs were normalized with respect to their maximum in a grasp (Table 3.S3). Different analyses were devised for the transient (dynamic analysis) and the plateau (stationary analysis) phases of the pressure sensor signal (Fig. 3.3A). Maxima and average were inspected in the two cases respectively. For the velocity task, instead, FRs were normalized with respect to their maximum in a movement or grasp (Table 3.S3), then the maximum and the slope were computed for every motion repetition (Fig. 3.4A). The slope was defined between the FR maximum and the beginning of the movements that was triggered by the GUI.

***Decoding***

As anticipated in the Results, the decoding algorithms relied on features that consisted of a time series (100 ms resolution) representing a linearized relationship between the motoneurons firing rate and the movement parameters (force, velocity), and of a set of other time series that were used to separate signal portions where the subjects were resting and where producing a movement.

The choice of the exponential of the AFR in the case of force decoding, which could be unintuitive for the reader, was driven by the fact that this function grows faster than the inverse of the saturation relation between firing rate and force (Equation 1), for data values higher than 1 and is comparable for values between 0 and 1.

More in detail, the decoders first picked a state between rest and activity. In the former case, the output prediction was rest, in the latter was a value characterizing the motion parameters (1 to 4 in the case of force, 1 to 3 for

velocity). This value was assigned according to the least Euclidean distance between Feat1 (the so indicated main feature in Results, Table 3.S5) and the centroids of the mentioned classes. Such centroids were defined on a training set folded by a leave-one-out strategy.

The AFR and the features as well as the classifiers output were computed every 100 ms, so it represents the delay of the decoder.

Finally, the classification accuracy was computed as follows:

$$\frac{\sum_{classes} \frac{number\ of\ correctly\ predicted\ events}{number\ of\ events}}{\sum_{classes} number\ of\ events}$$

A class prediction was considered to be correct when, within the time interval imposed to the subject by the GUI request, the mode of the not-resting estimations matched the desired output. On the other hand, a rest estimation was considered correct only if the decoder did not provide any activity prediction.

The empirical chance level has been computed according to the definition of (Combrisson and Jerbi, 2015) by implementing in Matlab the equation:

$St(\propto)$=$binoinv(1-\propto, n, c)*100/n$;

$\propto$ (set at 0.05) represents the significance level, $n$ the size of the dataset and $c$ the number of classes to discriminate. $St(\propto)$ is the statistically significant threshold. Decoding performance beyond such value are considered significant.

***Model of the reflex pathway***

*Single motoneuron dynamics*

We modelled the firing behaviour of 5 motoneurons using the approach proposed by Izhikevich (Izhikevich et al., 2003), which is described by the following subthreshold equations:

$$\dot{v} = 0.04v^2 + 5v + 140 - u + r_m I$$

$$\dot{u} = a(bv - u)$$

with auxiliary after-spike-resetting condition being:

*if* $v \geq 30$ *mV, then* $\{v = c \text{ and } u = u+d\}$.

*v* and *u* are the membrane potential and the auxiliary adaptation variable of a single neuron and *I* is the input current that was normalized in a way that $r_m = 1$. Parameters were tuned as in (Izhikevich et al., 2003) to induce a Regular Spiking Dynamics (a=0.02, b=0.2, c=-65, d=8).

The input to each neuron was randomly generated from a Poisson distribution with the same time varying mean for all the cells, and it was constituted by the sum of two components, the stimulus and the feedback current ($I_{stim}$ and $I_{feedback}$, respectively).

*Central drive*

The stimulus current was assumed to be linearly proportional to the target force (Fuglevand et al., 1993) and convoluted with a 20 ms Gaussian window to avoid excessively sharp transitions.

In the case of the force task, $I_{stim}$ was given by a square wave with a 4 seconds period with amplitude proportional to the desired force.

In the case of the *velocity task*, we built the input as follows. In a basic approximation, when the muscle stretches of a length *x* the force it exerts respects Hooke's law ($F = -kx$), hence, in order to achieve a constant velocity the same force must be applied in the opposite direction. Since we kept the

assumption that input and generated force correlate linearly as in the previous task, for each constant value of velocity $\bar{v}$ we have:

$$I_{stim}(t) = \alpha F(t) = \alpha k x(t) = \beta \bar{v} t, \ onset < t < \bar{x}/\bar{v};$$

where $\bar{x}$ is the length of the path which is the same for all speeds. As a consequence the peak input is the same for all speeds:

$$\max(I_{stim}) = \max(\beta \bar{v} t) = \frac{\beta \bar{v} \bar{x}}{\bar{v}} = \beta \bar{x}$$

In a separate set of simulations we also tested the hypothesis of an input whose intensity was proportional to the speed, injecting in the network the alternative stimulus:

$$I_{stim}(t) = \beta' \bar{v}, \qquad onset < t < \bar{x}/\bar{v}$$

The two stimuli for this task and the associated responses are shown in Fig. 3.7A and Fig. 3.7E.

*Generation of muscle force*

Following (Contessa and De Luca, 2013), in our model each spike elicited a reaction $F$ in the muscle with a bi-exponential time course:

$$F_{spike}(t) = A_{spike} \sum_{t*<t} \left( e^{t*-t/\tau_2} - e^{t*-t/\tau_1} \right)$$

where t* are the spike times occurred before t, and $\tau_1$ *and* $\tau_2$ chosen so to have a rise time of 60 ms and an half-relaxation time of 80 ms (Contessa and De Luca, 2013). The amplitude $A_{spike}$ is not fixed but is larger for spikes fired by stronger motor units. If we take into account that motor units are known to be recruited in order of strength (Henneman et al., 1965, Llewellyn et al., 2010) it results that if they are *n* at time t and then become *n+m* at time t+1, each of the new *m* active units elicits a force stronger than the "old" *n* active ones. In other words, force grows super-linearly with the number of spikes fired, i.e., with the overall firing rate.

Starting from these considerations, we developed an *ad hoc* phenomenological model to describe the superlinear relationship between the amplitude of the global force exerted by the muscles and the overall motoneurons firing rate.

$$F_{tot}(t) = A_{tot}\left(\sum_{t*<t}\sum_{i=1}^{5} FR_i(t^*)\left(e^{(t^*-t)/\tau_2} - e^{(t^*-t)/\tau_1}\right)\right)^k \qquad (2)$$

We achieved the results shown in Fig. 3.6 with $A_{tot} = 0.4$ and $k = 5$ but they were qualitatively similar at least for $0.2 < A_{tot} < 0.5$ and $3 < k < 5$.

*Feedback*

The sensory feedback was sent simultaneously to all the motoneurons in the network (Lusher et al., 1979, Mendell and Henneman, 1968). We implemented a simple model of force feedback that may correspond to the average current input to motoneurons resulting from the firing produced by homologues Ib and heterologous Ia and II fibers. Then we implemented a similar model of the movement feedback mimicking the average current input to motoneurons due to the activity of homologues Ia and II fibers.The relationship between force and feedback was defined as (Mileusnic and Loeb, 2006):

$$I_{feedback\_force}(t+\Delta) = F_{coeff}\sum_{t'=t-W}^{t'=t}\left(\left(1+\alpha\left(t'-\frac{W}{2}\right)\right) * F_{tot}(t')\right)$$

The width of force integration $W$ was set at 0.5 seconds as in (Contessa and De Luca, 2013). The optimal value of the delay $\Delta$ between force and feedback was found to be 0.15 seconds, but results were similar for delays as low as 0 seconds. The optimal value of the slope of integration $\alpha$ was found to be 1, but results were similar from $\alpha$=4 down to $\alpha$=0 (flat integration). The feedback was excitatory, inhibitory, or null depending on

$F_{coeff}$ (respectively, >, < or = 0). The results obtained in Fig. 3.6 were for $F_{coeff}$ = -0.4 and $F_{coeff}$ = 0.2, in case of inhibitory and excitatory feedback, respectively. However, results were qualitatively similar for $F_{coeff}$ > -0.8 for inhibitory feedback while for excitatory feedback a value of $F_{coeff}$ = 0.4, was already sufficient to induce epileptic activity (Fig. 3.S4).

When speed was different from zero, we added a second term representing the feedback depending on velocity and position (Maltenfort and Burke, 2003):

$$I_{feedback}(t+\Delta) = \sum_{t'=t-W}^{t'=t} \left( \left(1 + \alpha \left(t' - \frac{W}{2}\right)\right) \left(XV_{coeff} v(t') * x(t') - F_{tot}(t')\right)\right) \quad (4)$$

where $v(t)$ and $x(t)$ are velocity and position respectively, corresponding to experimental measurements. For the sake of simplicity, both delay and window of integration were the same we implemented in the force feedback relation. Positive, negative and null $XV_{coeff}$ lead to excitatory, inhibitory, or absent feedback respectively.

The results obtained in Fig. 3.7 are obtained with values $XV_{coeff}$ = -0.8 and +0.8, respectively in case of inhibitory and excitatory feedback. However, results were qualitatively similar for a broad range of $XV_{coeff}$ values in case of excitatory feedbacks (up to $XV_{coeff}$ = 8), while for $XV_{coeff}$ > 1.6 inhibitory feedback prevented firing activity (Fig. 3.S4).

It is important to notice that calibrating α, $F_{coeff}$, and $XV_{coeff}$ by the experimental recording takes into account other factors affecting the motoneurons firing such as proprioception discharge coming from

contralateral and/or antagonist muscles (Jankowskab, 2013b), or presynaptic inhibition on afferent fibers (Fink et al., 2014).

*Implementation*

Simulations were implemented with in-house developed codes in Matlab R 2013 (Natick USA). Each stimulation pattern was presented 10 times and results were averaged over presentations.

### *Data analysis and statistics*

Data were exported and analyzed in Matlab R2013 (Natick USA). All data were reported as mean values ± S.D. or S.E.M. when indicated. The normality of the data distributions was verified by means of a Lilliefors test. Two tails ANOVA or Kruskall-Wallis tests were executed on the distributions according to the results of the Lilliefors test. Tukey-Kramer correction was applied in the case of multiple class comparisons.

**ACKNOWLEDGMENTS**

This work was partly supported by the EU Grant CP-FP-INFSO 224012 TIME project (Transverse Intrafascicular Multichannel Electrode system), by the EU Grant FET 611687 NEBIAS Project (NEurocontrolled BIdirectional Artificial upper limb and hand prosthesiS), by the EU Grant FP7-NMP 228844 NANOBIOTOUCH project (Nanoresolved multi-scan investigations of human tactile sensations and tissue engineered nanobiosensors), by the project NEMESIS (Neurocontrolled mechatronic hand prosthesis) funded by the Italian Ministry of Health, by the national project PRIN/Hand-Bot ('Biomechatronic hand prostheses endowed with

bio-inspired tactile perception, bi-directional neural interfaces and distributed sensori-motor control', CUP: B81J12002680008), by INAIL/PPR2 ('Control of hand prosthesis by invasive neural interfaces'), funded by the National Institute for Insurance against Industrial Injuries (CUP: E58C13000990001), and by the Swiss National Competence Center in Research in Robotics.

**CONTRIBUTIONS**

**F.P** designed the study, set-up and conducted the experiments, realized the decoding algorithms, collaborated at the development of the model of the neuromuscular system, analyzed the data, discussed the results, and wrote the paper; **A.M** developed the neuromuscular system model, discussed the results and wrote the paper; **J.R.** collaborated at the development of the decoding algorithms and at the data analysis, discussed the results and wrote the paper; **F.G.** collaborated at the design of the experiment, obtained the ethical approval, and performed microneurography; **G.G** performed the peripheral nerve ultrasound and wrote the paper**; E.G.** collaborated during the preparation of the experiments; **L.Z.** collaborated during the preparation of the experiments, discussed the results and wrote the paper; **M.C.** collaborated at the data analysis, discussed the results and wrote the paper; **S.R** designed the study, supervised the experiments, collaborated at the data analysis, discussed the results and wrote the paper; **S.M.** designed the study, supervised the experiments, discussed the results and wrote the paper.

## FIGURES

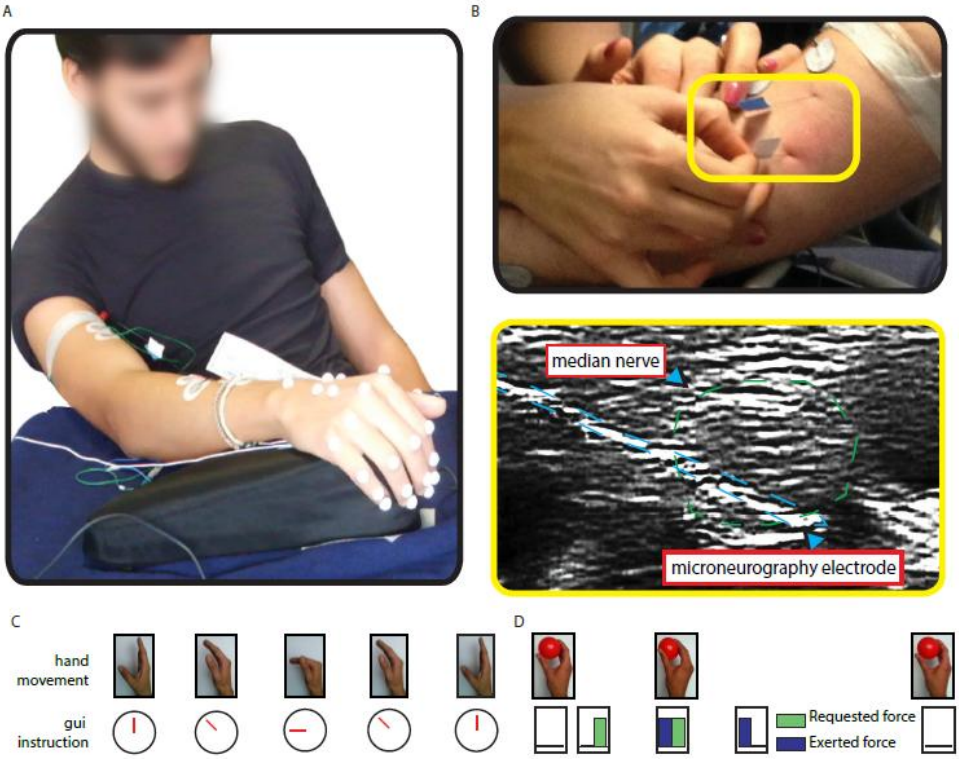


**Fig. 3.1. Efferent microneurography experimental setup.** (**A**) The subject sits relaxed on a chair with the arm on a support, placed on a table. (**B**) The microneurography electrodes inserted by the neurologist (top) and their ecographic image (bottom). (**C-D**) Once the microneurography electrodes are correctly placed, a GUI, showed on a screen, guides the subject to execute velocity (C) and force (D) protocols (see Experimental Procedures).

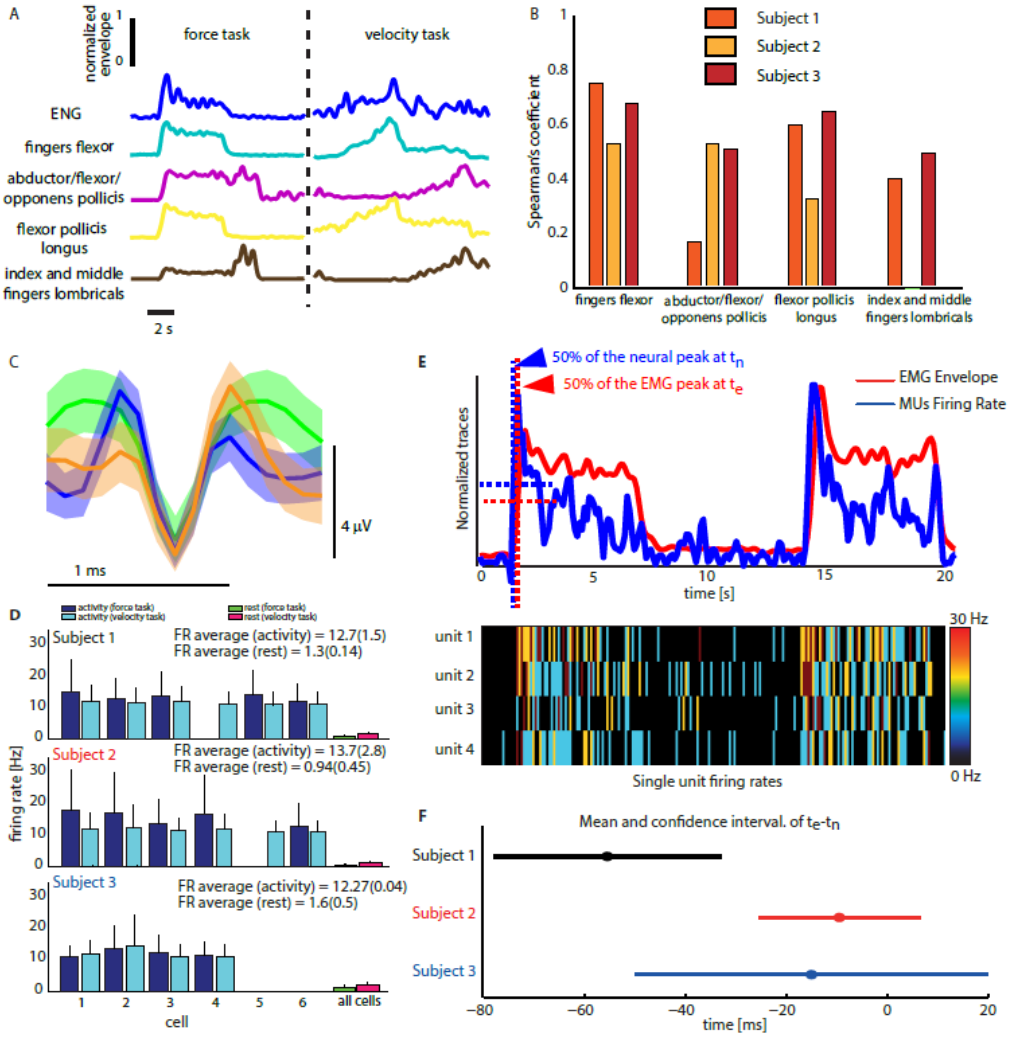


**Fig. 3.2. ENG and sEMG relationship.** (**A**) Normalized envelope of the neural and muscular activities during a cylindrical grasp (force task) and a middle finger interphalangeal joint flexion (velocity task). Data are extracted from Subject 1. (**B**) Correlation between microneurographic and muscular recordings, over all the participants. (**C**) Examples of spike waveforms sorted from subject 1. (**D**) Firing rate of the recorded axons during movements (blue for force tasks and light blue for velocity tasks) and during rest (green for force tasks and fuchsia for velocity tasks) for the three subjects. (**E**) Neurons firing rate (saturated at 30 Hz, bottom), and their average (top, blue line). Along with them, the sEMG envelope of the most correlated muscle (flexor digitorum, red) is showed. Signals portions are extracted from Subject 1. The 50% of the maximum of the neural signal occurs (at $t_n$) before the one of the sEMG (at $t_e$). (**F**) ($t_e$-$t_n$)

distributions represented by mean and confidence interval (n=15, 25, 9 respectively for subject 1, 2 and 3).

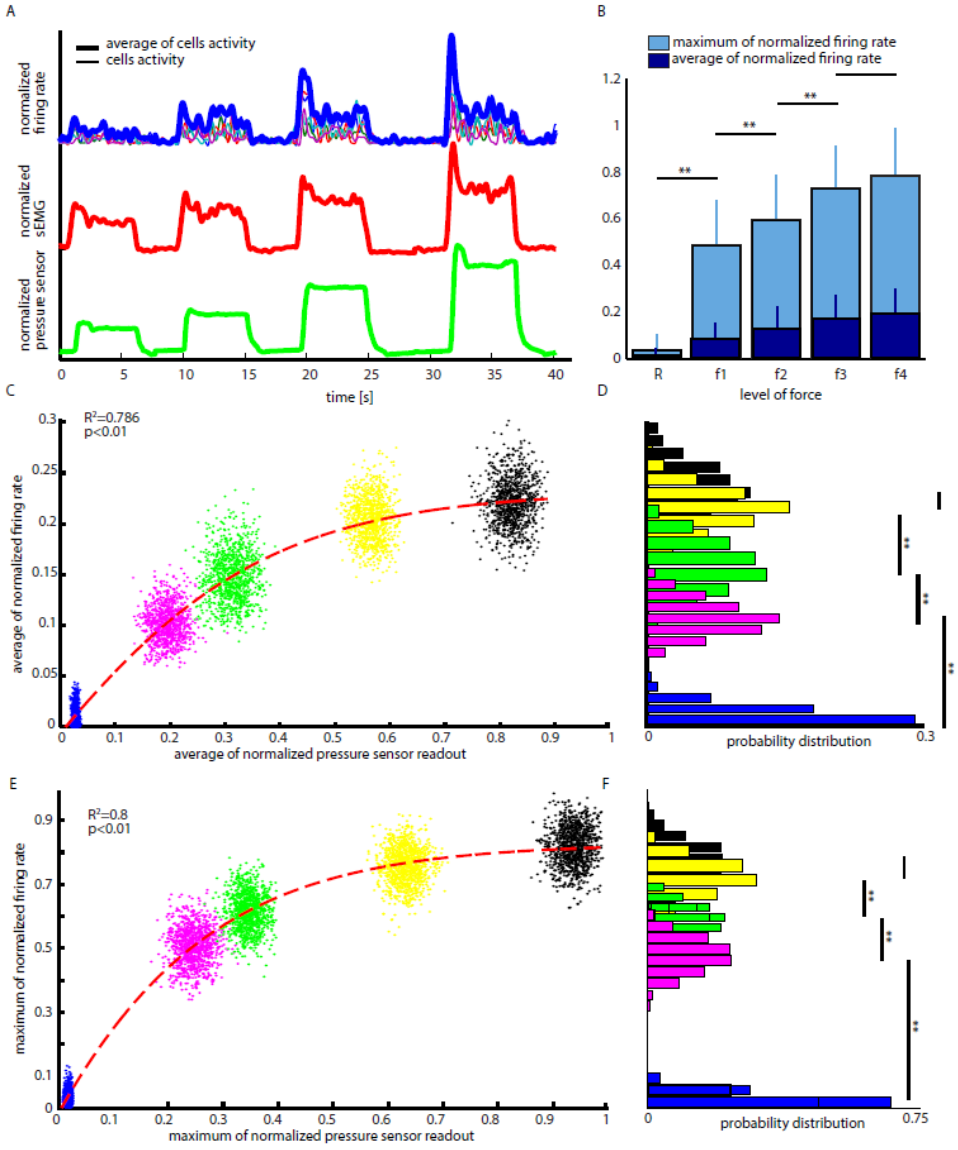


**Fig. 3.3. Neural activity correlates with grasping force.** (**A**) FRs normalized to 110 Hz and their average (blue line), flexor digitorum sEMG (red), and pressure sensor readout normalized to 7.7 kPa (green). Signals portion is extracted from Subject 1 while exerting a cylindrical grasp. Data are representative of n=110 repetitions (40, 46 and 24 including rest, respectively for subject 1, 2 and 3). (**B**) Barplot representing the FRs normalized to their maximum in the grasps, with respect to the variation of the exerted force, in the case

of static and dynamic analysis (light blue and blue, respectively). Data are represented as averages ± SD. (**C**) Relation between the force exerted during the grasps and the alpha motoneurons firing rate. The former is computed as the average over the interval in which the sensor readout is stationary. The latter is calculated analogously. Pressure sensor readout is normalized as aforementioned, alpha motoneurons firings are normalized to their maximum (Table 3.S3). Colors represent different requested levels of force. A saturation function fitting ($R^2$=0.786, p<0.01) is proposed (dashed red line). Data are bootstrapped (5000 samples, each of which obtained by averaging 10 samples randomly chosen from the original distribution composed of 526 points). (**D**). Probability distribution of the subsets in (**C**). Their correspondence is color-coded. (**E**) Relation between the peaks of alpha motoneurons firings and sensor readout. The proposed saturation function is equal to the one showed in (**C**). Data are bootstrapped as in (**C**). P-values are determined by ANOVA with Tukey-Kramer test for multigroup comparison. ** p<0.01. The tests reported in (**D, E**) are executed on the not bootstrapped dataset.

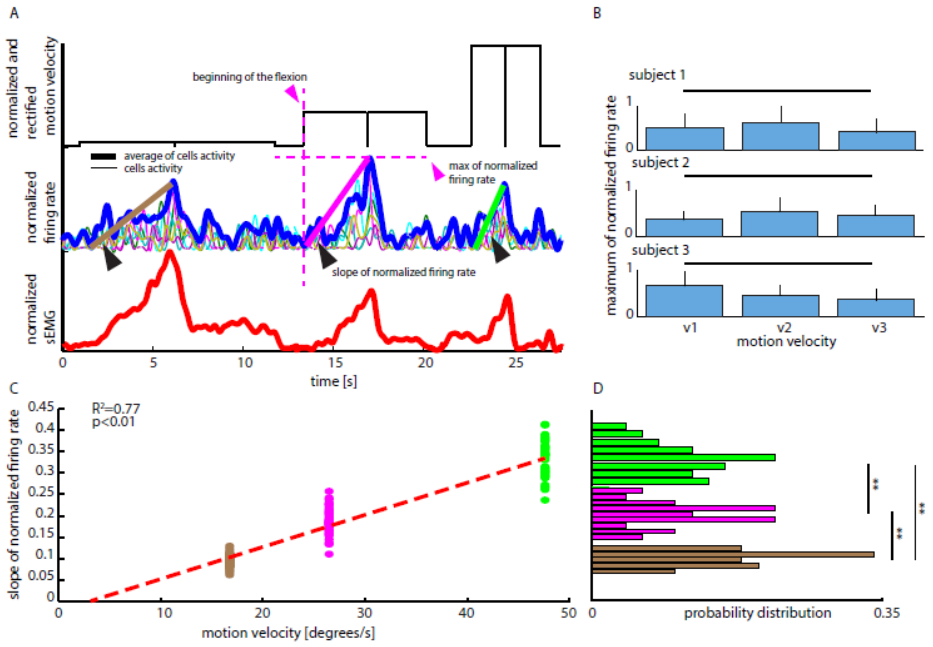


**Fig. 3.4. Discharging alpha motoneurons properties during velocity task.** (**A**) Motion velocity normalized to 47.37 degree/s, neurons FRs normalized to 60 Hz along with their average (normalized, blue line) and normalized fingers flexor sEMG (red). Signals portion

is extracted from a middle finger interphalangeal joint flexion executed by Subject 1. Data are representative of n=63 repetitions (36, 18 and 9 respectively for subject 1, 2 and 3). (**B**) The range of FRs is constant for different velocities, for the three subjects. FRs are normalized to their maximum (Table 3.S3). Data are represented as average ± SD. (**C**) Relation between the slope of the normalized mean firing rate and the required velocity of motion (only during flexion). Colors correspond to different velocities. A linear fitting ($R^2$=0.77, p<0.01) is proposed (dashed red line). Data are bootstrapped (150 samples each of which obtained by averaging 5 samples randomly chosen from the original distribution composed of 54 points). (**D**). Probability distribution of the subsets in (**C**). Their correspondence is color-coded. P-values are determined by Kruskalwallis with Tukey-Kramer test for multigroup comparison. ** p<0.01. The tests reported in (**D**) are executed on the not bootstrapped dataset. The analysis has been conducted on the portions of the recorded neural activity in which the subjects were executing a flexion.

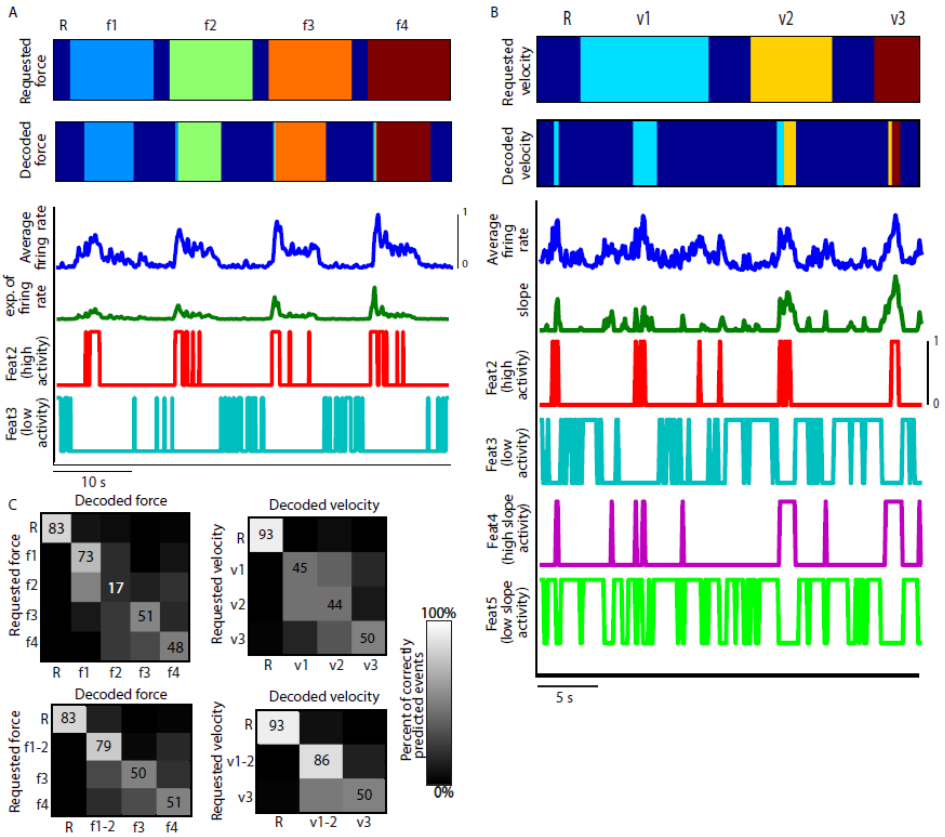

**Fig. 3.5. Decoding.** (**A**) Force prediction, (**B**) Velocity prediction. Requested versus decoded action, normalized FRs average and features. Signals are extracted from subject 1. Data are representative of n=45 repetitions in (**A**) and of n=36 in (**B**), equally distributed among the subjects. (**C**) Confusion matrices of the requested versus decoded action (rest included) representing the performance of the different decoders when predicting 4 or 3 forces and 3 or 2 velocities, top or bottom respectively. They were obtained by the sum of the single normalized matrices computed for the each subject separately. They were calculated, after bootstrapping, over 246 samples (50, 100, 96 respectively for subject 1, 2 and 3), 1100 samples (175, 175, 750 for subject 1, 2 and 3), and 425 samples (150, 150, 125 for subject 1, 2 and 3), respectively for those corresponding to (**A**) and (**B**). f1,2,3,4=force 1,2,3,4, v1,2,3=velocity 1,2,3.

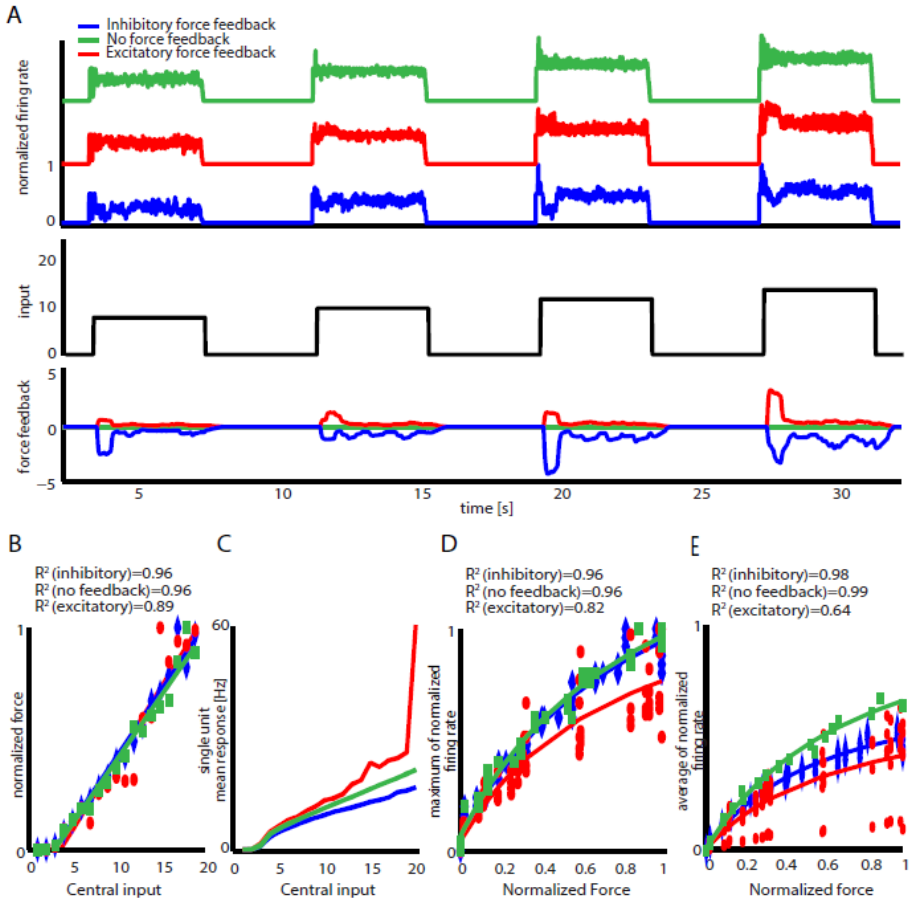


**Fig. 3.6. Force Task Modeling**

(**A**) Normalized firing rate in response to increasing force input in case of no force feedback (green line), excitatory force feedback (red line, strength=0.2), inhibitory force feedback (blue line, strength=0.4). Note that since for input=20 excitatory feedback induced an outshoot (see panel C) normalization was computed relatively to input=19. Color code is the same for all panels. (**B**) Average normalized force as a function of the central input. Solid lines indicate linear fits obtained in the three cases for inputs >2. The titles report fitting quality ($R^2$). (**C**) Average (and standard deviation) of the single unit responses as a function of central input for the three feedbacks. The standard deviation for the five units is so close to the average that lines cannot be discriminated. (**D**) Peak of normalized firing rate as function of resulting force. Markers indicate different trials for no force feedback (green squares), excitatory force feedback (red circles), inhibitory force feedback (blue diamonds). Solid lines indicate fits obtained in the three cases with Equation 3. Title reports fit quality for the three cases. (**E**) Average normalized response for the three feedbacks as a function of the normalized force (as in Fig. 3.4D). Solid lines indicate fits obtained in the three cases with Equation 4. Title reports fit quality for the three cases.

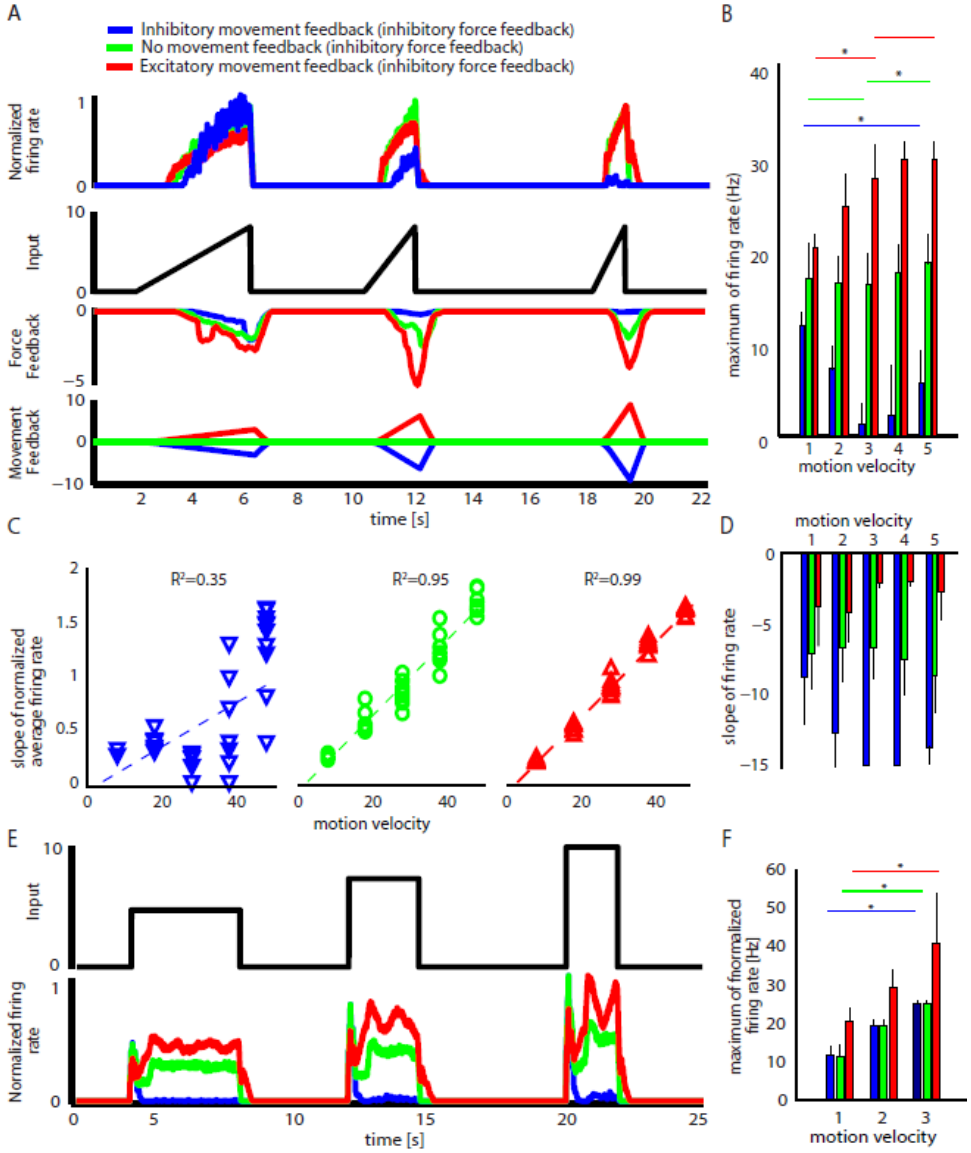


**Fig. 3.7. Velocity task modeling**

(**A**) From top to bottom are shown: (i) normalized response firing rate in case of no movement feedback (green), inhibitory (blue, strength=0.2) and, excitatory (red, strength=0.2) movement feedback, (ii) central input for three different speeds (top, black), (iii) force feedback evolution for the same time interval in the three cases and (iv) movement feedback evolution. (**B**) Peak firing rate for five different speeds for the three cases. Markers over bars indicate significance of differences between sets. (**C**) Slope of firing rate increase following onset of stimulus as a function of motion velocity in the three cases. Dashed line indicates linear fit and title reports fit quality. (**D**) Slope of firing

rate decrease following offset of stimulus as a function of motion velocity for the three cases. (**E**) Squared input proportional to the speed (top, black) and normalized response firing rate (bottom) in case of no movement feedback (green), negative (blue), and positive (red) movement feedback. (**F**) Peak firing rate for the three different speeds for the three cases. Markers over bars indicate significance of differences between sets.

## SUPPLEMENTARY MATERIAL

In these materials are included, in the order, figures and tables that are cited in the main paper.

## SUPPLEMENTARY FIGURES

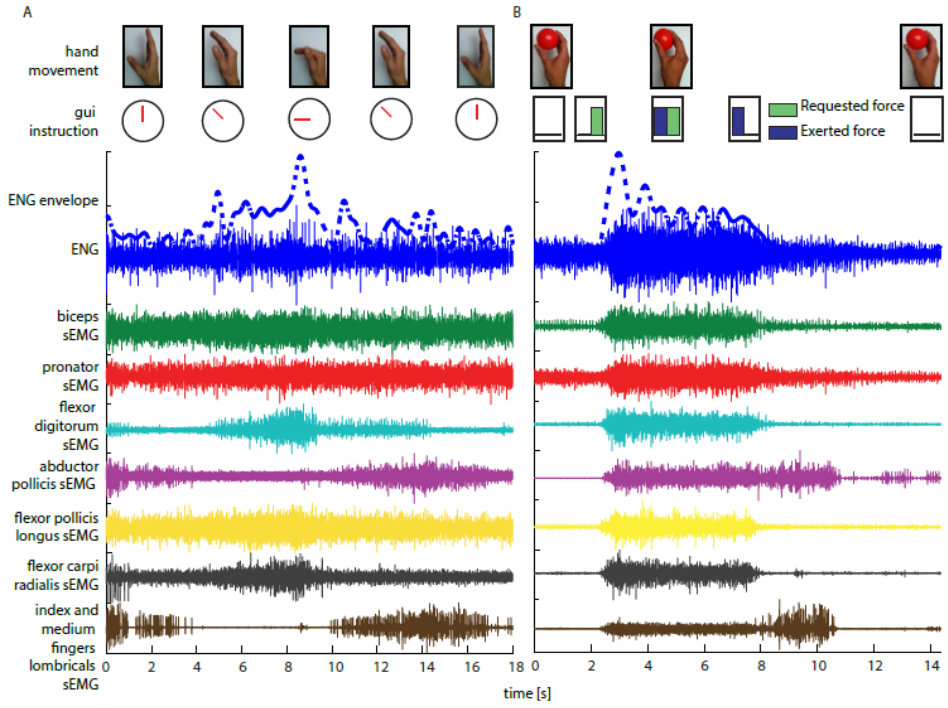


**Fig. 3.S1. Velocity and Force tasks.** (A) Velocity task. (B) Force task. Movement executed by the subjects (pictures), normalized ENG (blue) and its envelope (dashed blue), normalized sEMG of the acquired muscles (biceps (green), pronator (red), flexor digitorum (light blue), abductor pollicis (violet), flexor pollicis longus (yellow), flexor carpi radialis (black), lombricals (brown)). Data are extracted from subject 1.

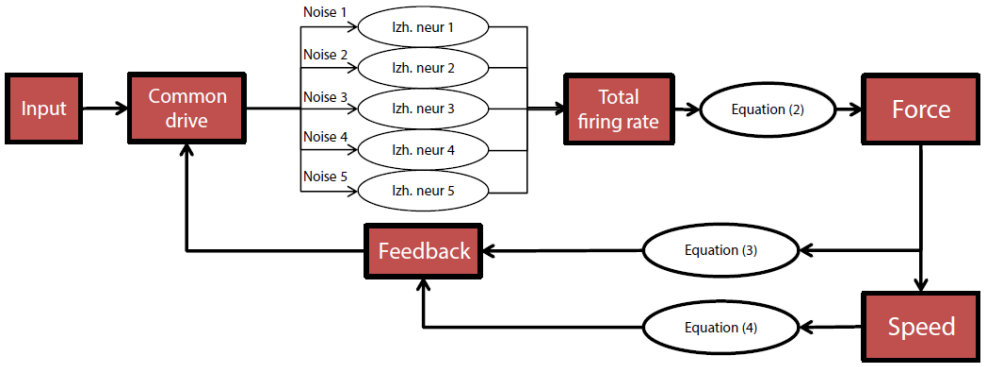


**Fig. 3.S2. Scheme of the network implemented in the computational model**

Illustrative representation of the different elements of the network model and their interactions

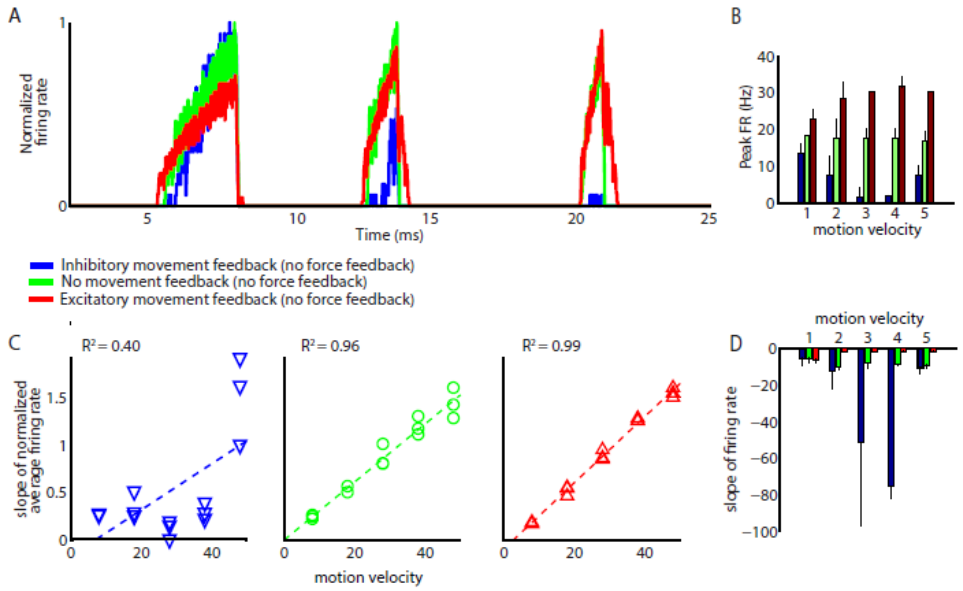


**Fig. 3.S3. Impact of force feedback on velocity regulation.** The same simulation presented in Fig. 3.6 is run here without accounting for the contribution of the force feedback. (**A**) Normalized firing rate of the artificial alpha motoneurons in case of no movement feedback (green), inhibitory (blue, strength=0.8) and, excitatory (red, strength=0.8) movement feedback, (**B**) Peak firing rate for five different speeds for the three cases. (**C**) Slope of firing rate increase following onset of stimulus as a function of motion velocity in the three cases. Dashed line indicates linear fit and title reports fit quality. (**D**) Slope of firing rate decrease following offset of stimulus as a function of motion velocity for the three cases.

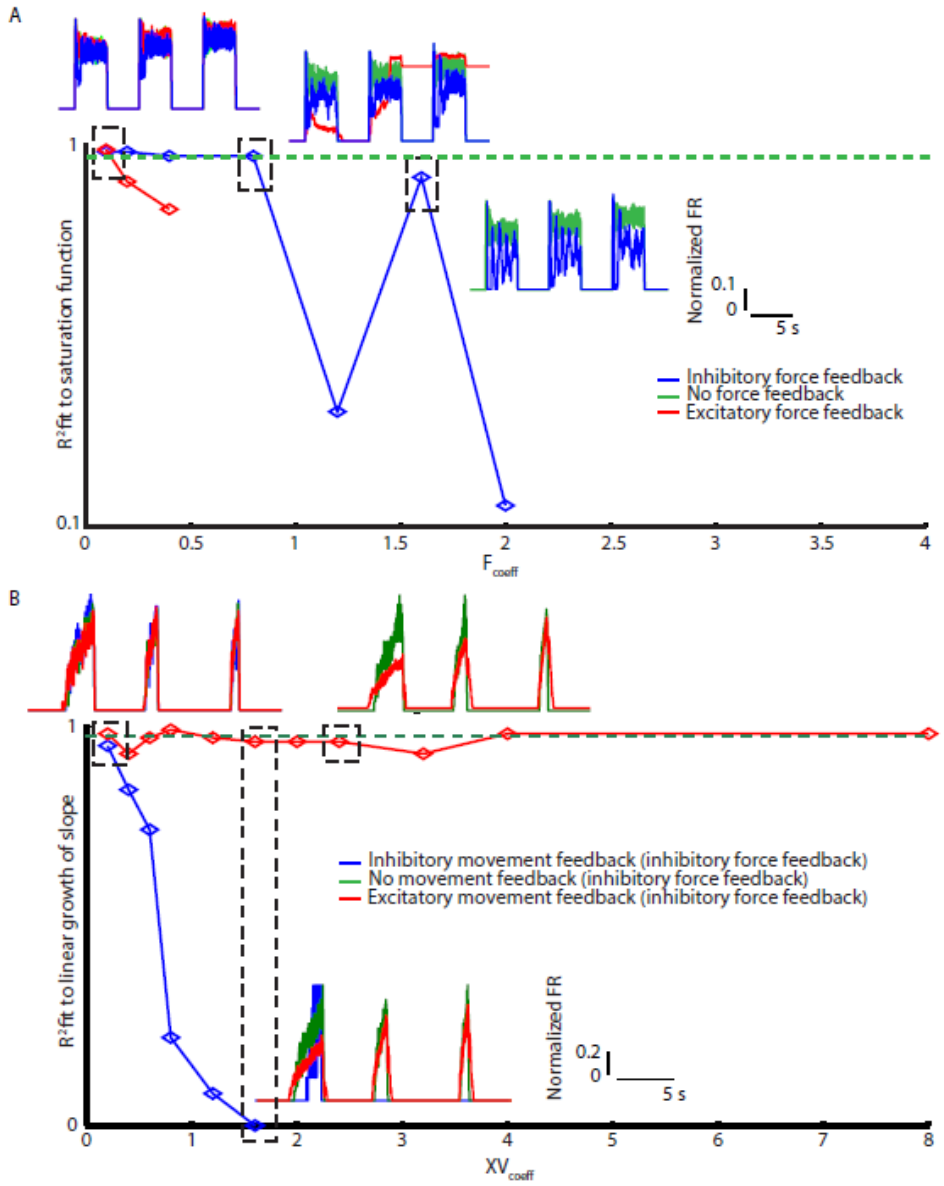


**Fig. 3.S4. Robustness of modeling results.** (**A**) Mean quality ($R^2$) of the fitting executed on the simulated firing rate peaks and stationary phases by equation 1 (*force task*), as a function of $F_{coeff}$. The relation is reported for inhibitory (blue) and excitatory (red) force feedback and compared with the case in which alpha motoneurons do not receive any proprioceptive feedback (green). The simulated dynamics of the cells firing is showed in correspondence of $F_{coeff}$ = [0.2, 0.8, 1.6]. (**B**) $XV_{coeff}$ variation determines the quality of

linear fitting ($R^2$) performed on simulated cells firing slope. In blue and red are showed the cases of inhibitory and excitatory movement feedback respectively. Results for $XV_{coeff}$ = 0 are in green. The firing dynamics of the simulated alpha motoneurons is displayed for $XV_{coeff}$ = [0.2, 1.6, 2.4].

## SUPPLEMENTARY TABLES

**Table 3.S1**. Hand muscles (extrinsic and intrinsic) recorded during the experiments.

| **Recorded hand muscles** |
|---|
| Fingers flexor |
| abductor/flexor/opponens pollicis (intrinsic muscles) |
| Flexor pollicis longus |
| Index and medium lombricals |

**Table 3.S2**. Movements required during the experiments. After every motion the subject had to return to the rest position (palm toward the experimental table).

| **Required movements** |
|---|
| (single or multiple) MCP fingers flexion |
| (single or multiple) IP fingers flexion |
| Thumb adduction |
| Thumb flexion |
| Thumb opposition |
| Hand closure |
| Cylindrical grasp |
| Pinch |
| Tridigital grasp |

**Table 3.S3.** Range (computed as difference between maximum and minimum) of the firing rate of the extracted cells for the three subjects for both velocity and force tasks.

**Firing rate range (Hz)**

| | Subject 1 | Subject 2 | Subject 3 |
|---|---|---|---|
| | Velocity tasks | | |
| Cell 1 | 60 | 50 | 30 |
| Cell 2 | 40 | 70 | 100 |
| Cell 3 | 50 | 30 | 40 |

| | | | |
|---|---|---|---|
| Cell 4 | 40 | 30 | 30 |
| Cell 5 | 30 | 50 | |
| Cell 6 | 30 | 40 | |
| | Force tasks | | |
| Cell 1 | 110 | 90 | 30 |
| Cell 2 | 40 | 90 | 70 |
| Cell 3 | 70 | 60 | 50 |
| Cell 4 | 60 | 80 | 40 |
| Cell 5 | 60 | 60 | |

**Table 3.S4.** Correlation index (Spearman) between ENG and sEMG of acquired muscles, for the velocity and force tasks. The selected muscles are highlighted. In the case of subject 3, considered that several muscles showed a similar correlation with the ENG, we picked the one suggested by the clinician during the experiments.

| **Recorded muscles** | **Correlation in force task** | **Correlation in velocity task** |
|---|---|---|
| **Subject 1** | | |
| Fingers flexor | 0,7936 | 0,6998 |
| abductor/flexor/opponens pollicis (intrinsic muscles) | 0,1632 | 0,1683 |
| Flexor pollicis longus | 0,7843 | 0,4088 |
| Index and medium lombricals | 0,6645 | 0,1348 |
| **Subject 2** | | |
| Fingers flexor | 0,8257 | 0,1111 |
| abductor/flexor/opponens pollicis (intrinsic muscles) | 0,7708 | 0,2849 |
| Flexor pollicis (intrinsic muscle) | 0,3260 | 0,321 |
| **Subject 3** | | |
| Fingers flexor | 0,894 | 0,4495 |
| abductor/flexor/opponens pollicis (intrinsic muscles) | 0,614 | 0,397 |
| Flexor pollicis longus | 0,8886 | 0,4 |
| Index and medium lombricals | 0,837 | 0,141 |

**Table 3.S5.** Features set exploited in the cases of velocity, force and grasp decoding. Tu1, Tu2 and Tl1, Tl2 are thresholds chosen to identify the intervals in which the neuronal activity is high (as during the execution of motions) or low (as during rest). ti represents the time instant (picked every 100 ms in the case of grasp and force and every 100 ms in

the case of velocity decoding). AFR=(FRs average). *tmin* represents the minimum firing rate identified before subjects' activity.

| | **Forces** | **Velocities** |
|---|---|---|
| Feature 1 | $Feat1(t_i) = e^{AFR(t_i)}$ | $Feat1(ti) = \frac{AFR(t_i) - AFR(t_{min})}{t_{min} - t_i}$ |
| Feature 2 | $\begin{cases} 1, & \text{feat1}(t_i) \geq \text{Tu1} \\ 0, & \text{feat1}(t_i) < T\text{u1} \end{cases}$ | $\begin{cases} 1, & AFR(t_i) \geq \text{Tu1} \\ 0, & \text{AFR}(t_i) < T\text{u1} \end{cases}$ |
| Feature 3 | $\begin{cases} 1, & \text{feat1}(t_i) \leq \text{Tu1} \\ 0, & \text{feat1}(t_i) > T\text{u1} \end{cases}$ | $\begin{cases} 1, & AFR(t_i) \leq \text{Tu1} \\ 0, & \text{AFR}(t_i) > T\text{u1} \end{cases}$ |
| Feature 4 | | $\begin{cases} 1, & \text{feat1}(t_i) \geq \text{Tl2} \\ 0, & \text{feat1}(t_i) < T2 \end{cases}$ |
| Feature 5 | | $\begin{cases} 1, & \text{feat1}(t_i) \leq \text{Tl2} \\ 0, & \text{feat1}(t_i) > T\text{l2} \end{cases}$ |

# Chapter 4 Restoring natural sensory feedback in real-time bidirectional hand prostheses

The content of this chapter has been published as Raspopovic, S., Capogrosso*, M., Petrini, F. M.*, Bonizzato, M.*, Rigosa, J., Di Pino, G., ... & Micera, S. (2014). Restoring natural sensory feedback in real-time bidirectional hand prostheses. Science translational medicine, 6(222), 222ra19-222ra19.

* Equal contribution

**ABSTRACT**

Hand loss is a highly disabling event that dramatically affects the quality of life. In order to achieve a close to natural replacement for the lost hand, the user should be provided with the rich sensations that we naturally perceive when grasping or manipulating an object. In fact, ideal bidirectional hand prostheses should involve both a reliable decoding of the user's intentions and the delivery of nearly "natural" sensory feedback through remnant afferent pathways, simultaneously and in real time. However, current hand prostheses fail to achieve these requirements, particularly because they lack any sensory feedback. Here, we show that by stimulating the median and ulnar nerve fascicles using transversal multichannel intrafascicular electrodes, according to the information provided by the artificial sensors from a hand prosthesis, physiologically appropriate (near-natural) sensory information can be provided to an amputee during the real-time decoding of different grasping tasks to control a dexterous hand prosthesis. This feedback enabled the participant to effectively modulate the grasping force of the prosthesis with no visual

or auditory feedback. Three different force levels were distinguished and consistently used by the subject. The results also demonstrate that a high complexity of perception can be obtained, allowing the subject to identify the stiffness and shape of three different objects by exploiting different characteristics of the elicited sensations. This approach could improve the efficacy and "life-like" quality of hand prostheses, resulting in a keystone strategy for the near-natural replacement of missing hands.

## INTRODUCTION

Sophisticated hand control is a peculiar characteristic of higher primates. Dexterous manipulation is achieved through a complex relationship between motor commands, executed movements, and sensory feedback during hand activities. Hand loss causes severe physical debilitation and often distress because skillful object grasping and manipulation is compromised, thus depriving the person of the most immediate and important source of tactile sensing in the body. For these reasons, replacing a lost hand and its precise functionalities is a major unmet clinical need that is receiving attention from engineers, neurophysiologists, and clinicians. An ideal hand prosthesis should reproduce the bidirectional link between the user's nervous system and the peri-personal environment by exploiting the post-amputation persistence of the central and peripheral neural networks and pathways devoted to hand motor control (Reilly et al., 2006) and sensing (Goodwin, 2004, Schady et al., 1983, Marchettini et al., 1990, Schady et al., 1994). In particular, real-time and natural feedback from the hand prosthesis to the user is essential to enhance the control and the functional impact of prosthetic hands in daily activities, prompting their full acceptance by users within an appropriate "body scheme" that does not require continuous visual monitoring, as with current artificial hands (Atkins et al., 1996, Biddiss et al., 2006).

Recent notable advances in the field of hand prostheses have included designing devices with multiple degrees of freedom and equipped with

different sensors (Carrozza et al., 2006, Johannes et al. 2011). These developments have made the need for more effective bidirectional control even more compelling. A promising solution is represented by targeted muscle reinnervation (TMR), which consists of rerouting the residual nerves of the amputees over the chest muscles (Kuiken et al., 2007b, Kuiken et al., 2009). Individuals with arm or hand amputations can chronically use TMR-based prostheses, which could theoretically allow for a certain amount of sensory feedback (Marasco et al., 2009, Kuiken et al., 2007b). However, because the superficial electromyogram (sEMG), used as a control signal, is recorded from the same body region (i.e., the chest) that must be mechanically stimulated to provide feedback, real-time bidirectional control could be difficult to achieve. In this scenario, TMR subjects must contract muscles and simultaneously perceive a touch sensation on the skin overlying the same muscles, therefore possibly producing the so-called neurophysiological "sensory gating" (Kristeva-Feige et al., 1996).

In parallel, the rapid development of neural interfaces for the peripheral nervous system (Navarro et al., 2005) has provided potential for new tools through which bidirectional communication with nerves in the stump could be potentially restored. Initial feasibility demonstrations of the induction of some sensations (Dhillon et al., 2005) and preliminary trials of the sporadic control of non-attached prostheses (Rossini et al., 2010, Jia et al., 2007) have recently been performed. However, to date, no evidence has been gathered for the real-time use of these neural interfaces for the effective bidirectional control of dexterous prosthetic hands performing different grasping tasks.

In this case study, our aim was to restore touch sensation in a person with hand amputation using transversal intrafascicular multichannel electrodes (TIMEs) (Boretius et al., 2010) connected to artificial hand sensors and to intuitively use this sensation to achieve bidirectional control of a hand prosthesis. Our hypothesis was that the participant would be able to exploit the dynamic tactile information induced by neural stimulation that

is triggered by the sensors of the hand prosthesis, during real-time simultaneous control of a dexterous prosthetic hand, to adaptively modulate grasping force, thus closing the user-prosthesis loop. The active sites of the electrodes were used to deliver electrical stimuli to the peripheral nerves that were proportional to the readouts of artificial sensors in the hand prosthesis. sEMG signals were used to decode different grasping tasks to verify whether the sensory information provided could be used in real time (i.e., with the delay imperceptible by the user). If this goal could be accomplished, then the hand prosthesis could have practical relevance in daily activities.

## RESULTS

TIMEs were implanted into the median and ulnar nerves of an amputee's residuum to investigate the possibility to restore natural sensory feedback and integrate it into the user control loop of a dexterous prosthetic hand (Fig. 4.1A). Median and ulnar nerves (Fig. 4.1, B and C) were chosen as their innervation territory covers almost entirely the palmar and the fingers sensory fields. The participant (D.A.S.) suffered a transradial left arm amputation 10 years ago, as a consequence of a traumatic event. During all experiments with restored touch, he was acoustically and visually isolated (Fig. 4.1A) in order to show that he was relying exclusively on the induced tactile sensation, without using other sensory modalities. The motor commands (palmar grasp, ulnar grasp, tridigital grasp, hand opening and rest) were decoded by processing sEMG signals, while the sensory feedback (encoding) was triggered by intrafascicular stimulation of the median and ulnar nerves by using TIMEs (Fig. 4.1, D and E) according the information of the hand prostheses sensors. The subject performed more then 700 trials to verify his ability to modulate force during grasping and to identify specific physical characteristics of objects.

### Peripheral nerve stimulation

Sensory tactile feedback was restored by delivering electrical current through one TIME active site placed in the median nerve and one placed in

the ulnar nerve. The sensations elicited corresponded to the physiological sensory mapping of touch within the innervation territories of the median and ulnar nerves (Fig. 4.1D), confirming that this property was not lost several years after sensory deprivation.

Then, we determined the range of electric charge usable (Fig. 4.1D) to provide a dynamically graded sensory feedback for real-time control. The lower threshold corresponded to the minimum stimulus charge needed to elicit the first distinct touch sensation. Saturation was positioned just below the pain threshold reported by the participant. When repeatedly tested, the mapping of sensations over the representation of the missing hand, assessed using a patient report, was stable and repeatable throughout the four weeks of study, both for the median and the ulnar nerve (Fig. 4.1E). Stimulation of fascicles inside the ulnar nerve produced the sensation of gradual touch in the little finger, whereas stimulation inside the median nerve produced progressive sensations located in both the index finger and the thumb.

The charge range for the ulnar nerve was stable over four weeks, while for the median nerve, the charge range increased over time (Fig. 4.1D). Meanwhile, the maximum charge injected into both nerves (8 and 24 nC) was much lower than the highest charge theoretically injectable using TIME electrodes (120 nC). The injected charge range used in this study was consistent with the range 0.3 - 60 nC used by Dhillon *et al.* (Dhillon et al., 2005) for the stimulation of the human median and ulnar nerves with intrafascicular electrodes.

**Real-time fine force control**

We first assessed whether the induced natural (physiologically plausible) dynamic sensory feedback could lead to a voluntary and reliable modulation of grasping force of the prosthesis. During these fine force trials ($n$ = 449), the participant was blindfolded and acoustically shielded (Fig. 4.1A). The subject was asked to repeatedly produce three different force levels on a pressure sensor chamber, using the induced sensory

feedback to modulate the force when performing pinch, ulnar, and palmar grasps.

*Assessment of the performance during closed-loop grasping control*

The participant was able to accurately control the grasp force in both single-level press-and-release trials and in the continuously modulated "staircase task" (Fig. 4.2A). In the staircase task, the participant needed to gradually increase the applied force in three steps lasting approximately 2 seconds each and then gradually return to the baseline, while in the single-level trials he was instructed to maintain it until feeling confident with exerted level of force. In certain trials, when the participant recognized—through the sensory feedback—that he had applied too much pressure (Fig. 4.2A, red arrow), he corrected the grasp accordingly, eventually meeting the task requirement and clearly exploiting the induced sensory feedback.

Over the course of 7 days, the subject could produce three levels of stable and discrete pressure with both the index and the little finger under voluntary control, reaching a success rate >90% in the last sessions for both fingers (Fig. 4.2B). The accuracy of execution increased from the first day until the end of the experiment**.** The percentage of correct performance increased from an initial 67% to 93% for the index finger and from 56% to 83% for the little finger, demonstrating that the subject had most likely undergone a learning process by integrating the restored sensation into closed-loop control strategies (Fig. 4.2B). For this one subject, the predominant source of error was confined to the execution of the medium level of force (as reflected in Fig. 4.1B confusion matrices). With both, index (Fig. 4.S1A) and little finger (Fig. 4.S1B), the subject was able to apply consistently three significantly different force levels [Tukey-Kramer test, $p<0.001$ single press-and-release trials ($n = 76$)].

To compare the performance of the hand prosthesis to that of an intact hand, the participant was asked to perform the same task with his intact (and dominant) right hand and with his left hand prosthesis with visual and acoustic feedbacks, but without any nerve stimulation. The obtained

pressure profiles were evaluated by means of several parameters defining the precision and shape of the staircase (a list of all the parameters is provided in Fig. 4.S2). All data were processed using principal component analysis (PCA) and plotted in the space of the first three principal components, which explained more than 80% of the variance. Each ellipsoid represents one distribution and it is centered at the mean value with semi-axes equal to the standard deviation along each principal component (Fig. 4.2C). Trials executed solely with the artificial tactile feedback (in blue) were much more similar to those of the intact hand (in green) than the ones with prosthesis control by visual feedback (in red). The data variability in the absence of tactile feedback was greater than for the other two cases, as shown in the PCA representation in Fig. 4.2C, as the standard deviations for the case without tactile feedback are approximately double than in the case of tactile feedback induction. The performance with visual-only feedback was also significantly different from the one with the natural hand (Kruskall-Wallis $p<0.05$), whereas the performance of the natural hand versus the prosthetic hand with tactile feedback was similar (Kruskall-Wallis $p=0.31$) (Fig. 4.2C).

We also investigated whether the participant was able to integrate multiple and independent pressure sensory inputs when performing a palmar grasp (which delivered inputs from the median and ulnar region simultaneously). The results indicate that the dynamic information of the index and little fingers were effectively integrated and exploited to modulate palmar grasp fine force control, with 82.7% overall accuracy (Fig. 4.2D).

*Falsification experiments*

To evaluate whether the control of the exerted force was only due to the restored touch sensations over phantom hand fingers, and to falsify the hypothesis that the subject learned to regulate the force applied by modulating the timing of hand actuation, two different control conditions were designed and tested. In one test (placebo, or "p"), among many trials with stimulation, we randomly selected several press-and-release trials in

which the nerve stimulation was switched off, while asking the patient to reach a low level of force; no force control was possible in this configuration ("low-p" in Fig. 4.3A), resulting in the maximum possible force in all these trials ($n$ = 15). In another test, the velocity of hand actuation was modified without notifying the subject, in order to falsify the hypothesis that the user could still learn the force level exerted from the prosthesis closure time.

The achieved performances in Fig. 4.3B suggest that the participant was not relying on the timings of closure to reach a desired level of pressure. In fact, if this was the case, then both the slower and faster velocity should have resulted in poor or at least reduced performances compared with the normal one. Instead, at higher velocities, the subject had more difficulty in finely controlling the movements (with performances of 75.7% for the index finger and 67.0% for the little finger over all 131 sessions), whereas at lower velocities, the participant was able to finely grade the force showing the best performance (88% and 94% performances for index and little fingers, respectively, over all 118 sessions). We speculate that this is because, at lower actuation speeds, it was easier to grade the exerted force and understand the intensity of the sensation. These results indicate that the force control exclusively relied on the induced sensory tactile feedback in this subject.

**Functional grasping**

We next investigated the possibility of integrating the restored sensation in a manipulation task similar to activities of daily living. During this task, an object was placed on the palm of the hand prosthesis, and the participant was instructed to recognize its position with respect to the hand and to perform the most appropriate grasp for handling. Three objects were placed at different locations: a cylindrical object, engaging the entire palm, and two smaller objects located on the median or ulnar sides. To recognize the object position, the participant, who was blindfolded and acoustically shielded, used an explorative palmar grasp (sensing phase in Fig. 4.4A). The real-time muscle electrical activity (sEMG

envelope), the decoded hand commands, the synchronous readouts of the hand sensors, and the current injected within nerves (tactile traces) are represented in Fig. 4.4A. Once identifying the position of the object using the sensory information available, the participant re-opened the hand and performed a location-appropriate grasp (palmar for the cylindrical object, pinch or ulnar grasp for the median and ulnar located small objects-specific grasp phases in Fig. 4.4A).

As soon as the participant realized that the object was steadily grasped, he handed the object to the experimenter sitting in front of him (in case of median position), to the experimenter on his right (for ulnar position), or lifted it up (for whole-palm sensing). The participant was able to perform this task with an average accuracy of ~97% over 52 trials performed on days 5 to 7 (Fig. 4.4B and movie S1).

**Sensing the environment: recognition of object properties**

In this experiment, the participant's ability to use the restored hand sensation to identify the physical properties of an object, such as stiffness and shape, was verified. In case of stiffness, the underlying hypothesis was that dynamics of the restored sensation could help discriminate specific object characteristics. Such discrimination would be based on the subject's cognitive ability to decode stiffness by processing the artificial tactile feedback dispatched from the sensors of the prosthetic hand. In particular, because the stimulation currents injected into the nerves follow the sensor readout, it was expected to change very rapidly with a hard object and very slowly with a soft object.

The participant, blindfolded and acoustically shielded, was provided with three objects: a piece of wood (hard), a stack of plastic glasses (medium), and a cotton pack (soft). He was instructed to explore the object with a palmar grasp and to apply force until he could perceive its stiffness. As expected, the sensor readout in the hand significantly differed according to the object's stiffness: stiffer objects caused the sensor output (blue traces in Fig. 4.5A) and, consequently, the intensity of the injected current (red traces in Fig. 4.5A) to cross the range from minimum contact to saturation

quicker than softer objects. The value of the average current amplitude derivative (0.67 ± 0.31, 0.19 ± 0.09, and 0.08 ± 0.04 μA/s for high, medium, and low stiffness, respectively) was significantly different for different object stiffnesses (Tukey-Kramer test, $p<0.001$) (Fig. 4.5B and Fig. 4.S3). The evolution over time of the induced sensory response was consistently well-separated, suggesting that this dynamic information could have been used by the subject to distinguish among the three presented stiffness (Fig. 4.S3).

It is reasonable to hypothesize that the subject might have intuitively exploited this information to distinguish between the three levels of stiffness within 3 seconds. As a result, the subject was able to consistently recognize the proposed object with an overall level of performance of 78.7% (Fig. 4.5B). A clear improvement was observed in intra-session performance, which might suggest a learning process or acquaintance with the task, boosting the performance to high accuracy in three sessions executed from in days 6 and 7 of experiments with half-day separation (Fig. 4.5B and movie S2). By examining the confusion matrix in Fig. 4.5B, the majority of errors were observed to be caused by the misjudgment of the medium stiffness toward either soft or hard. The soft object was never confused with the hard one and vice versa.

Furthermore, we tested whether the participant, who was blindfolded and in acoustic isolation, was able to use the differential recruitment of the restored sensation in different hand sites, to recognize object shape, keeping stiffness constant (hard/high, in this case). Three different items were independently presented (Fig. 4.5C): a cylindrical object (a bottle), a large spherical object (a baseball)—both of which covered the entire hand palm—and a small spherical object (a mandarin orange), which covered only part of the hand palm. The participant was able to correctly classify all three shapes with an average accuracy of 88% (Fig. 4.5D). Although the baseball was large enough to cover the entire hand, the subject could feel that the spherical shape produced a different sensation than the cylindrical bottle. To achieve this discrimination ability the participant

referred to the use of the perceived delay between the contact of the index and little finger with the object surface. This delay was indeed significantly different between the spherical and the cylindrical shapes (Kruskall-Wallis $p<0.01$) (Fig. 4.5D and Fig. 4.S3).

**DISCUSSION**

In the case study presented here, sensory feedback was achieved by stimulating peripheral nerve fascicles, which in turn allowed real-time closed-loop control of a prosthetic hand by a human subject with a transradial amputation. To restore the lost sensory feedback, four TIMEs were implanted in the median and ulnar nerves fascicles, and two stimulation sites that were able to elicit distinct and repeatable sensations on the innervation territories of the two nerves (Shady et al., 1983, Marchettini et al., 1990, Shady et al., 1994) were then selected at the end of systematic testing of all the contacts and then connected to the artificial hand sensors. Sensations were elicited in a range from slight contact to just below the reported pain threshold, to dynamically control the intensity of stimulation delivered, according to the prosthetic hand sensor readouts.

The participant controlled the prosthesis through voluntary contractions of the remaining muscles on the stump, being able to perform different (ulnar, pinch, and palmar) grasps, and hand opening by online processing of sEMG signals. The grasps were performed in terms of position control such that he was able to finely modulate the fastening and opening of the prosthetic hand. The complex and fine manipulation tasks in the natural human hand require a deep and complex interaction between motor commands and sensory feedback (Johansson et al., 2006, Flanagan et al., 2006). Current solutions are not able to provide a natural (i.e., physiologically appropriate) sensory feedback to amputees for real-time closed-loop prosthetic use. In present study we developed a system able to perform control and to deliver sensory feedback with an imperceptible delay (Farrell et al., 2007) for the user. Our approach allowed the user to

perform several tasks with very promising results. In the fine force control task, the subject indeed mastered a precise closed-loop control of the force elicited by his voluntary contraction, using either median or ulnar natural feedback of pressure intensity. With a series of "placebo" trials, it was confirmed that the high performance obtained was only due to the restored sensation, which allowed the user to master force control in the absence of any other feedback (visual or auditory). The possibility of adding physiologically appropriate touch sensations to hand prosthesis could enhance the controllability and thus acceptability (Atkins et al., 1996, Biddiss et al., 2006) of such a device, bringing it closer to the natural manipulation strategy.

This level of precise force control is not reachable with currently available prostheses, owing to the lack of natural sensory feedback offered to the user. Moreover, the participant's performance rapidly increased during a week of tests and training, indicating that the participant intuitively and precisely integrated the information provided by the restored feedback in his control loop. This finding was also confirmed by the trials in which the participant recognized, through the sensory feedback, having exceeded the pressure level requested and corrected the grasping force accordingly. Moreover the present approach featured an emerging, higher level of complexity than controlling only different levels of force of single fingers, when the participant was able to successfully integrate both the median and ulnar sensory feedbacks into a full-palm control of exerted pressure.

Successively, the participant's ability to exploit the prosthetic sensory-motor loop in a task involving different object sensing and various available motor commands was tested. Our hypothesis was that this complex sensory integration could be exploited to gain control of the hand prosthesis in manipulation tasks, even without visual or auditory feedback. The participant rapidly mastered the task, demonstrating the ability of integrating the sensory information in real-time control for several grasps of the prosthetic hand. Thus, the subject achieved appropriate grasping and manipulation of some common objects.

Therefore, single sensations dispatched along separate neural pathways can be combined to achieve a comprehensive, physiological, and functional prosthetic agency experience.

Restoring the sensory pathway should not only serve as a method to improve the controllability of the prosthesis, but also to help in regaining the ability to explore the environment. Our hypothesis was that the close to natural sensory feedback delivered from the prosthesis sensors would allow the user to actively sense the environment, being able to recognize object properties, such as stiffness, size, and shape. Tests conducted with a baseball, a mandarin orange, and other visually dissimilar objects indicated that the subject was indeed able to intuitively integrate the sensory information received to recognize that the objects were different and therefore needed to be handled with differently grasps and levels of force. The subject probably used a discrimination approach very similar to the physiological one based on the tactile information provided by the different average slope of the force-time and contact-time curves associated with the fingertips for different objects (Srinivasan et al., 1995). Stiffer objects reach the maximum of the perceived force faster than less stiff objects. Thus, the participant benefited from the same characteristic behavior in the sensation elicited by the nerve stimulation and encoded it to achieve discrimination of three different object compliances after only three sessions. The patient recognized the object stiffness in less than 3 seconds, and the recognition for stiffer objects was even faster. We believe that this short time is compatible with real-life applications (*26*).

The sensory information naturally received while exploring an object's shape is a complex mixture of redundant and overlapping inputs coming from different sensory receptors and fibers (Frisoli et al., 2011, Goodwin et al., 1997). However, as shown in our case, even sensing a differential recruitment of two parts of the hand is sufficient to recognize the shape of some familiar objects. For objects characterized by different shapes covering all the palmar prosthetic hand, the timing of activation of the two sensors is in fact different. The subject to discriminate among the objects

can use this kind of information. The restored sensation can thus induce an artificial, although close-to-natural, neural coding that allows the subject to intuitively integrate the combined stimulation of different neural pathways without any training. The successful combined use on multiple channels provides clear evidence of the build-up of natural perceptions due to the homology and real-time properties of this neural coding. The participant's ability to control different levels of grasping force, execute functional manipulations and identify some simple object properties as three levels of compliance and three different shapes, provides powerful evidence of the impact that this approach could have in real-life applications.

However, this study was conducted on one participant over a limited amount of time, and future studies will show on larger populations of amputees accurately the performance and limits of this artificially induced sensory feedback integration into the control of prosthesis. The other limitation is the fact that the tests were conducted continuously over the course of 1 week, so it is not clear whether or not the user would retain or even improve performances over a longer period of not being used. Moreover, many other sensations, or more sophisticated perceptions that might be elicited with this implants, were not tested.

Restoring sensory feedback is necessary to improve the usability of a hand prosthesis in daily life activities, where regaining control of the force output or being able to recognize object properties would increase the quality of life of people who suffer from hand amputation. The concept of this closed-loop bidirectional control, using a stimulating neural interface, could also be extended to enable the stimulation of a larger number of sites on the nerve implants. By coupling these locations for stimulation with the readouts of as many sensors embedded in the hand prosthesis, a wider variety of sensations could be delivered to the user, both in terms of position (e.g., palm sensing) and type of sensation (e.g., proprioception). To translate this technology to common clinical practice and even every-day use several goals have to be achieved. First, the equipment used for

stimulation should be miniaturized and fully implantable. The control unit for decoding of motor intention from sEMG signals and encoding of sensation by stimulation should be programmed on-chip and introduced in the socket of the prosthetic hand. Overall, this approach opens up new possibilities for hand prosthesis users, paving the way for the development of natural, dexterous, and effective bidirectional control of these devices.

## MATERIALS AND METHODS

### Study design

To verify whether a restored natural sensory feedback could be integrated in the user control loop of a dexterous prosthetic hand, TIMEs were implanted into the median and ulnar nerves of an amputee's residuum. Touch sensations were elicited on the median and ulnar innervation territories and exploited in the bidirectional control of a sensorized prosthetic hand. In this case study, the experiments were aimed at testing the subject's ability to modulate the grasping strength by measuring the force output with a pressure sensor, and to explore the possibility to integrate the sensations into functional tasks and for the identification of daily object physical properties. Because there are no references for this type of experiment, we aimed to make as high as possible number of trials ($n$ = 700) within the limited time on disposition. More in particular, we made many trials in experiments with the force control (both for evaluation as for falsification), because that is the essential for proof-of-concept, and also the basic principle for all other experiments done.

Data were acquired in several sessions distributed in 7 days. Session lasted as long as the subject was comfortable with the time spent. Therefore, trials were interrupted when the subject asked it. Data were considered outliers when they exceeded 2 SD from the mean.

### Subject recruitment

All procedures were approved by the Institutional Ethics Committees of Policlinic A. Gemelli at Catholic University, where the surgery was performed, IRCCS S. Raffaele Pisana (Rome), where the experiments took place, and Campus Bio-Medico University, whose clinical personnel collaborated during the experiments. The protocol was also approved by the Italian Ministry of Health. One male participant (D.A.S.), age 35 years, was selected for the experiments from a group of 31 candidates with hand amputation because of the stump characteristics (trans-radial amputation, sufficient number of remnant muscles) and his psychophysical abilities (expert user of EMG-driven hand prostheses). He suffered a transradial left arm amputation 10 years ago, as a consequence of a traumatic event.

**Bidirectional prosthesis and real-time control**

The surgical procedure for implanting TIMEs is described in Supplementary methods. The bidirectional prosthesis comprised a set of commercial devices (Prensilia IH2 Azzurra robotic hand, 2 GRASS QP511 analogical amplifiers, Multichannel System STG4008 stimulator) and the TIMEs developed in the homonymous EU project. The artificial hand was connected to the stump of the volunteer by a custom-made socket (Ortopedia Italia). The artificial hand and the stimulator were controlled by custom-developed software in Labview (National Instrument). The prosthetic hand was equipped with tension sensors measuring the force exerted by the index and the little finger.

The users' residuum sEMG signals were used to decode the intended grasp. Decoded hand motion was driven in terms of progressive position control, resulting in a gradual opening or closing of the hand. The sensors embedded in the hand were used as inputs for the delivery of the afferent neural stimulation. Current-controlled stimulation was delivered through the TIME active sites (two in the median nerve and two in the ulnar nerve, with overall 56 active stimulating and 8 ground sites), eliciting a sensory perception reliably localized within the territories of the stimulated median or ulnar sensory fascicles. The stimulation was provided at fixed

frequency and width of a biphasic train of pulses, whereas the current amplitude was modulated proportionally to the sensors readouts.

**sEMG-based control**

The sEMG signals were collected differentially, from the five muscular positions. Data were acquired at 12 kHz, band-pass filtered (100-1000 Hz), and grouped into intervals of 100 ms. For each interval features where extracted and fed to a Multi Layer Perceptron Network providing the classification output every 100 ms. Signal processing, feature extraction and validation, and decoding are described in detail in the Supplementary Methods.

**Restoration of sensory feedback**

The ability of the electrodes to elicit sensations by means of electric current stimulation was tested during different trials. The experiments consisted of stimulating single contacts of the four electrodes, with a train of cathodic rectangular biphasic pulses. The frequency of the delivered pulses was 50 Hz and the length of the stimulation train was 500 ms for every trial. The injected charge was varied within the safety limits indicated for the electrodes by the manufacturers and by the ethical committee. Elicited sensations reported by the subject (type, location, and strength in a scale from 1 to 10) were recorded.

Two stimulation sites able to elicit sensations on the sensory innervation territories of the two nerves were selected: a touch sensation on index and thumb for the median innervated territory, and a touch sensation on the little finger for the ulnar innervated territory, were reported by the subject (Fig. 4.1, D and E). Sensations were elicited in a range that went from slight contact to pain threshold (corresponding to 14-24 nC and 4-8 nC, for median and ulnar nerve, respectively). These properties were exploited to dynamically control the intensity of stimulation delivered, accordingly to the prosthetic hand sensor readouts.

### Transformation of sensors readouts in stimulation patterns (encoding)

The readout of the sensors embedded in the prosthetic hand was used as an input for a proportional delivery of afferent neural stimulation. Sensors positioned in the index and little fingers were used to acquire the level of contact applied on the two sides of the robotic hand. A real-time algorithm dedicated to the sensory loop was able to read both hand sensors outputs and to encode the respective sensory stimulation. Simultaneously, the algorithm dedicated to the control loop was able to acquire, process, and decode the sEMG signals and to deliver the motion command to the robotic hand. The details of the algorithm and sensor encoding are described in Supplementary Methods.

### Experimental design

Several protocols were designed and implemented to demonstrate that the restored sensory feedback could allow the participant to effectively use the bidirectional hand prosthesis. In particular, four experiments were carried out: fine force control task ($n$ = 560 trials), functional exploration and grasping tasks ($n$ = 52 repetitions), stiffness recognition ($n$ = 66 repetitions), and object shape recognition ($n$ = 32 repetitions). The details of each of these four experiments is in Supplementary Methods.

During all the experiments, the participant was blindfolded and acoustically shielded in order to eliminate both visual and auditory feedback. He did not receive any systematic and prolonged training but he quickly learnt by himself how to use and control the bidirectional robotic hand.

### Data collection and normalization

During the experiments with the bidirectional prosthesis the following information were recorded: index and little finger sensors readouts, stimulation parameters (current amplitude, frequency and pulse width), desired fingers position, pressure sensor output, residual muscles stump sEMGs and MLP decoded intention.

All the data traces shown in the paper are normalized for formatting and simplicity of visualization reasons. All the traces corresponding to the pressure sensor chamber were normalized with respect to the maximum pressure exerted by the hand, which was of about 1.5 kPa (after sensor calibration). Because hand sensors were measuring the tension in the fingers' tendons, these values correspond to a measure of the force exerted at the tip of the finger, which was comprised in the range 0 to 60 N. Current values were saturated within the 15% (S15) to 75% (S75) of the sensors readouts (Fig. 4.1). Stimulation current traces were normalized to the maximum stimulation current: 240 μA (at 100 μs) for the index finger and 160 μA (at 50 μs) for the little finger.

**Data analysis and statistics**

The acquired data were exported and processed offline in Matlab R2012 (The Mathworks). All data were reported as mean values ± S.D. or S.E.M. when indicated. Performances were evaluated in terms of confusion matrices measuring the number of outcomes for each possible answer with respect to each requested task. Because data distributions were not Gaussian (Kolmogorov-Smirnov, 95% CI), statistical evaluations were performed using the two-tailed Kruskall-Wallis test (a nonparametric analysis of variance) with 95% CI. The two-tailed Tukey-Kramer test was applied in the case of multiple groups of data.

**ACKNOWLEDGMENTS**

The authors are grateful to the Participant D.A.S. who freely donated six weeks of his life for the advancement of knowledge and for a better future of people with hand amputations. **Funding:** This work was supported by the EU Grant CP-FP-INFSO 224012 (TIME project), the project NEMESIS (Neurocontrolled mechatronic hand prosthesis) funded by the Italian Ministry of Health, the EU Grant FP7-611687 NEBIAS (NEurocontrolled BIdirectional Artificial upper limb and hand prosthesiS), the EU Grant FP7-NMP 228844 NANOBIOTOUCH (Nano-resolved multi-scan investigations of human tactile sensations and tissue engineered nanobiosensors). The

work was also supported by the Swiss National Science Foundation through the National Centre of Competence in Research (NCCR) Robotics. **Author contributions:** S.R. designed the study, developed the software, performed the experiments and wrote the paper; M.Capo., M. B. and F. P. developed the software and the overall system integration, performed the experiments, analyzed the data and wrote the paper; J. R. developed the software and collaborated during the experiments; G.D.P. selected the patient, collaborated during the design of the study and during the experiments; J. C., G. G., L. C., A.L.C., and C.M.O. collaborated during the integration of all the components of the device and collaborated during the experiments; M.Cont., C.C., and M.C.C. developed the robotic hand; W. J. and E. G. collaborated during the preparation and execution of the experiments; T. B. and T. S. developed the TIME electrodes; E. F. performed the surgery; P.M.R. selected the patient, designed the study, supervised the experiments and wrote the paper; and S. M. designed the study, supervised the experiments, and wrote the paper. All the authors read and approved the manuscript. **Competing interests:** C.C. and M.Cont. have financial interests in the company Prensilia SRL, which manufactures artificial hands similar to the one used in this study; S.R., M. Capo., M.B., F.P. and S.M. are inventors of a pending patent application concerning part of the methods in this work. **Data and materials availability:** Raw data and the custom-developed Labview software will be made available by MTA upon reasonable request to S. M.

**FIGURES**

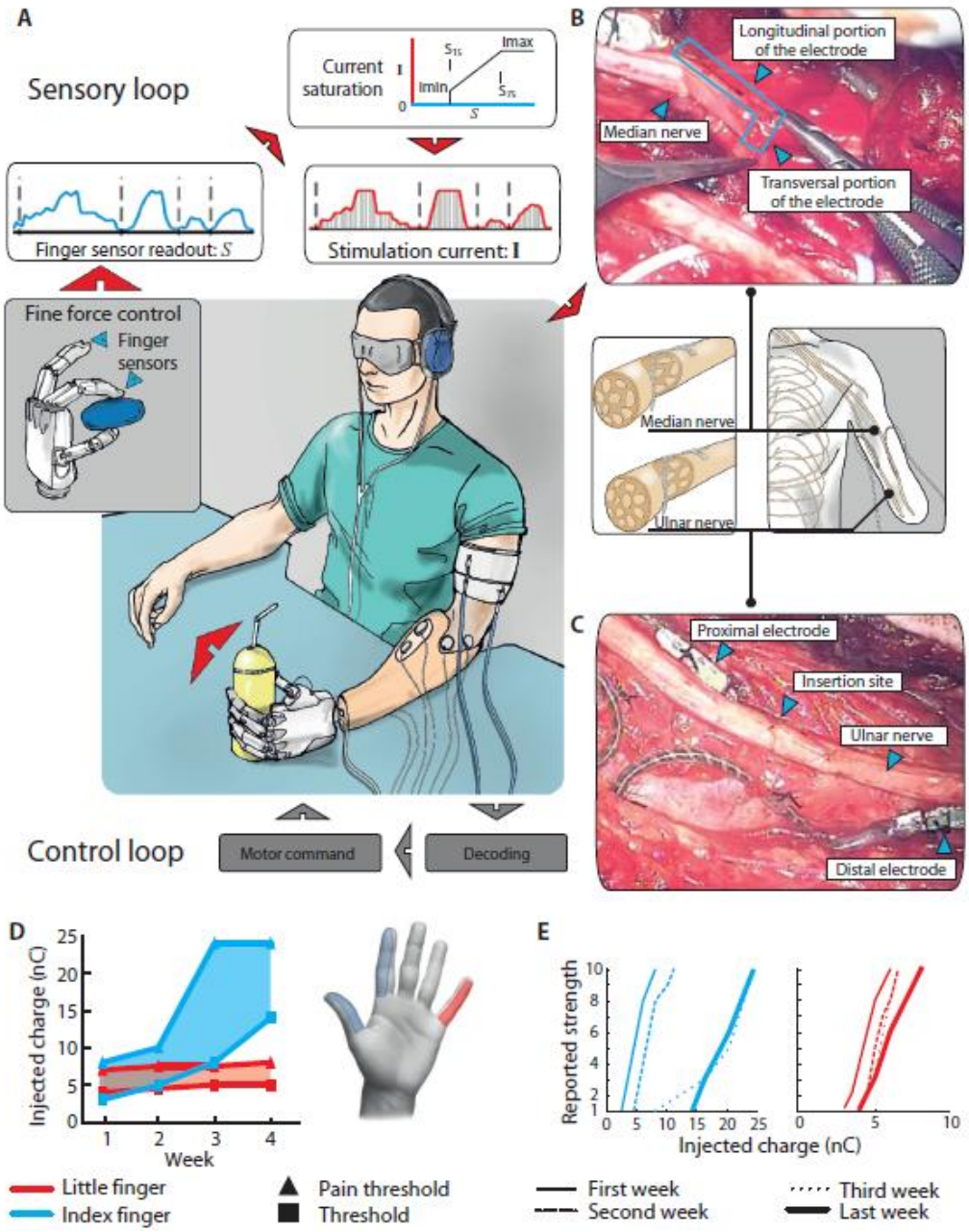


**Fig. 4.1. Bidirectional control of hand prosthesis and characterization of neural stimulation.** During experiments, the participant was blindfolded and acoustically shielded. The real-time bidirectional multiple-grasp control of the hand prosthesis involved both a reliable decoding of the user's motor command, immediately converted into hand motion (control loop), and a simultaneous readout from prosthesis sensors fed back to the user through intrafascicular nerve stimulation (sensory loop). The decoding

was performed by processing sEMG signals, while the encoding was simultaneously achieved by intrafascicular stimulation of the median and ulnar nerves using TIMEs. **(A)** The current is delivered as a function of the prosthetic hand sensor readouts. $S_{15}$ and $S_{75}$ are the 15% and 75% of the range of sensor values, respectively. **(B**) A photograph of the surgical insertion of a TIME electrode in the median nerve of the participant. **(C)** A depiction of the subject's ulnar nerve with the two implanted electrodes. **(D)** Time course of the reported threshold and saturation of sensation over 4 weeks in the little finger (red) and index finger (blue). The sensation threshold corresponded to the minimal sensation of touch reported, while saturation ("pain threshold") was defined as the charge that elicited a nearly painful touch as reported by the subject. **(E)** Sensation strength reported on a scale from 1 to 10 for each of the four weeks.

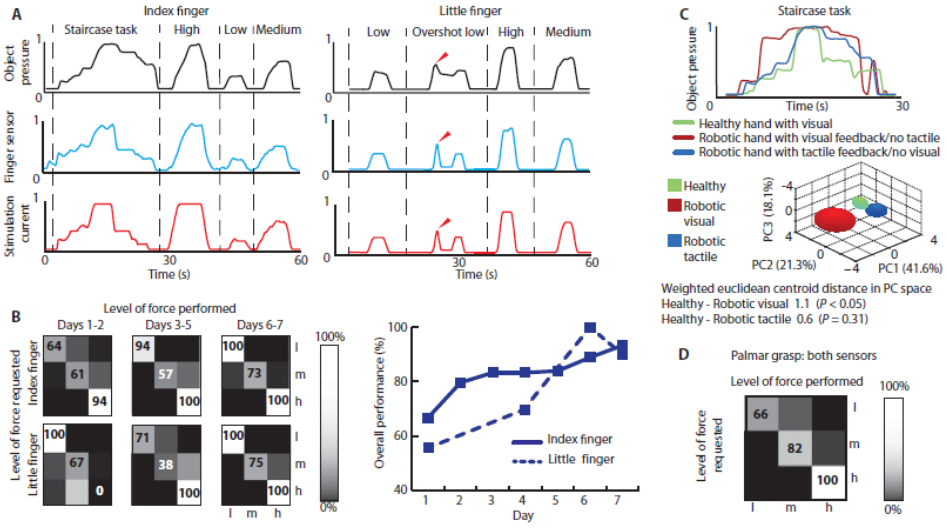


**Fig. 4.2 - Fine force control.** (**A**) External pressure sensor outputs (black) normalized to 1.5 kPa, hand sensor readings (blue) normalized to 60 N, and stimulation current amplitude (red) normalized to 240 μA and 160 μA, for the index and little finger, respectively, during force control task for the index and little fingers. A red arrow indicates when the subject recognized an overshoot in the exerted pressure. Data are representative of *n* = 200 trials. (**B**) Confusion matrices of the requested versus exerted force levels for the index (*n* = 128 repetitions in 7 sessions) and little finger (*n* = 72 repetitions in 4 sessions). On the right, data are presented as the overall performance improvements during the experiment time course. (**C**) Performance of the hand without tactile feedback (visual only) compared in the PCA space with that of the hand prosthesis with induced tactile feedback (no visual) and that of the healthy hand (*n* = 21 repetitions). The ellipsoids represent the location of each data group in the PC space (center: mean; semi-axis: S.D.). (**D**) Confusion matrix for force control task with a palmar

grasp (*n* = 111 repetitions in 2 sessions). In matrices in (B and D): l=low, m=medium, h=high force levels.

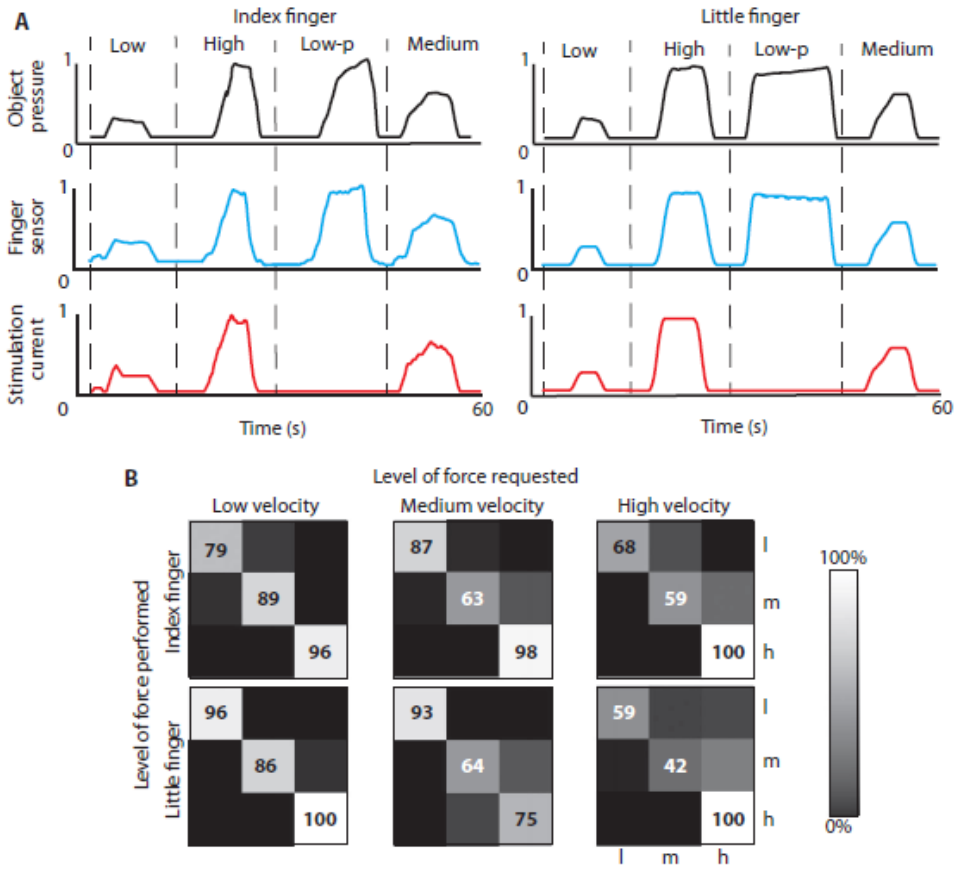


**Fig. 4.3 - Fine bidirectional control is due to integration of the restored sensation into the bidirectional loop.** (**A**) This test was similar to Figure 3B except with placebo trials. Examples of placebo trials, randomly mixed during the sessions of the fine force protocol, are shown in "low-p". During these trials, the participant was asked to apply the minimum level of force but with the electrical stimulation turned off (no feedback from the sensors of the hand prosthesis). External pressure sensor outputs (black) normalized to 1.5 kPa, hand sensor readings (blue) normalized to 60 N, and stimulation current amplitude (red) normalized to 240 μA and 160 μA for the index and little finger, respectively, during force control task for the index and little fingers. (**B**) Confusion matrices of the requested versus performed force levels for the index and little finger at different velocities. The performance at different velocities of the robotic hand motors actuation was evaluated to exclude the possibility that the participant could have learned to control the force by associating the control with the time needed for hand prosthesis closure (*n* = 294 in 7 sessions for the index finger and *n* = 155 in 4 sessions for the little finger). In matrixes: l=low, m=medium, h=high force levels.

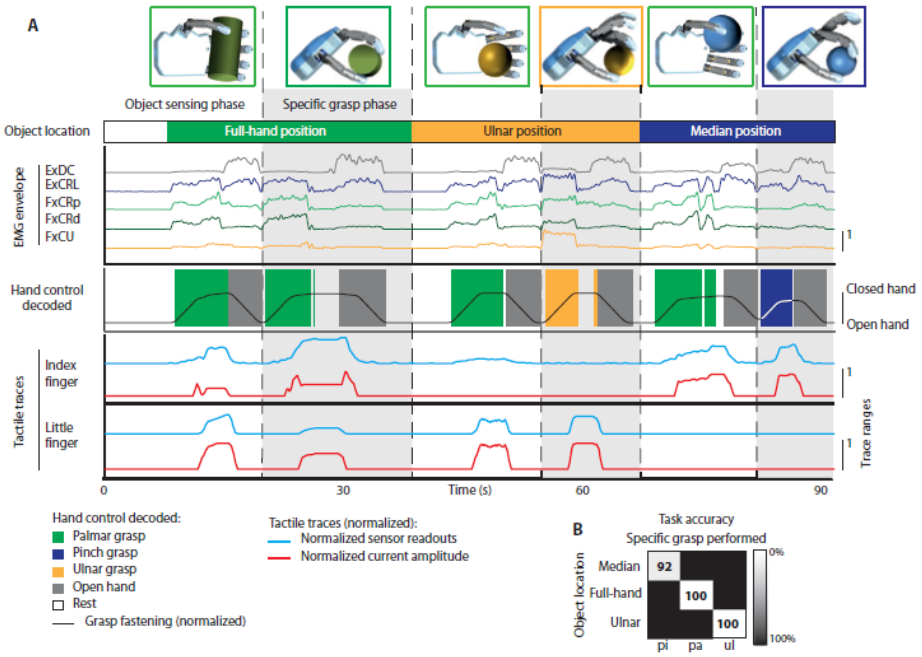


**Fig. 4.4 - Object sensing and selection of the appropriate grasp for handling. (A)** Three task repetitions involving a different palmar location of the object. Sensing phase: the participant performed a palmar grasp to detect the object position, then released the grip. Specific grasp phase (shaded): the participant performed the appropriate grasp for handling the item. The object was then displaced with a translation movement by the arm and released. sEMG signals at five sites (ExDC, ExCRL, FxCRp, FxCRd, and FxCU) were recorded and processed to decode the user's hand motor commands, which drove the opening/closing of the hand prosthesis. The sensory feedback, encoded in terms of the intensity of intrafascicular nerve stimulation, arithmetically depended on the finger sensor traces (tactile traces). (**B**) Confusion matrix indicating a 97.3% mean class accuracy for selected grasps ($n$ = 52). Main diagonal is accuracy for each class. pi, pinch; pa, palmar; ul, ulnar.

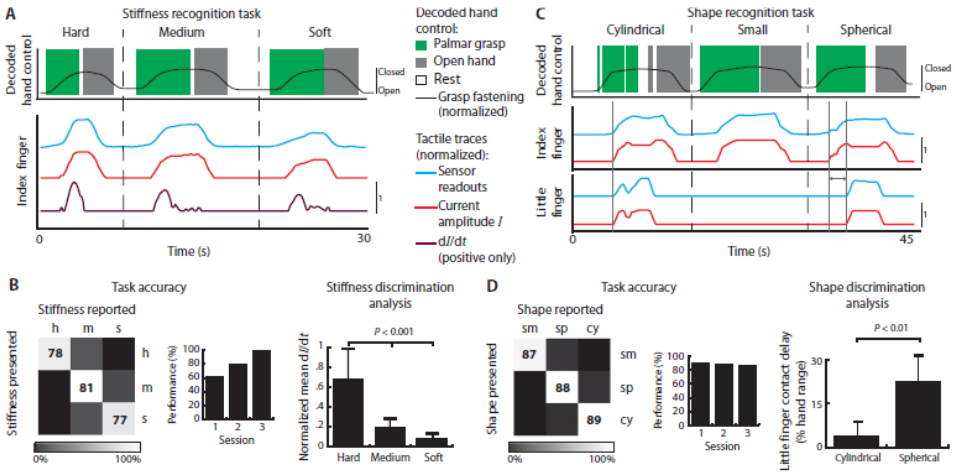


**Fig. 4.5 - Object stiffness and shape recognition. (A** and **B)** Stiffness recognition, discrimination, and accuracy tasks. (A) Hand control decoded from sEMG activity and index finger robotic hand sensor readout and stimulation current amplitude, with its positive time derivative. (B) Confusion matrix and performance quantified for each of three sessions (n=66 repetitions per session) and current time derivative (positive, d$I$/dt) for the three objects. Data are averages ± SD. P-values determined by Kruskall-Wallis with Tukey-Kramer test for multigroup comparison. (**C** and **D**) Shape recognition, discrimination, and accuracy analysis. (C) Decoded motor commands, sensors readouts and stimulation amplitude. The solid vertical lines and the grey double arrow indicate the stimulation onset delay between the median and ulnar sites. (D) Confusion matrix assessing task accuracy, based on the shape of the sensed object reported by the subject, and quantification of performance for each of three sessions ($n$ = 32 total). The contact delay between the index and little finger during manipulation differed between objects that engaged the full hand or partial hand. Data are averages ± SD. P-values determined by Kruskal Wallis test.

## SUPPLEMENTARY MATERIALS

## MATERIALS AND METHODS

### Surgical procedure

In general anesthesia, through a 15 cm-long skin incision on the medial aspect of the left arm, the median and ulnar nerves were exposed to implant a proximal and a distal TIME in each nerve (Fig. 4.S1). The microelectrodes and a segment of their cables were brought into the operating area across four small skin incisions, two laterally and two medially to the main surgical cut. The cable segments were placed in

subcutaneous pockets and secured with sutures. Then, using an operating microscope (Zeiss, Pentero), the single microelectrode was implanted transversally within the nerve fascicles; appropriate microsutures secured the nerve implant in order to maintain a stable positioning of the individual contacts with the adjacent fascicles. Particular care was used to avoid any mechanical stress due to the movements of the transcutaneous cable by means of specific cable loops (Fig. 4.S1C). This implantation procedure lasted seven hours, to guarantee the stability of well-functioning microelectrodes (including impedance measurements of individual contacts).

After 30 days, under an operating microscope the four microelectrodes were removed, in accordance with EU guidelines. At the time of removal, however, the TIME electrodes were still performing extremely well, and their presence did not cause any discomfort to the subject. The follow-up of the clinical condition of the participant 6 months after the end of the protocol did not reveal any subjective or objective side effects. sEMG-based control of the hand prosthesis (decoding) The sEMG signals were collected differentially (surface disk electrodes in a bellytendon montage) at five sites on the stump, corresponding to the three muscle bellies of Flexor Carpi Ulnaris (FCU), Extensor Carpi Radialis Longus (ECRL) and Extensor Digitorum Communis (EDC) and two additional recording sites located on a proximal and distal position of Flexor Carpi Radialis (FCRp and FCRd), with a grounding site at the Olecranon to complete the setup. Data were sampled at 12 kHz, analogically band-pass filtered between 100 and 1000 Hz, and amplified by 104. They were then collected at intervals of 100 ms. These 1200 samples per channel were then divided in two bins of 50 ms. The following parameters were extracted (Englehart et al., 2003, Zecca et al., 2002) for each of these sequences:

- Signal Variance;
- First half of the Fast Fourier Transform (FFT) components integrated;
- Second half of the FFT components integrated;

• Difference between the amplitude of the first and the second half of the samples in the bin.

All the features extracted were stacked in a vector and processed by a 3-layer multilayer perceptron (MLP) network that provided one output node for each possible hand motion, plus an additional one for the rest state. The decoded state competition at the final layer was solved by a winner-takes-all strategy. The MLP was trained using a supervised learning approach after a set of sEMG data had been collected in a specific initial session of approximately 50 seconds, in which the subject was asked to perform a sequence of three 2s-long repetitions for each hand movement that had to be classified by the network ('Pinch Grasp', 'Little Finger Grasp', 'Palmar Grasp', 'Hand Opening'), separated by 2s rests. The hyper-parameters of the MLP (number of hidden neurons, learning factor, momentum factor, and number of training iterations) were one-off extracted on an initial dataset. Parameters optimization was performed through grid-search, in a leave-one-out cross-validation. During online classification, possible chatter from the MLP output was smoothed using hidden Markov model (HMM) filtering; i.e., the current state of the user's desired hand control x(t), which was assumed to have generated the last observed instance of the EMG signal feature vector y(t), was estimated by choosing the most likely value of the distribution $P(x(t)|y(1),\ldots y(t))$. The HMM transition weights were fixed at 0.5 to keep the current state, and at 0.1 to switch to any new state. The final output was transferred to the hand prosthesis within a soft real-time deadline set at 100 ms, when the next sEMG signal block was made available. This means that the user's motor intention was evaluated by the decoder 10 times per second, in each of this time points the participant was in control of the grasp position and could a) increase progressively the fastening of the current grasp, b) release progressively the current grasp, c) switch to another grasp in the repertoire just by changing the pattern of recorded muscle activation accordingly. Switching between grasps was allowed only when no contact was reported by the hand sensors. The desired hand motion resulted in a progressive opening or closing of the fingers involved in the user-selected

grasp by approximately 2% of their motion range per output valuation cycle when the finger sensors did not report contact with an object, and 0.5% in the other case. Performance of sEMG-based control of the hand prosthesis (decoding) In order to evaluate the performance of the decoding algorithm, a test using the datasets collected during the decoder training procedure was carried out. Each of these datasets features 3 repetitions for each of the 4 possible hand motions, as described in the paragraph "sEMG-based control of the hand prosthesis (decoding)" of the main body of the manuscript. MLP decoding precision over 7 such datasets, assessed in a leave-one-out fashion over trial segments, was 90.2% (mean class accuracy). By applying HMM filtering to the MLP output, the decoding performance increased to 93.5% of the tested datasets.

**Transformation of sensors readouts in stimulation patterns (encoding)**

The relationship between the hand sensors readout and the amplitude of the stimulation current biphasic pulses delivered was implemented as follows:

$c=(cmax - cmin)*(s- s15)/(s75- s15)+ cmin$, when $s15 \leq s \leq s75$;

$c=0$, when $s15 < s$;

$c=cmax$, when $s > s75$;

where:

c is the amplitude of stimulation current; s is the sensor readout; s15 and s75 represent 15% and 75% of the maximum range of the sensor readout, which characterize, respectively, the contact point of the robotic hand with an object and a value tuned to exploit the full range of sensations for all objects; cmin and cmax are the stimulation current amplitudes that elicited, respectively, the minimum and the maximum (i.e., below pain threshold) touch sensations, as reported by the subject. The injected train of biphasic pulses had a frequency of 50 Hz, and each pulse lasted 100 and 50 μs, respectively, for index and little fingers. cmin and cmax were 100

and 240 μA and 80 and 160 μA, respectively, for index and little fingers. Under the condition of object contact, the stimulation was continuously delivered and its current amplitude was updated every 100 ms. Specifically, the soft real-time algorithm dedicated to the sensory loop was able to read both hand sensors outputs and to encode the respective sensory stimulation within this time frame of 100 ms. Simultaneously, the algorithm dedicated to the control loop was able to acquire, process, and decode the sEMG signals and to deliver the motion command to the robotic hand, all within the same 100 ms frame, which is imperceptible for a prosthesis user (Farrell et al., 2007). In the case of multiple sensor contacts, a threshold on the maximum injectable current was applied to avoid an excessive current delivery that could have resulted in painful sensations.

**Experimental design details**

*Real time fine force control*. During the fine force control task the subject was instructed to apply, using the bidirectional robotic hand, three different force levels over a pressure sensor chamber and to hold them for approximately 2s. Depending on the experiment, he was engaged either in repeated up-down transitions from the lowest to the highest sensed pressure level and vice versa ("staircase" task) or single level press-and-release trials, where he was asked to replicate a randomly generated sequence of pressure levels. We designed three further tests. First, the user was asked to execute the "staircase" task with visual and acoustic cues but without sense of touch to compare his performance while controlling a bidirectional or a myoelectric prosthesis to natural hand control. Then, we randomly selected a few press-and release trials in which was switched off the nerve stimulation while asking the patient to reach a medium or low level of force to show the unfeasibility of the task without the induced sense of touch. Finally, in order to exclude the possibility that the participant could have learnt to control the force by associating it with the time necessary for the hand prosthesis to close after a voluntary command, the subject was asked to execute the fine force

control task while the robotic hand actuation speed was switched in a random order, and without notification to him, to three possible different values. The experiments were repeated for pinch, ulnar, and palmar grasps. Overall, the subject performed 560 trials during fine force control testing. The index finger trials were 294 in total divided into 7 sessions (82 trials at low velocity, 128 at normal velocity and 84 at high velocity), the little finger trials were 155 divided into 4 sessions (47 for low velocity, 72 for normal velocity and 36 for high velocity) and the cylindrical grasp force trials were 111 in total divided into 2 sessions. The cases of self-correction—reported in Fig. 4.1A with a red arrow—are particular examples that occurred in sporadic cases in which the subject initially made an error, sensed it, and adjusted to a correct pressure level. We consider these traces representative examples of bidirectional prosthesis control.

*Functional grasping*. In the functional exploration tasks the subject controlled a voluntary palmar grasp in order to understand, through sensory feedback, the location (ulnar, median, or full palm) over his prosthesis of three different objects: a cylindrical one, engaging the whole palm and two smaller ones located in the median or ulnar sides. According to the recognized item positioning the participant had to grasp it with an appropriate command (palmar for the cylindrical object, pinch or ulnar for the median and ulnar located small objects) and to deliver it to the person sitting in front of him or at his right side (in both the median and ulnar locations, but with different arm motion directions) or to raise it (full palm case). A total of 52 repetitions were performed.

*Sensing of environment: Object properties recognition*. During the object stiffness recognition task the participant was asked to grasp objects with different stiffness and to rely on the sensory feedback to understand the specific physical property. The items were a hard piece of wood, a medium stiffness- stack of plastic glasses, and a soft cotton pack. Finally, in the object size/shape recognition task, the subject was asked to perform a palmar grasp to explore the object (three possible shapes), then report his

sensation and release the grasp. The three different items were: a cylindrical object (a bottle), a big spherical object (a baseball), both covering the whole hand palm, and a small spherical object only partially covering the hand palm (a mandarin orange) placed either in the median or ulnar area of the hand. A total of 66 and 32 repetitions were carried out for the stiffness and shape recognition tasks, respectively.

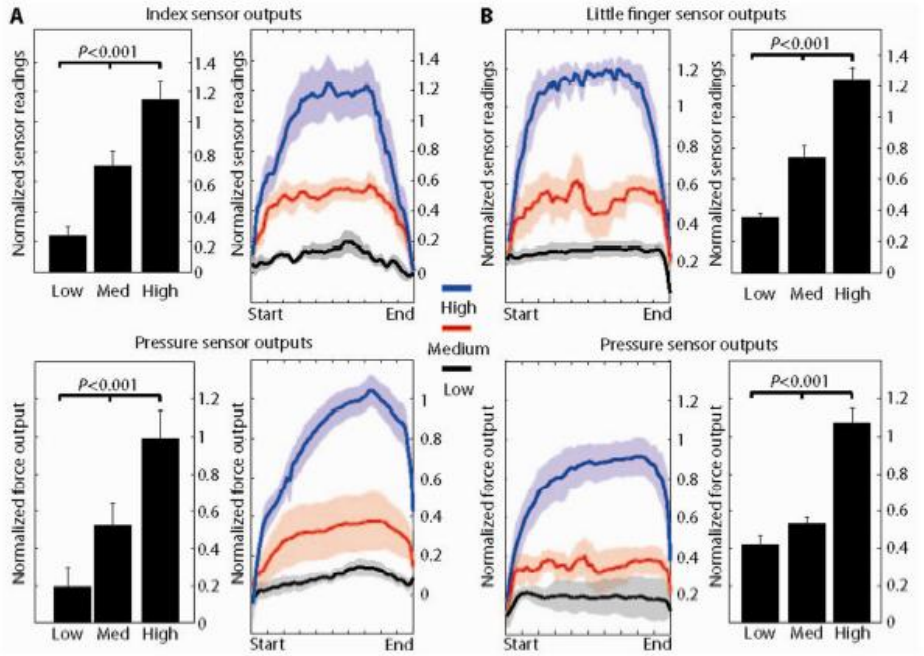


**Fig. 4.S1. Force reproducibility.** (A and B) Statistical analysis and reproducibility of the force output are presented for the index finger (A) and little finger (B). A Kruskall-Wallis test with a Tukey-Kramer post-hoc test for multi group comparison was performed over all the index and little fingers single press-and-release trials (n = 76). The test shows three significantly different levels achieved in terms of the maximum force-per-level reached. Time course plots (4.7 seconds median duration, interquartile range 3.8 s) show the shape of the executed levels normalized over each cycle length as an average ± S.E.M. in shaded regions (n = 7 sessions for the index finger and 4 sessions for the little finger).

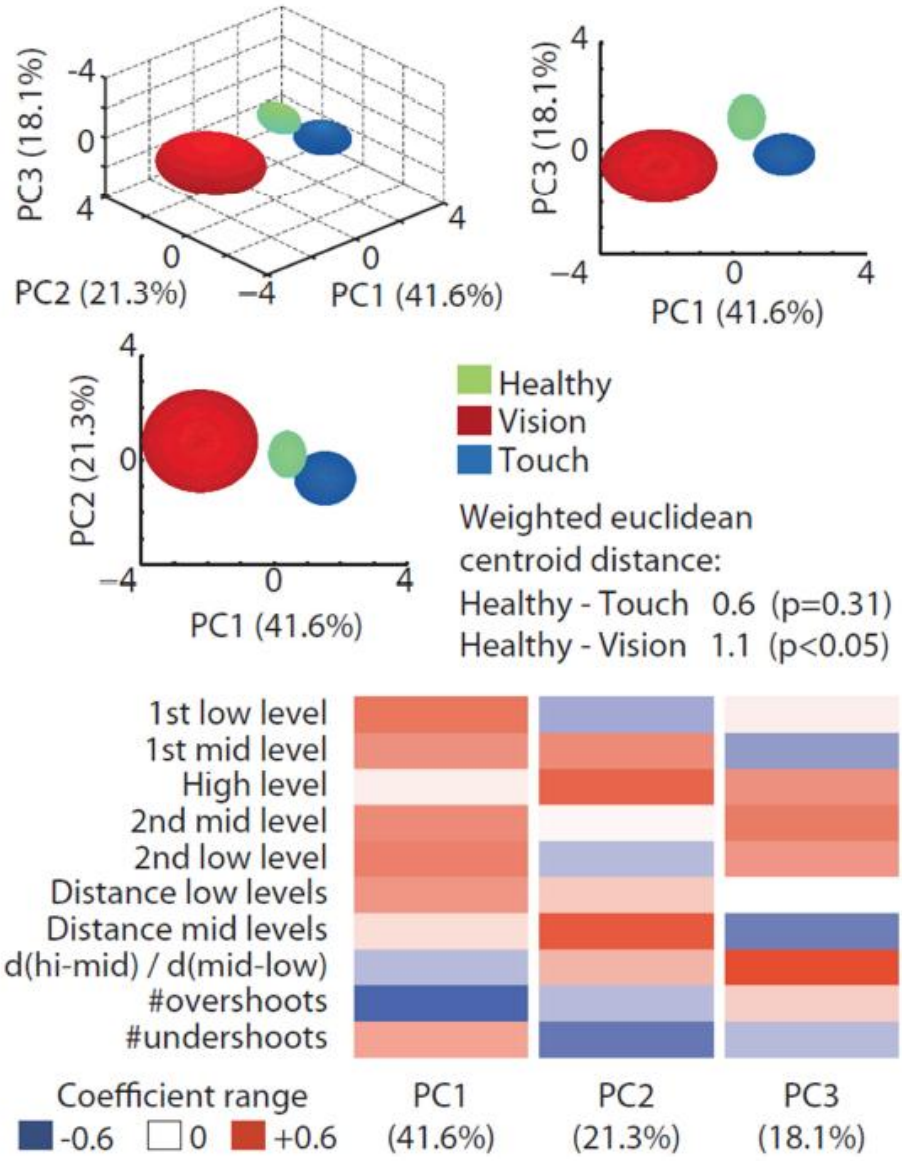


**Fig. 4.S2. PCA analysis of the staircase task.** A PCA analysis of parameters describing the staircase profiles was performed to evaluate the performance of the healthy hand against the prosthetic hand with induced sensory feedback (subject being blindfolded and acoustically shielded) and without sensory feedback (but visual and acoustic feedback available). Ellipsoids represent the location of each data group in the PC space (center: mean; semi-axis: S.D.). The extracted parameters measured each level position, repeatability (distance between repetitions of the same level), staircase shape (distances between levels), and control accuracy (number of overshoots or undershoots).

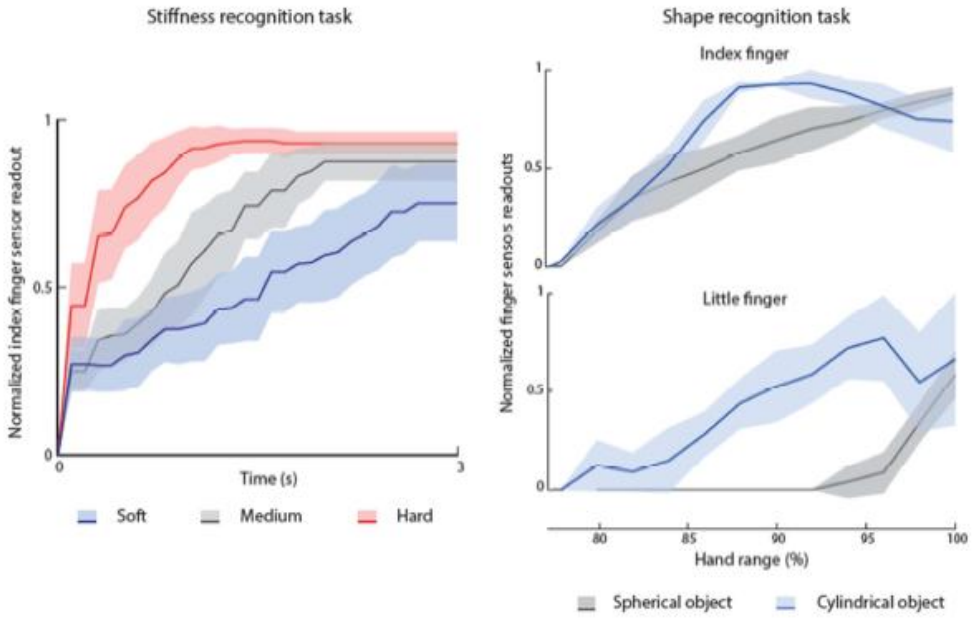


**Figure 4.S3. Variability of sensor data in stiffness and shape recognition tasks.** The sensors' profiles for all trials are averages ± S.E.M. (shaded area). Profiles are plotted from threshold to saturation.

# Chapter 5 Sensory substitution in amputees: intraneural versus transcutaneous nerve stimulation for bidirectional prosthetic control

**ABSTRACT**

Sensory feedback is essential for a sophisticated and effortless hand control. Appropriate sensations from the periphery and its interaction with the external world are essential for correct agency and ownership of the hand. Sensory feedback in amputees could be conveyed both by direct neural stimulation via implantable devices or by means of superficial transcutaneous electrical nerve stimulation (TENS).

In this work, we systematically compared intraneural and superficial nerve stimulation effects, both in open (sole stimulation) and in closed-loop (i.e. integrated in a bidirectional prosthesis). The same transradial amputee has been stimulated by TIME electrodes implanted in median and ulnar nerves and by TENS.

We provided the two types of stimulation, in single and multi-polar configuration.

We showed that intraneural single channel stimulation elicits close-to-natural touch sensations over discrete areas of phantom hand, while TENS provides a more fuzzy-localized paresthesia.

For the first time, we unveiled the effects of multipolar stimulation, which evoked, in some cases, linear combinations and, in others, non-linear summation of single-sites sensations. Unexpectedly, in the latter condition, the referred perceived area was completely different from those related to the single sensations.

Finally the control performance during the bidirectional prosthetic control was evaluated when TENS feedback was used, and compared to results reported with the intraneural stimulation. We showed that similar performances can be achieved with the two approaches.

Overall these results pave the clear guidelines into the possibilities of use of non-invasive and invasive solutions for sensory feedback in the next generation prosthetic devices.

## INTRODUCTION

Tactile feedback plays a pivotal role in objects manipulation (Johansson and Flanagan, 2009) and in grasp force modulation, which is essential for a sophisticated and effortless hand control, especially during high precision tasks. For the successful control of grip forces such that they are adequate to prevent accidental slips but not so large that they cause unnecessary fatigue or damage to the object or hand, it is essential the correct interplay between voluntary commands and perceived feedback.

Moreover, appropriate sensations from periphery are essential for the embodiment of the hand (Botvinick and Cohen, 1998; Armel and Ramachandran, 2003; Ehrsson et al., 2004; Tsakiris and Haggard, 2005; Longo et al., 2008; Moseley et al., 2008, Blanke et al., 2002).

The first powered hand prosthesis appeared over 50 years ago (Bottomley et al., 1965) and enabled the users to perform one-degree-of-freedom movements.

Even if lot of research has been done in development of more sophisticated robotic devices, or controlling algorithms, clinically relevant advancements were not achieved until the last 15 years. The invention of

Targeted Muscle Reinnervation (Kuiken et al., 2009) enabled subjects with shoulder disarticulation and transhumeral amputation to homologously and reliably command several DoFs of a robotic arm. Very recently the selective and continuous recording of intramuscular electrical activity (Pasquina et al., 2014) permitted an amputee to move independently single prosthetic fingers (i.e. the thumb).

On the other side, even if the need for sensory feedback has been expressed almost a decade ago (Biddiss et al., 2006), just recently technology became mature enough to enable the feasibility of the close-to-natural sensory substitution by means of intraneural electrodes (Dhillon et al., 2005, Rossini et al., 2010). On the parallel track the use of transcutaneous electrical nerve stimulation has been proposed (Kaczmarek et al., 1991, Patterson et al., 1992), but without the achievement of significant results.

Recently, the proof-of-concept of the restoration of the sensory feedback, by means of intraneural stimulation, during the multi-degree-of-freedom bidirectional control of prosthesis, has been shown (Raspopovic et al., 2014). Successively the longevity of sensory feedback restoration has been demonstrated within one-degree-of-freedom control, by means of cuff-like electrodes (Tan et al., 2014, Ortiz-Catalan et al., 2014).

However it is still unclear what can be achieved by means of non invasive methods with respect to surgically implanted electrodes, what could be the effects of multipolar stimulation (which is often proposed but not tested in humans), and how the addition of sensory feedback to prosthesis could be assessed (Farina et al., 2014).

To reply to those questions, we systematically compared the sensory feedback provided by means of invasive and non-invasive nerve stimulation strategies. In particular, we implanted the median and ulnar nerves of a transradial amputee with TIME electrodes (Boretius et al., 2010) for a month (Raspopovic et al., 2014). We characterized the subject's responses to single and multi-polar stimulation and we integrated the sensory feedback restoration in the closed-loop control of a

bidirectional prosthesis (Raspopovic et al., 2014). Then, we repeated this experiment with the same volunteer, recurring to the use of TENS. With the goal to prepare the perfect set-up for the exploitation of non-invasive nerve stimulation, we first run a trial on healthy subjects.

In order to assess quantitatively the effect of the different strategies of sensory feedback restoration, we designed a set of principles, accounting for the patient perception experience and the received augmentation: (i) **efficiency** (in terms of selectivity and modulability), objectively reflected in the proper sophisticated and effortless prosthesis control; (ii) **natural-like** sensation subjectively reported by the user and objectively manifested by the absence of necessity for a training before the use of the device; and (iii) **generalization** (the unexpected use of sensory feedback for a more sophisticated building of sensations) showed by the ability to use the sensory feedback for tasks not planned a-priori.

## RESULTS

### Open loop sensory feedback restoration by intraneural stimulation

In order to evaluate the effect of invasive sensory feedback restoration we implanted 4 intraneural electrodes, in equal number in the median and ulnar nerves of a volunteer with hand amputation. Such implant was executed proximally to the elbow (Fig. 5.1A), hence, the procedure is amenable for all types of transradial amputees.

Then, we injected through all the active sites of the electrodes (alone or in combination) trains of cathodic biphasic pulses. Their amplitude and duration were varied, respecting the safety limits of injectable charge for the electrodes. Frequency was fixed at 50 Hz. Feedbacks from the amputee were acquired in terms of sensation intensity (in a scale between 1 and 10), location, extension, type.

Impressively, the participant reported close-to-natural and very localized sensations (Fig. 5.1B), covering, in overall, the majority of the areas innervated by median and ulnar nerves. More in particular, by median

nerve stimulation, sensations over the first two fingers and underlying palm were elicited. Instead, when the stimulation was delivered through the electrodes implanted within the ulnar nerve, the subject referred sensations over the small finger, underlying palm, and lower (close to dorsal) palm.

Types of sensations ranged from natural touch, waving pressure, needle pinch, to movement like (which was reported very closely to muscles activation), and vibrations. Remarkably the positioning of the sensations, other than being clearly delineated, was stable for all the intensities of injected currents while the reported area increased slightly with them (Fig. 5.1B). Most importantly, we observed that the sensation intensity was modulable with the charge delivered to the subject's nerves from minimal perceivable touch, until close to pain sensation (Fig. 5.1C). This property is essential for achieving fine force control with the bidirectional prosthesis (Raspopovic et al., 2014).

As following step we performed an extensive mapping of the effects deriving from several channels simultaneous (multipolar) stimulation. In particular, the active sites that gave pleasant sensations to the amputee were stimulated simultaneously and studied. The stimulation parameters were changed similarly to what reported for the single channel characterization procedure.

Remarkably, two different types of results were observed: the linear summation of effects (green and red in Fig. 5.2A) or, unexpectedly, the transformation of the sensation location (blue). Moreover, double channel charge was inferior with respect to the single channels thresholds (Fig. 5.2B).

**Open loop sensory feedback restored by TENS**

In order to evaluate whether non-invasive stimulation could elicit a reliable sensation to integrate in the closed loop control of a bidirectional prosthesis, we injected current through electrodes located at different positions over the arm and forearm of 8 healthy volunteers (Fig. 5.3A). We

delivered trains of biphasic cathodic pulses at a frequency of 50 Hz, on one or two electrodes (corresponding to two different nerves) at time.

The current amplitude and the width of the pulses ranged respectively, between 2-6 mA and 20-500μs. We took record of subjects' referred location, area, type and intensity of the sensation (in a scale between 1 and 5) on the hand as well as on the skin under the electrodes (in loco sensation), and muscle activation.

A clear sensation on the hand was reported, only for some of the configurations corresponding to sites where median and ulnar nerves are anatomically close to the skin, in particular above the elbow for the ulnar nerve and at the level of the wrist for both nerves. It is interesting to notice that increasing over 10 mA the amplitude of the injected current would have probably elicited hand sensations for all the tested electrodes configurations. However, considering the unpleasantness of the stimuli on the skin, reported by the volunteers, we discarded this possibility.

As expected, the superficial stimulation resulted to be not extremely selective. Indeed, once the sensation was reported, it covered almost all the receptive areas of the median or the ulnar nerves (Fig. 5.3B). Remarkably, though, the intensity of the reported sensation could be modulated in relation of the injected charge from the minimum perception to discomfort (Fig. 5.3C). The extension of the perception, moreover, increased with the injected charge (Fig. 5.3D). In all the subjects, only paresthesia was reported.

When multipolar stimulation was provided to subjects (Fig. 5.4A), as in the case of invasive stimulation, they referred two kinds of feedback (Fig. 5.4B). The area of the evoked sensations over the hand resulted or from linear summation or from nonlinear combination of the areas produced by separated single electrodes stimulation. Furthermore, we found that the threshold for eliciting a sensation in the case of double channels stimulation was inferior than the single channels ones (Fig. 5.4C). The type of sensation reported was paresthesia.

In conclusion, superficial stimulation resulted to be a non-selective tool for sensory feedback restoration. Additionally, since the electrodes configurations that are efficient for eliciting sensations are mainly in the forearm, its transferability may be limited only to trans-radial amputees.

However, the observed sensation modulability provided strong justification for trial on amputees with the bidirectional prosthesis.

Because of these results, on the same subject underwent intraneural electrodes implant, we explored the possibility of eliciting a reliable sensation over the phantom hand.

Relying on the pilot run with healthy subjects, we investigated whether the participant presented a spot on the skin where the nerve was superficial. We found, by tactile exploration, that he had the neuroma in the middle of the forearm, hence we placed, for the following experiments, the electrodes just proximally to this location (Fig. 5.5A).

Comparably with the case of healthy subjects, the reported type of sensation was paresthesia, for all the delivered stimuli. Coherently with the mentioned pilot, the stimulation was not selective and the extension of the reported sensation was highly dependent on the injected charge (Fig. 5.5B). The charge necessary for eliciting a reliable sensation was quite high (almost twice the values observed in normal-bodied tests, Fig. 5.5C). The perceived intensity was modulable but only up to a certain extent because of the unpleasantness of the in-loco stimulation (Fig. 5.5C). Interestingly, the sensation did not cover all the receptive areas of median or ulnar nerves, probably because it was not possible to recruit all the necessary afferent fibers, due to the limit imposed by the in loco current injection.

Finally, when the multipolar stimulation was performed, the reported perception covered a hand area, corresponding to the non-linear combination of the separated single channels sensations (Fig 5D, E).

In conclusion, these results suggest that the sensory feedback restored by invasive stimulation was more efficient and more natural-like (as qualitatively reported from the subject) than by TENS.

**Closed loop bidirectional prosthesis control**

Successively, in order to quantitatively evaluate the naturalness of the sensation elicited by TENS and compare it with the intraneural case (that we have already reported in Raspopovic et al., 2014), we integrated it in the closed loop control of the bidirectional prosthesis and performed the full set of experimental measurements as in (Raspopovic et al., 2014).

Tests were first performed to assess whether the induced dynamic sensory feedback could lead to a voluntary and reliable modulation of the grasping force exerted with the prosthesis. During these trials, the participant was blindfolded and acoustically shielded. He was asked to repeatedly produce three different force levels on a dynamometer, relying on the induced sensory feedback, when performing pinch, ulnar, and palmar grasps (Fig. 5.6).

The participant was able to accurately control 3 different levels of grasp force in single-level press-and-release trials (Fig. 5.6A). He succeeded in the required task by voluntarily controlling pinch, ulnar and power grasp, reaching an overall success rate higher than 80% in the last two sessions (Fig. 5.6B, C). These results, though, are slightly inferior to those obtained with the intraneural feedback (inset in Fig. 5.6B). 89.3% for pinch, 83.3 % for ulnar and 80% for palmar, with respect to 91%, 91.6% and 82.6%, were achieved in the noninvasive and invasive cases, in the order.

To evaluate whether the results were only due to the restored sensations, two different control conditions were designed and tested ("placebo" tests). In one test, during press-and-release trials we switched-off the nerve stimulation, while asking the patient to reach a medium or low level of pressure: the maximum possible force was always exerted, hence, no control was ever possible in this configuration (Placebo in Fig. 5.7A). In another test, the velocity of hand actuation was changed without notifying

it to the subject, in order to falsify the hypothesis that the user could still learn the force level exerted from the prosthesis closure time (Fig. 5.7B).

The achieved performances imply that the participant was not relying on the timings of closure to reach a desired level of pressure. In fact, if this was the case, then both the slower and faster velocity should have resulted in poor or at least reduced performances. Performances were stable at higher velocities (overall accuracy of ~70% for the index finger, ~93.3% for the little finger, and ~91% for power), as at lower ones (74%, 82%, 91% rate of success over all sessions). These results prove that the force control exclusively relied on the induced sensory tactile feedback.

The statistical analysis of the performances, as measured from the hand sensors and from the dynamometer, demonstrates that with index finger (Fig. 5.8A), little finger (Fig. 5.8B) and power grasp (Fig. 5.8C), the subject was able to apply consistently three significantly different force levels (Tukey-Kramer test, $p<0.001$ on all trials), relying on the sensory feedback.

## DISCUSSION

Restoration of sensory feedback in amputees is a problem with several possible pathways to solution. Two of them, intraneural and transcutaneous stimulation of residual nerves, which are on different ends of the invasiveness level, were robustly studied and compared in the present work.

The striking difference between intraneural and transcutaneous stimulation is that the minimum elicitable area over the hand is much bigger in the latter case, confirming the expected higher selectivity of invasive sensory restoration approaches. Indeed, only isolated nerve portions, or even only the single fascicles are solicited when intraneural stimulation is used, while with the transcutaneous one the whole nerve is stimulated.

The types of sensations reported in the case of intraneural stimulation were mainly close to natural and physiologically plausible touch, while in the case of the transcutaneous stimulation, paresthesia was dominantly reported by healthy subjects and amputee, combined with substantial in-loco sensation. This is an essential consideration connected to the fatigueless control of the prosthesis, for which, in our opinion, is mandatory to have as natural as possible sensations.

Together with selectivity and quality of the sensation, the other important feature for a successful bidirectional control is modulability. This is an essential requirement in order to obtain fine and controllable force manipulation.

Here we showed that, nevertheless the number of sensation intensities evoked by TENS stimulation (Fig. 5.2B) was smaller with respect to the intraneural case, the user could similarly integrate the feedback in order to achieve the control of 3 levels of force. It has to be noticed, however, that in-loco sensations could have been used as a non-homologues code by the amputee to obtain such a performance.

On this other side, in this work, we did not investigate about the capability to exploit non-invasive homologous sensory feedback for the encoding of higher level sensations (objects shape or compliance). Such exploration should be conducted as prosecution of this study.

Finally, in this work, other than a systematic comparison between invasive and noninvasive sensory restoration strategies, we characterized for the first time, the effect of bipolar stimulation. We showed, surprisingly, that combining different single channel stimulations, generates sensations referred in hand areas not directly elicited by means of them.

As a matter of fact, these sensations could be effectively exploited in the functional tasks of bidirectional control. The power of the multipolar stimulation is in the enhancement of the single-channel elicitable sensations, both by being able to make the linear combination of them, but also by permitting the stimulation of areas that were un-reachable by means of single active sites. Moreover, the current necessary to perform

multipolar stimulation was typically lower than the sum of the two monopolar stimulations. This is beneficial both for the battery of the stimulator, but also for diminishing the nerve damage and for increasing electrode lifetime.

With respect to other useable approaches, the number and extension of referred sensations in the case of cuff electrodes (Tan et al., 2014) is similar to the TIME electrode outcomes. The main difference lies in the fact that the quantitative naturalness of the sensation is higher in the case of intraneural stimulation. Indeed, while in the cuff-like preparation the sensations enabled only an on-off control (at least such type of tasks was presented in the cited work), in the case of intraneural stimulation it was possible to exploit the range of sensations for fine force manipulation and tasks that require dynamic force recognition (e.g. stiffness recognition). Moreover, we did not make any comparison with other non-homologues approaches (Antfolk et al., 2013), since our philosophy is that, on long-term, only by simple, intuitive and effortless bidirectional control the user can capture the prosthesis as part of its own body (Blanke et al., 2002).

In conclusion, as guideline for the use of superficial or invasive feedback for sensory substitution in amputees, it has to be considered a very non-linear trade-off among several factors.

The quality of reachable control is similar when the invasive and non-invasive approaches are used within the bidirectional prosthesis, in terms of precision (performance level). But, in the first place, for higher level amputees, the invasive approach remains the more viable with respect to superficial stimulation. Indeed, the arm height on which electrodes have to be placed in case of TENS is lower than the site of intraneural electrodes implant. Therefore, the category of subjects to be treated is more limited. However, as indicated in our results, the positioning of the stimulating superficial electrodes found in the normal-bodied subjects could vary, in case of amputees, depending most probably, on the type and location of neuroma.

Finally, the quality of the sensation elicited with intraneural stimulation is much more natural and selective than in the case of TENS.

## MATERIALS AND METHODS

### Sensory feedback restoration

A 500 ms train of cathodic biphasic pulses, interleaved with a frequency of 50 Hz, was injected through the active sites of the intraneural electrodes and through superficial electrodes. A forced method of limits was implemented for characterizing the subject response to the current delivery.

During single channel stimulation, one of the current parameters (amplitude and pulse width) was fixed, while the other was increased ("scale injection") within the ranges that were compatible with the maximum injectable charge of the electrodes (120 nC). Feedbacks from the subjects were recorded in terms of type, location, extension and intensity of the elicited sensation.

We changed the two parameters, until we found a scale which elicited all the sensation intensities between minimum perceived and before pain.

The same procedure was conducted in order to implement the simultaneous stimulation of two channels.

### Bidirectional prosthesis integrating TENS and real-time control

The bidirectional prosthetic system was composed of several commercial devices (Prensilia IH2 Azzura robotic hand, Ripple Grapevine NIP signal acquisition system, Odroid U3 single board computer, Hasomed RehaStim stimulator). The robotic hand was attached to the stump of the subject using a custom-made socket (Ortopedia Italia). A custom-developed, multi-threaded C program running on the single board computer served as the central controller for the bidirectional system. The system ran with minimal delays (within 100 ms, Farrell et al., 2007), allowing for real-time control.

The subject's residual sEMG signals were used to decode the intended grasping patterns. The decoded information was subsequently fed to the robotic hand using progressive position control, allowing for gradual opening and closing of the fingers. The estimated force readout was used to drive the current-controlled stimulation delivered through two surface electrodes located on the stump (one location corresponding to stimulation of the median nerve, the other corresponding to stimulation of the ulnar nerve). The stimulation elicited referred sensations of tingling (paresthesia) over the phantom hand. The stimulation frequency and current amplitude were maintained at a fixed value throughout the experiments, whereas pulse width was modulated proportionally to the estimated force readout to provide the corresponding sensation.

**sEMG-based control**

The sEMG signals were acquired at 1 kHz from 4 differential channels. Every 100ms the buffered data was read, and the processing was applied on the whole window. After the data was filtered using a band pass filter (80-400 Hz), features were computed and passed on to the classifier (KNN, k=3), which provided one of 5 possible classes as an output. The classification output was thus refreshed with a frequency of 10Hz.

**Force readout (estimation of applied force)**

In order to estimate the force being generated by the hand without using explicit force sensors, an alternative, indirect method was used. The difference between the desired position imposed on the hand (value between 0-255), and the true, reported position (0-255) was computed. This difference is roughly correlated to the force being applied because of the internal controller of the hand, which will deliver increasing amount of current to the motors if the desired position cannot be reached.

**Transformation of sensor readouts in stimulation patterns (encoding)**

The estimated force readout from the robotic hand was used to compute the appropriate stimulation parameters, which were subsequently

delivered to the subject in order to provide a corresponding sensation. The estimated force was obtained from the little finger and the index finger. An encoding algorithm computed the stimulation parameters in real-time, every 20ms (50Hz), and triggered the sensory stimulation.

The relationship between the estimated force and the stimulation parameters was a simple linear slope with thresholds for minimum and maximum intensity. The values of these thresholds were determined during the first exploratory phase of the experiments and were subject specific.

## FIGURES

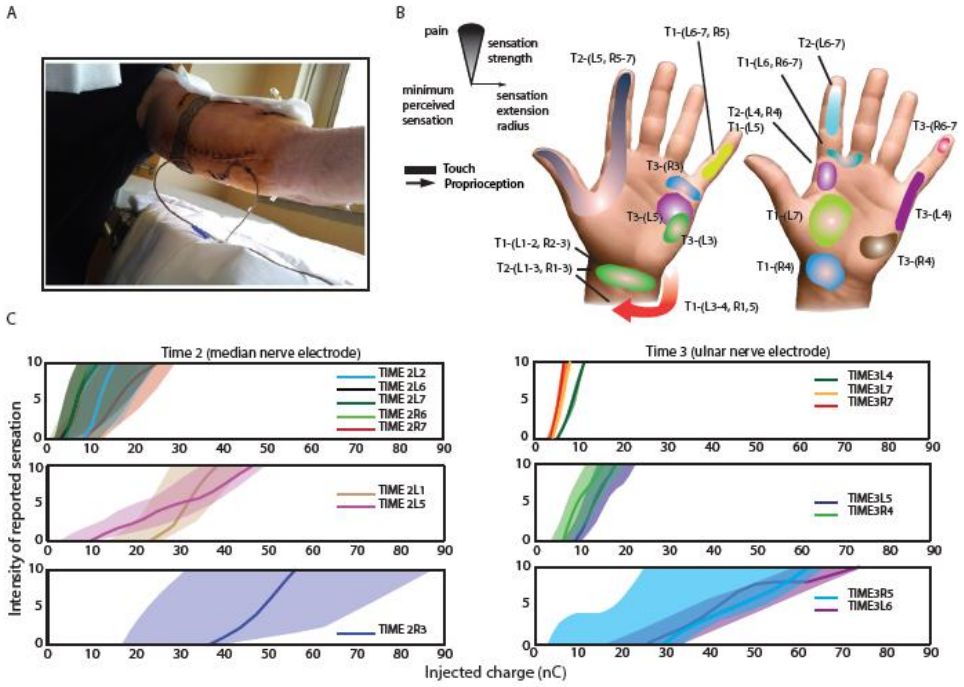


**Fig. 5.1. Single channel intraneural stimulation.** (**A**) Scar on the skin of an amputee due to the surgery for intraneural electrodes implant. Transcutaneous cables come out from holes in the skin aside the mentioned scar. (**B**) Location and extension of the sensation evoked in an amputee by intraneural stimulation. The active sites producing such sensations are indicated by letters. Two hand are showed for visual reason (**C**) Charge necessary to exploit the full dynamics of the referred sensation from minimum perceivable to almost pain. Data are showed in mean and SD, representing the variation in charge along three weeks of stimulation experiments.

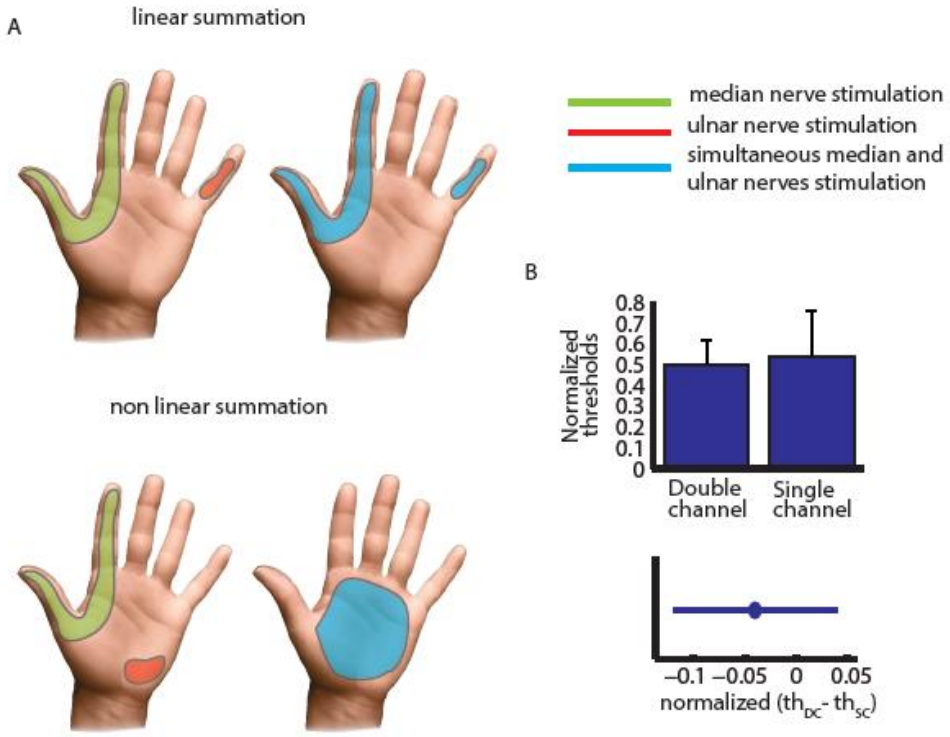


**Fig. 5.2. Intraneural multipolar stimulation. (A)** Two real examples of typical behaviors following mulipolar stimulation are showed: the single sensations are maintaining their positions when combined in the multipolar stimulation (green and red), or mapping into a new position (blue). (B) Double channel charge is inferior with respect to the single channels thresholds.

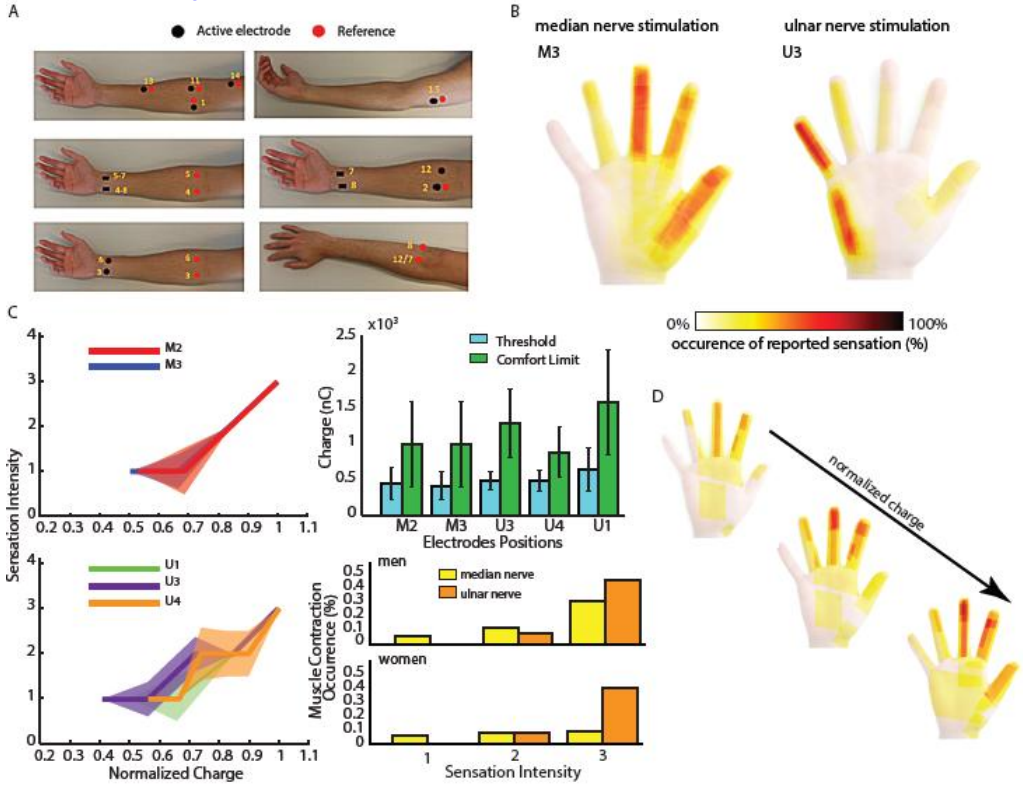


**Fig. 5.3. Single channel TENS on health subjects.**

(**A**) Single channels tested configurations. (**B**) Reported area of sensation (averaged over all the subjects) in case of stimulation with electrodes positioned on the wrist (M3, U3 configurations). (**C**) Intensity of the reported sensation as a function the injected charge (left). Results are normalized to the values showed on the top right and obtained pooling together all the subjects. Median (M2, M3) and ulnar (U1, U3, U4) configurations of electrodes over the wrist are displayed. Muscle contraction is sometime observed (30% of occurrence) when high amount of charge (order of 1000 nC) is injected. (**D**) The extension of the referred sensation increases with the delivered charge. M2=5, M3=7, U1=3, U3=8, U4=15.

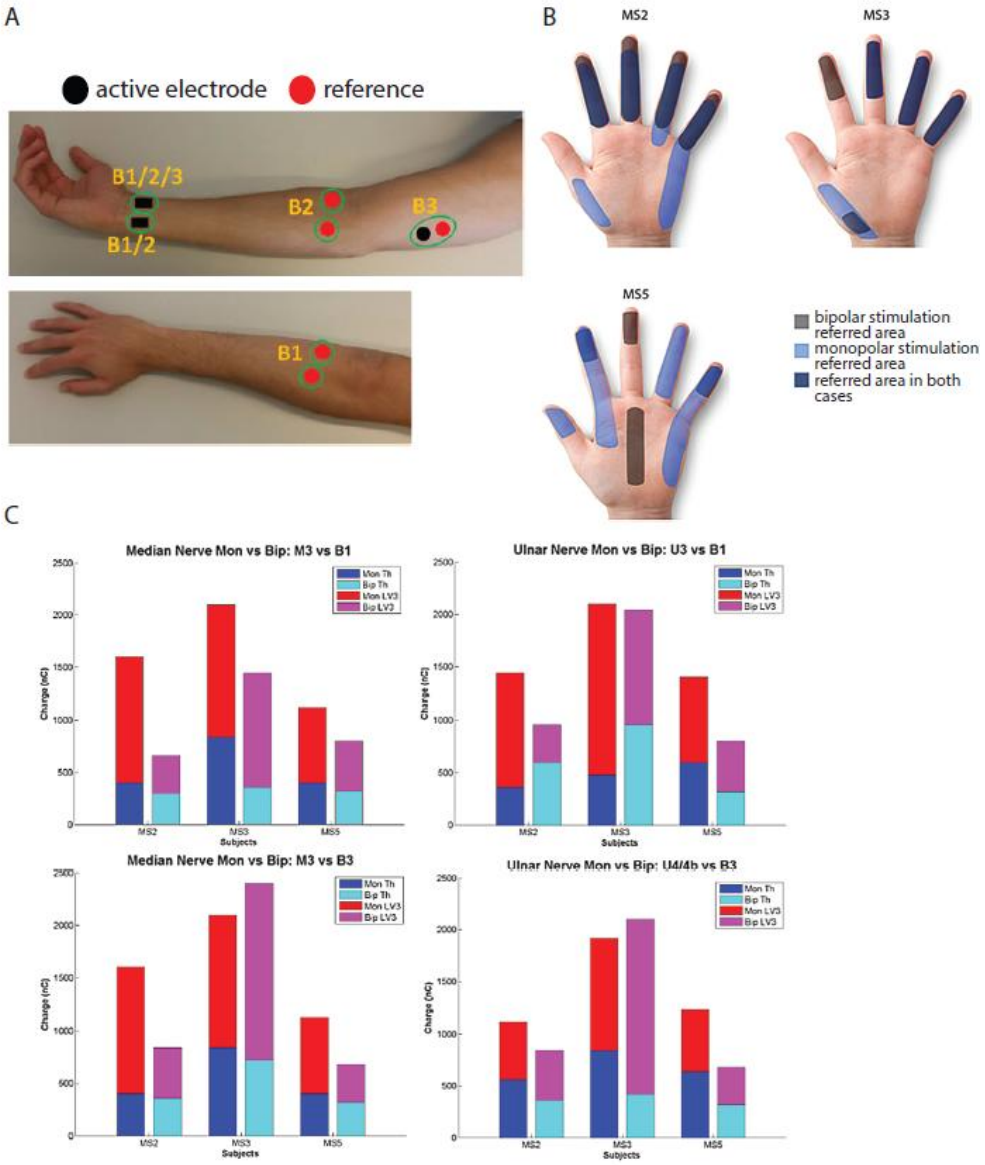


**Fig. 5.4. Transcutaneous multipolar stimulation.** (**A**) Multipolar configurations that produced a stable sensation on the subjects. (**B**) The single sensations are maintaining their positions when combined in the multipolar stimulation (MS2 and mainly MS3), or mapping into a new position (MS5 and index in the MS3). (**C**) The threshold currents necessary when the multipolar stimulation is performed are generally smaller with respect to those corresponding to single channels, similarly as in the intraneural case.

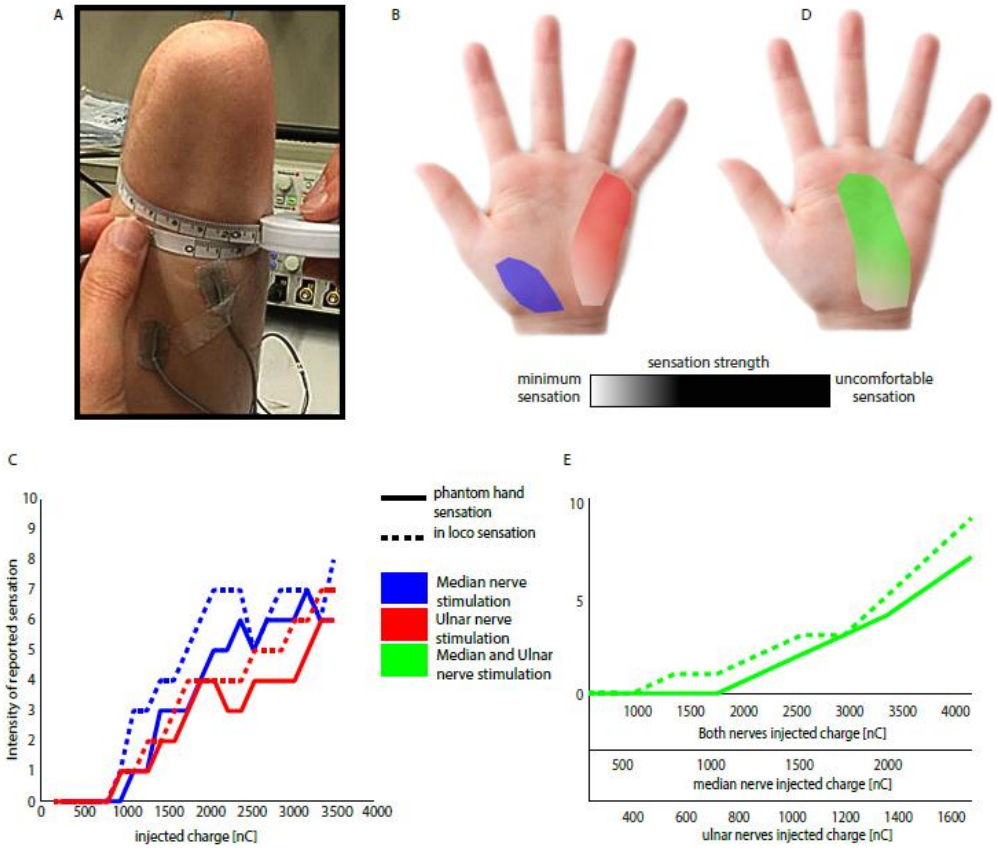


**Fig. 5.5. Transcutaneous stimulation mapping in an amputee.** (**A**) Superficial electrodes positioning. (**B**) Position and extension of the sensations evoked by median (blue) and ulnar (red) stimulation. (**C**) Intensity of the sensation reported over the phantom hand and in loco under the electrode for median and ulnar stimulation, respectively in blue and red. (**D**) Stimulation of both nerves produced paresthesia in area that is in the middle with respect to what referred for single channels stimulation. (**E**) Intensity of the sensation reported over the phantom hand and in loco under the electrode for simultaneous median and ulnar nerves stimulation.

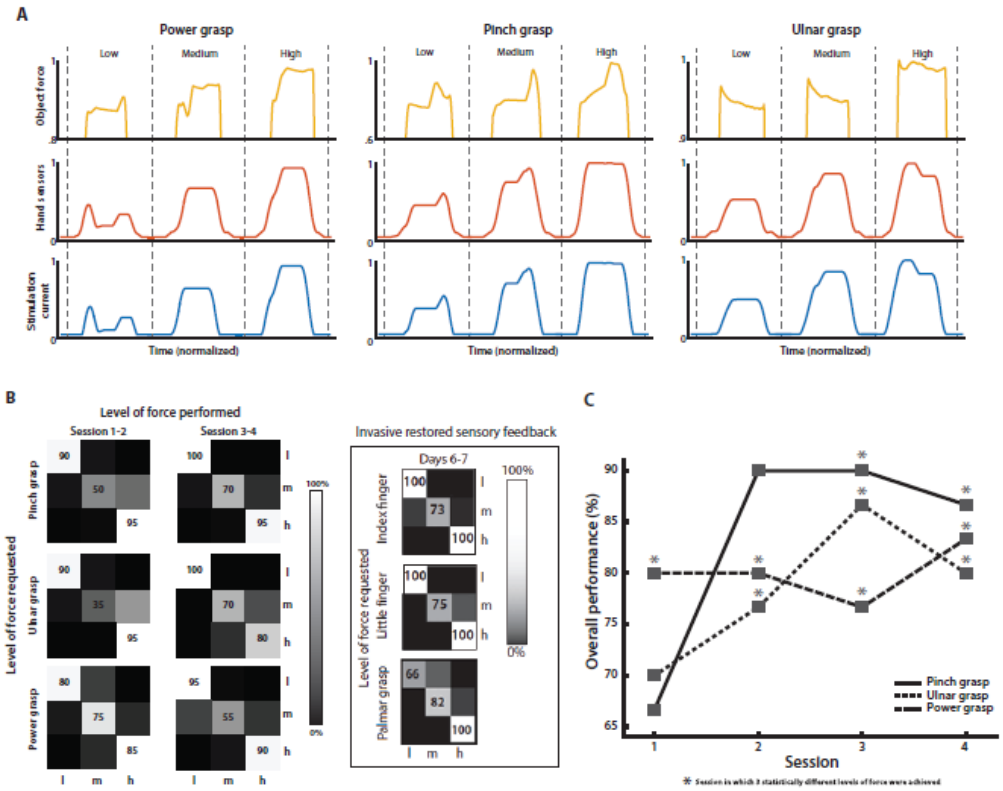


**Fig. 5.6. Fine force control.** (**A**) External pressure sensor outputs (yellow), hand sensor readings (red) and stimulation current charge (blue) during force control task for index and little fingers and power grasp. (**B**) Confusion matrices of the requested force levels for the index (N=120 repetitions in 4 sessions), little finger (N=120 repetitions in 4 sessions) and power grasp (N=120 repetitions in 4 sessions). In the inset results taken from the invasive trials (Raspopovic et al., 2014) are reported. (C) Overall performances trend during the experiment.

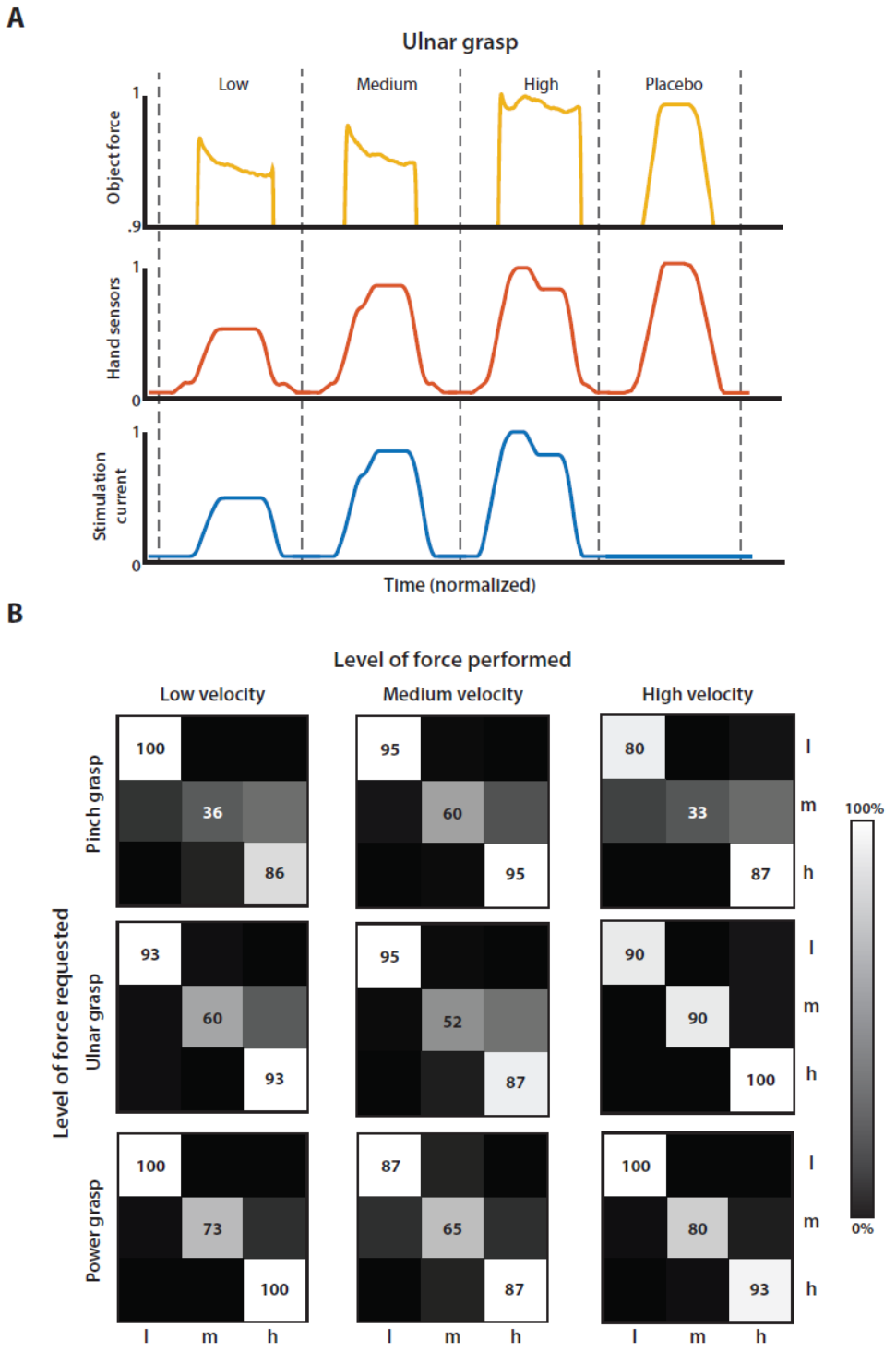


**Fig. 5.7. Fine bidirectional control is entirely due to the integration of the restored sensation into the bidirectional loop**. (**A**) Examples of placebo trials, randomly mixed during the sessions of the fine force protocol are shown in low-p. During these trials, the participant was asked to apply the minimum level of force but with the electrical stimulation turned off (no feedback from the sensors of the hand prosthesis). (**B**) The performance at different velocities of the hand motors actuation was evaluated to exclude

the possibility that the participant could have learned to control the force by associating the control with the time needed for hand prosthesis closure (N=120 in 4 sessions for the index finger, N=120 in 4 sessions for the little finger and N=120 in 4 sessions for power grasp).

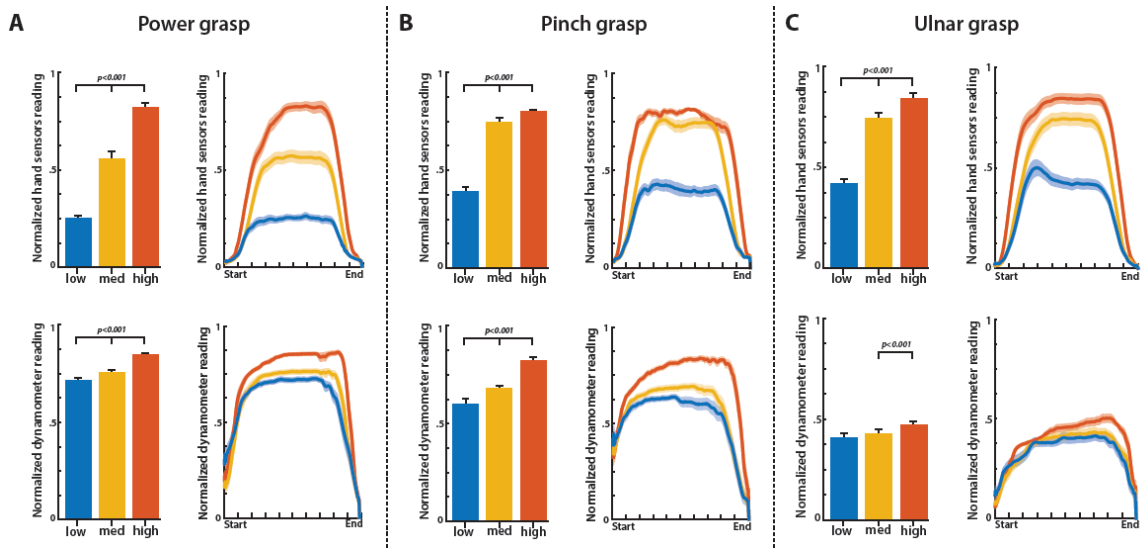


**Fig. 5.8. Force reproducibility.** Statistical analysis and reproducibility of the force output are presented for index finger (**A**), little finger (**B**) and power grasp (**C**). Three significantly different force levels were applied over the dynamometer for the case of power and pinch grasps. In the case of ulnar grasp force modulation, the two lowest force levels were not applied with the same accuracy (bottom). However, the subject always drove its own stimulation with 3 significantly different levels of current injected (top). Plots show the shape of the executed levels normalized over each cycle length as average +/- S.E.M. Kruskall-Wallis test with Tukey-Kramer correction was performed over all the repetitions reported in (**A**), (**B**) and (**C**).

# Chapter 6 Conclusions and perspectives

This work of thesis focused on improving both motor and sensory functionalities of the upper limb prostheses currently available on the shelf and in research. Novel strategies for interfacing upper limb nerves (information extraction and delivery) were inspired by a punctilious investigation and a deep comprehension of the system of interest (Chapter 2).

Human alpha motoneurons axons spiking activity was recorded for the first time by exploiting an innovative hybrid ecography and microneurography technique developed in the present thesis. Features correlated with kinematics and dynamics of the hand motion were extracted from alpha motoneurons firings. Those features were used to design novel decoding algorithms that were able to estimate from recorded ENG, in (quasi-)real-time, the velocity of motion and the force exerted. These parameters could be used for driving different DoFs of the next-generation neuroprostheses.

Hence, we proved that reliable spiking activity from alpha motoneurons axons in peripheral nerves could be recorded and that sophisticated information can be extracted, justifying chronic implant of electrodes in humans for motor control of prostheses. Moreover, these recordings validated a model of the neuromuscular system that could predict the behavior of alpha motoneurons in pathologic conditions in which proprioceptive feedback is missing (as it is in the case of amputees).

Further tests, however, should be conducted on amputees in chronic implants to verify the stability of recordings and for implementing proportional mapping algorithms to control prosthesis DoFs. During a long term implant, moreover, it could be possible to verify whether

amputees manage to modulate and eventually increase the amount of generated efferent activity, that was probably not exploited for several years after the lost of the limb.

On the sensory side, we demonstrated for the first time, that by median and ulnar nerves stimulation injected through transversal intraneural electrodes, it is possible to elicit tactile sensations on the phantom hand of an amputee in the closed-loop control of a bidirectional prosthesis. The type and location of the sensations were stable for a sub-chronic period of time. The injected charge was proportional to the readout of sensors embedded in the prosthesis. The movement of the robotic hand was driven by a decoder that was able to predict in (quasi-)real-time the user intention from remnant muscles sEMG.

The amputee was able to perfectly perceive the location, where objects were placed over the prosthesis. Remarkably, he managed to control the amount of force exerted with 3 different grasps (pinch, ulnar and power grasps) relying on the sensory feedback, while he could not do it without tactile sensations. Finally, exploiting the dynamics of the sensory feedback he was able to distinguish among objects with different compliance and shape.

Interestingly, we verified the physiologic principle (proposed by Muniak et al., 2007) according to which the amplitude of a mechanical stimulus on the skin is (partly) coded by increasing the number of afferent fibers recruited. This revolutionary work paved the way to a research in sensory feedback restoration in bidirectional prostheses.

In 2014, other than Raspopovic et al., 2014, also Tan et al. 2014, and Ortiz-Catalan et al.,2014 published very interesting results.

In particular, Tan et al. proved that peripheral nerve interfaces (in their case, FINE electrodes) are stable and reliable for long-term implants: the amputees involved in their study, in fact, have the electrodes in the body since more than 1.5 years. On the other hand, the aim of Ortiz-Catalan et al. was demonstrating the feasibility of prosthesis osteointegration, which is a promising technique for the long-term prosthesis stabilization. Aside,

they partially restored sensory feedback by stimulating the ulnar nerve of an amputee through a cuff electrode. Now, while the first two groups used percutaneous leads from the electrodes to an external stimulator, the last one, showed that, thanks to osteointegration, the cables (from the electrode to the external stimulator) could pass through the artificial bone.

Interestingly we found that when using the same bidirectional prosthesis, with the identical encoding principle but with transcutaneous nerve stimulation, an amputee was able to similarly control the amount of grasping force exerted over a pressure sensor. We had the unique possibility to conduct experiments with the bidirectional prosthesis on the same amputee, both with intraneural stimulation and TENS restored sensory feedback. This guaranteed both objective and subjective comparisons between the two approaches.

The amputee, in particular, reported a less natural and selective sensation than the one evoked by invasive stimulation. Moreover, in order to elicit a stable phantom hand sensation, high charge injection was required. This caused an unpleasant in-loco sensation on the skin under the superficial electrodes.

In the future, other neuro-inspired stimulation strategies should be tested in order to restore the huge range of sensations that human beings can perceive. A computational model of the physiology of the sensory system (along with an electrical model of the nerve) should support the design of these strategies. Moreover, microneurography should be used for testing novel algorithms before transferring to chronic implant.

In definitive, this work of thesis represents a breakthrough toward the development of naturally and effortless controllable bidirectional prostheses, which can be integrated in the appropriate body representation of amputees.

It is important to remember that all the achievements obtained in this work come from the exploration and comprehension of the phenomenon to interact with. Indeed, starting from the physiology of sensory system we have hypothesized and verified neuro-inspired strategies of stimulations.

Analogously, since human motoraxons behavior was not completely known under different conditions, we first experimentally investigated it and, then, implemented novel decoding algorithms relying on the obtained findings.

This is the philosophy I want to promote: only from the deep basic understanding is possible to implement optimal applications.

# Chapter 7 Bibliography

(Abraira and Ginty, 2013) Abraira, V. E., & Ginty, D. D. (2013). The sensory neurons of touch. Neuron, 79(4), 618-639.

(Atkins et al., 1996) D. Atkins, D. Heard, W. Donovan, Epidemiologic overview of individuals with upper-limb loss and their reported research priorities. *J Prosthet. Orthot.* **8**, 2 –11 (1996).

(Antfolk et al., 2013) C. Antfolk, M. D'Alonzo, M. Controzzi, G. Lundborg, B. Rosén, F. Sebelius, C. Cipriani, "Artificial redirection of sensation from prosthetic fingers to the phantom hand map on transradial amputees: vibrotactile vs mechanotactile sensory feedback discrimination," *IEEE Trans. on Neural Systems and Rehabilitation Engineering,* vol. 21, no. 1, pp. 112-120, 2013.

(Armel and Ramachandran, 2003) Armel KC, Ramachandran VS. Projecting sensations to external objects: evidence from skin conductance response. *Proc Biol Sci* 2003; 270: 1499–506.

(Bergenheim et al., 1999) Bergenheim, M., Roll, J. P., & Ribot-Ciscar, E. (1999). Microneurography in humans. In Modern techniques in neuroscience Research (pp. 803-819). *Springer Berlin Heidelberg*.

(Biddiss et al., 2006) E. Biddiss, D. Beaton, T. Chau, Consumer design priorities for upper limb prosthetics. *Disabil. Rehabil. Assist. Technol*. **2**, 346-57 (2006).

(Biddiss et al., 2007) Biddiss, Elaine, Dorcas Beaton, and Tom Chau. "Consumer design priorities for upper limb prosthetics." *Disability & Rehabilitation: Assistive Technology* 2.6 (2007): 346-357.

(Blanke et al., 2002) O. Blanke S.Ortigue T Landis, M Seeck "Neuropsychology: Stimulating illusory own-body perceptions" *Nature* 419, 269-270 (2002).

(Boretius et al., 2010) T. Boretius, J. Badia, A. Pascual-Font, M. Schuettler, X. Navarro, *et al*., A transverse intrafascicular multichannel electrode (time) to interface with the peripheral nerve. *Biosens. Bio- electron.* **26**, 62–69 (2010)

(Bottomley, 1965) A. Bottomley, Myoelectric Control of Powered Prostheses. *J. Bone & Joint Surg*. 47B, 411-415 (1965).

(Botvinick and Cohen, 1998) Botvinick M, Cohen J. Rubber hands 'feel' touch that eyes see. Nature 1998; 391: 756.

(Carrozza et al., 2006) M. C. Carrozza, G. Cappiello, S. Micera, B. B. Edin, L. Beccai L., *et al*., Design of a cybernetic hand for perception and action. *Biol. Cybern*. **95**, 629–644 (2006).

(Castellini and Passig, 2011) Castellini C., Passig G. (2011) "Ultrasound image features of the wrist are linearly related to finger positions," in Proceedings of IROS – International Conference on Intelligent Robots and Systems (San Francisco, CA: IEEE; ), 2108–2114 10.1109/IROS.2011.6094831

(Cipriani et al., 2012) Cipriani, C., D'Alonzo, M., & Carrozza, M. C. (2012). A miniature vibrotactile sensory substitution device for multifingered hand prosthetics. Biomedical Engineering, IEEE Transactions on, 59(2), 400-408.

(Citi et al., 2008) Citi, L., Carpaneto, J., Yoshida, K., Hoffmann, K. P., Koch, K. P., Dario, P., & Micera, S. (2008). On the use of wavelet denoising and spike sorting techniques to process electroneurographic signals recorded using intraneural electrodes. *Journal of neuroscience methods*, 172(2), 294-302.

(Connoly et al., 2008) C. Connolly, Prosthetic hands from Touch Bionics. *Industrial Robot*. **35**, 290-293 (2008).

(Contessa and De Luca, 2013) Contessa, P., & De Luca, C. J. (2013). Neural control of muscle force: indications from a simulation model. *Journal of neurophysiology*, *109*(6), 1548-1570.

(Cunningham et al., 2009) Cunningham, J. P., Gilja, V., Ryu, S. I., & Shenoy, K. V. (2009). Methods for estimating neural firing rates, and their application to brain–machine interfaces. Neural Networks, 22(9), 1235-1246.

(Curry and Timothy, 2011) Curry, Timothy B., and Nisha Charkoudian, (2011). The use of real-time ultrasound in microneurography. *Autonomic Neuroscience* 162.1: 89-93.

(De Luca et al., 2006) De Luca, C. J., Adam, A., Wotiz, R., Gilmore, L. D., & Nawab, S. H. (2006). Decomposition of surface EMG signals. Journal of neurophysiology, 96(3), 1646-1657.

(Dideriksen et al., 2010) Dideriksen, J. L., Farina, D., Baekgaard, M., & Enoka, R. M. (2010). An integrative model of motor unit activity during sustained submaximal contractions. Journal of Applied Physiology, 108(6), 1550-1562.

(Dideriksen et al., 2011) Dideriksen, J. L., Enoka, R. M., & Farina, D. (2011). Neuromuscular adjustments that constrain submaximal EMG amplitude at task failure of sustained isometric contractions. *Journal of Applied Physiology*, *111*(2), 485-494.

(Dhillon et al., 2004) Dhillon, G. S., Lawrence, S. M., Hutchinson, D. T., & Horch, K. W. (2004). Residual function in peripheral nerve stumps of amputees: implications for neural control of artificial limbs. The Journal of hand surgery, 29(4), 605-615.

(Dhillon and Horch, 2005) Dhillon, G. S., & Horch, K. W. (2005). Direct neural sensory feedback and control of a prosthetic arm. Neural Systems and Rehabilitation Engineering, IEEE Transactions on, 13(4), 468-472. (Dhillon et al., 2005).

(Edgerton et al., 2008) Edgerton, V. R., Courtine, G., Gerasimenko, Y. P., Lavrov, I., Ichiyama, R. M., Fong, A. J., ... & Roy, R. R. (2008). Training locomotor networks. Brain research reviews, 57(1), 241-254.

(Ehrsson et al., 2004) Ehrsson HH, Spence C, Passingham RE. That's my hand! Activity in premotor cortex reflects feeling of ownership of a limb. *Science* 2004; 305: 875–77.

(Enoka and Fuglevand, 2001) Enoka, R. M., and Fuglevand A. J. (2001). Motor unit physiology: some unresolved issues. *Muscle & nerve,* 24(1), 4-17.

(Englehart et al., 1999) Englehart, K., Hudgins, B., Parker, P. A., & Stevenson, M. (1999). Classification of the myoelectric signal using time-frequency based representations. Medical engineering & physics, 21(6), 431-438.

(Englehart and Hudgins, 2003) K. Englehart and B. Hudgins, "A robust, real-time control scheme for multifunction myoelectric control," IEEE Trans. Biomed. Eng., vol. 50, no. 7, pp. 848–854, Jul. 2003.

(Engstrom and Van de Ven C., 1999) Engstrom B, Van de Ven C. Therapy for Amputees. 3rd ed. Churchill Livingstone. Harcourt Brace and Company. ©1999. ISBN 0-443-05975-6).

(Farina et al., 2014) Farina, D., Jiang, N., Rehbaum, H., Holobar, A., Graimann, B., Dietl, H., & Aszmann, O. (2014). The Extraction of Neural Information from the Surface EMG for the Control of Upper-Limb Prostheses: Emerging Avenues and Challenges. *Neural Systems and Rehabilitation Engineering, IEEE Transactions on,* 22(4).

(Farrell et al., 2007) T. R. Farrell, R. F. Weir, The optimal controller delay for myoelectric prostheses. *IEEE Trans. Neural. Syst. Rehabil. Eng*. **15**, 111-8 (2007).

(Fink et al., 2014) Fink, A. J., Croce, K. R., Huang, Z. J., Abbott, L. F., Jessell, T. M., & Azim, E. (2014). Presynaptic inhibition of spinal sensory feedback ensures smooth movement. Nature, 509(7498), 43-48.

(Flanagan et al., 2006) J.R. Flanagan, M. C. Bowman, R. S. Johansson, Control strategies in object manipulation tasks. *Curr. Opin. Neurobiol.* **16**, 650-9 (2006)

(Fougner et al., 2012) Fougner, A., Stavdahl, O., Kyberd, P. J., Losier, Y. G., & Parker, P. A. (2012). Control of upper limb prostheses: terminology and proportional myoelectric control—a review. Neural Systems and Rehabilitation Engineering, IEEE Transactions on, 20(5), 663-677.

(Fougner et al., 2014) Fougner, A. L., Stavdahl, Ø., & Kyberd, P. J. (2014). System training and assessment in simultaneous proportional myoelectric prosthesis control. Journal of neuroengineering and rehabilitation, 11(1), 75.

(Fuglevand et al., 1993) Fuglevand, A. J., Winter, D. A., & Patla, A. E. (1993). Models of recruitment and rate coding organization in motor-unit pools. *Journal of neurophysiology*, *70*(6), 2470-2488.

(Freyschuss and Knutsson, 1971) Freyschuss, U., & Knutsson, E. (1971). Discharge patterns in motor nerve fibres during voluntary effort in man. *Acta physiologica Scandinavica*, 83(2), 278-279.

(Frisoli et al., 2011) A .Frisoli , M. Solazzi, M. Reiner, M. Bergamasco, The contribution of cutaneous and kinesthetic sensory modalities in haptic perception of orientation. *Brain Res. Bull.* **85**, 260-6 (2011).

(Gandevia et al., 1990) Gandevia, S. C., Macefield, G., Burke, D., & McKenzie, D. K. (1990). Voluntary activation of human motor axons in the absence of muscle afferent feedback the control of the deafferented hand. *Brain*, 113(5), 1563-1581.

(Gandevia and Hales, 1997) Gandevia, S. C., & Hales, J. P. (1997). The methodology and scope of human microneurography. *Journal of neuroscience methods*, *74*(2), 123-136.

(Gardner, 2010) Gardner, E. P. (2010). Touch. eLS.

(Gijsberts et al., 2014) Gijsberts, A., Bohra, R., González, D. S., Werner, A., Nowak, M., Caputo, B., ... & Castellini, C. (2014). Stable myoelectric control of a hand prosthesis using non-linear incremental learning. Frontiers in neurorobotics, 8.

(Goodwin et al., 1997) A. W. Goodwin, V. G. Macefield, J. W. Bisley, Encoding of Object Curvature by Tactile Afferents From Human Fingers. *J. Neurophysiol.* **78**, 2881-8 (1997).

(Goodwin et al., 2004) A.W. Goodwin, H.E. Wheat, Sensory signals in neural populations underlying tactile perception and manipulation. *Annu Rev Neurosci*. 27, 53-77 (2004).

(Gordon et al., 1966) A. Gordon AM, Huxley AF, Julian FJ (1966). "The variation in isometric tension with sarcomere length in vertebrate muscle fibres". J. Physiol. (Lond.) 184 (1): 170–92.

(Guo et al., 2013) Guo J. Y., Zheng Y. P., Xie H. B., Koo T. K. (2013). Towards the application of one-dimensional sonomyography for powered upper-limb prosthetic control using machine learning models. Prosthet. Orthot. Int. 37 43–49 10.1177/0309364612446652

(Hargrove et al., 2010) Hargrove, L. J., Scheme, E. J., Englehart, K. B., & Hudgins, B. S. (2010). Multiple binary classifications via linear discriminant analysis for improved controllability of a powered prosthesis. Neural Systems and Rehabilitation Engineering, IEEE Transactions on, 18(1), 49-57.

(Heckman and Binder, 1991) Heckman CJ, Binder MD, (1991). Computer Simulation of the Steady-State Input-Output Function of the Cat Medial Gastrocnemius Motoneuron Pool, Journal of neurophysiology, Vol. 65, No. 4.

(Heckman and Enoka, 2012) Heckman, C. J., & Enoka, R. M. (2012). Motor unit. *Comprehensive Physiology*.

(Helmholtz, H. 1850). Messungen über den zeitlichen Verlauf der Zuckung animalischer Muskeln und die Fortpflanzungsgeschwindigkeit der Reizung in den Nerven. Archiv für Anatomie, Physiologie und wissenschaftliche Medicin. 276

(Henneman et al., 1965) Henneman, E., Somjen, G. & Carpenter, D. O. (1965). Functional significance of cell size in spinal motoneurons. J. Neurophysiol. 28, 560-580.

(Hodgkin and Huxley, 1952) Hodgkin, A. L. and Huxley, A. F. (1952). A quantitative description of membrane current and its application to conduction and excitation in nerve. The Journal of Physiology, 117(4):500–544.

(Holobar et al., 2007) Holobar, A., & Zazula, D. (2007). Multichannel blind source separation using convolution kernel compensation. Signal Processing, IEEE Transactions on, 55(9), 4487-4496.

(Hultborn, 2006) Hultborn, H. (2006). Spinal reflexes, mechanisms and concepts: from Eccles to Lundberg and beyond. Progress in neurobiology, 78(3), 215-232.

(Huxley et al., 1949) Huxley AF & Stämpfli R. Evidence for saltatory conduction in peripheral myelinated nerve fibres. J Physiol. 108:315-39, 1949.

(Izhikevich et al., 2003) Izhikevich, E. M. (2003). Simple model of spiking neurons. *IEEE Transactions on neural networks*, *14*(6), 1569-1572.

(Jankowska, 1992) Jankowska, E. (1992). Interneuronal relay in spinal pathways from proprioceptors. Progress in neurobiology, 38(4), 335-378.

(Jankowska, 2013a) Jankowska, E. (2013). Spinal interneurons. Neuroscience in the 21st Century: From Basic to Clinical, 1063-1099.

(Jankowska, 2013b) Jankowska, E. (2013). Spinal Reflexes. Neuroscience in the 21st Century: From Basic to Clinical, 1463-1484.

(Jiang et al., 2009) Jiang, N., Englehart, K. B., & Parker, P. A. (2009). Extracting simultaneous and proportional neural control information for multiple-DOF prostheses from the surface electromyographic signal. Biomedical Engineering, IEEE Transactions on, 56(4), 1070-1080.

(Jia et al., 2007) Jia, X., Koenig, M. A., Zhang, X., Zhang, J., Chen, T., & Chen, Z. (2007). Residual motor signal in long-term human severed peripheral nerves and feasibility of neural signal-controlled artificial limb. *The Journal of hand surgery*, *32*(5), 657-666.

(Jiang et al., 2012a) Jiang, N., Vest-Nielsen, J. L., Muceli, S., & Farina, D. (2012). EMG-based simultaneous and proportional estimation of wrist/hand kinematics in uni-lateral trans-radial amputees. J Neuroeng Rehabil, 9, 42-53.

(Jiang et al., 2012b) Jiang, N., Dosen, S., Müller, K. R., & Farina, D. (2012). Myoelectric control of artificial limbs—Is there a need to change focus. IEEE Signal Process. Mag, 29(5), 152-150.

(Jian et al., 2013) Jiang, N., Muceli, S., Graimann, B., & Farina, D. (2013). Effect of arm position on the prediction of kinematics from EMG in amputees. Medical & biological engineering & computing, 51(1-2), 143-151.

(Johannes et al., 2011) M. S. Johannes, J. D. Bigelow, J. M Burck, S. D. Harshbarger, M. V. Kozlowski, T. Van Doren, An Overview of the Developmental Process for the Modular Prosthetic Limb. *Johns Hopkins APL Tech Dig*, **30**, 207–216 (2011).

(Johansson and Flanagan, 2009) Johansson, R. S., & Flanagan, J. R. (2009). Coding and use of tactile signals from the fingertips in object manipulation tasks. Nature Reviews Neuroscience, 10(5), 345-359.

(Kaczmarek et al., 1991) K. A. Kaczmarek, J. G. Webster, P. Bach-y-Rita, e W. J. Tompkins, «Electrotactile and vibrotactile displays for sensory substitution systems», *IEEE Trans. Biomed. Eng.*, vol. 38, n. 1, pagg. 1–16, gen. 1991.

(Kim et al., 2010) Kim, K., Colgate, J. E., Santos-Munné, J. J., Makhlin, A., & Peshkin, M. A. (2010). On the design of miniature haptic devices for upper extremity prosthetics. Mechatronics, IEEE/ASME Transactions on, 15(1), 27-39.

(Kristeva-Feige et al., 1996) R. Kristeva-Feige, S. Rossi, V. Pizzella, L. Lopez, S. N. Erné, J. Edrich, P. M. Rossini A neuromagnetic study of movement-related somatosensory gating in the human brain. ***Exp Brain Res*.** **107**, 504-14 (1996).

(Kuhn et al., 2010) Kuhn, A., Keller, T., Lawrence, M., & Morari, M. (2010). The influence of electrode size on selectivity and comfort in transcutaneous electrical stimulation of the forearm. Neural Systems and Rehabilitation Engineering, IEEE Transactions on, 18(3), 255-262.

(Kuiken et al., 2004) Kuiken, T. A., Dumanian, G. A., Lipschutz, R. D., Miller, L. A., & Stubblefield, K. A. (2004). The use of targeted muscle reinnervation for improved myoelectric prosthesis control in a bilateral shoulder disarticulation amputee. Prosthetics and Orthotics International, 28(3), 245-253.

(Kuiken et al., 2007) Kuiken, T. A., Marasco, P. D., Lock, B. A., Harden, R. N., & Dewald, J. P. (2007). Redirection of cutaneous sensation from the hand to the chest skin of human amputees with targeted reinnervation. Proceedings of the National Academy of Sciences, 104(50), 20061-20066.

(Kuiken et al., 2007b) T. A. Kuiken, L. A. Miller, R. D. Lipschutz, B. A. Lock, K. Stubblefield, *et al.,* Targeted reinnervation for enhanced prosthetic arm function in a woman with a proximal amputation: a case study. *Lancet* **369**, 371–380 (2007).

(Kuiken et al., 2009) T. A. Kuiken, G. Li, B. A. Lock, R. D. Lipschutz, L. A. Miller, *et al.,* Targeted muscle reinnervation for real-time myoelectric control of multifunction artificial arms. *JAMA* **301**, 619–628 (2009).

(Lederman et al., 1987) S. J. Lederman, R.L. Klatzky, Hand movements: a window into haptic object recognition. *Cognit. Psychol.* **19**, 342–368 (1987).

(Lewicki, 1998) Lewicki, M. S. (1998). A review of methods for spike sorting: the detection and classification of neural action potentials. *Network: Computation in Neural Systems*, 9(4), R53-R78.

(Llewellyn et al., 1965) Llewellyn, M. E., Thompson, K. R., Deisseroth, K., & Delp, S. L. (2010). Orderly recruitment of motor units under optical control in vivo. *Nature medicine*, *16*(10), 1161-1165.

(Longo et al., 2008) Longo MR, Cardozo S, Haggard P. Visual enhancement of touch and the bodily self. Conscious Cogn 2008; 17: 1181–91.

(Lowery and Erim, 2005) Lowery, M. M., & Erim, Z. (2005). A simulation study to examine the effect of common motoneuron inputs on correlated patterns of motor unit discharge. Journal of computational neuroscience, 19(2), 107-124.

(Lusher et al., 1979) Luscher, H. R., Ruenzel, P., Fetz, E., & Henneman, E. (1979). Postsynaptic population potentials recorded from ventral roots perfused with isotonic sucrose: connections of groups Ia and II spindle afferent fibers with large populations of motoneurons. *J Neurophysiol*, *42*(4), 1146-1164.

(Macefield et al., 1996) Macefield, V. G., Fuglevand, A. J., & Bigland-Ritchie, B. R. E. N. D. A. (1996). Contractile properties of single motor units in human toe extensors assessed by intraneural motor axon stimulation. Journal of Neurophysiology, 75(6), 2509-2519.

(Malagodi et al., 1989) Malagodi MS, Horch KW, Schoenberg AA (1989). An intrafascicular electrode for recording of action potentials in peripheral nerves. Ann Biomed Eng 17:397–410.

(Maltenfort et al., 2003) Maltenfort, Mitchell G., and R. E. Burke (2003). Spindle model responsive to mixed fusimotor inputs and testable predictions of β feedback effects. *Journal of neurophysiology* 89.5.

(Marasco et al., 2009) P. D. Marasco, A. E. Schultz, T. A. Kuiken, Sensory capacity of reinnervated skin after redirection of amputated upper limb nerves to the chest. *Brain* **132**, 1441–8 (2009).

(Marchettini et al., 1990) P. Marchettini, M. Cline, J. L. Ochoa, Innervation territories for touch and pain afferents of single fascicles of the human ulnar nerve. Mapping through intraneural microrecording and microstimulation. *Brain* **113**, 1491-500 (1990).

(Mercier et al., 2006) Mercier, C., Reilly, K. T., Vargas, C. D., Aballea, A., & Sirigu, A. (2006). Mapping phantom movement representations in the motor cortex of amputees. Brain, 129(8), 2202-2210.

(Mendell and Henneman, 1968) Mendell, L. M., & Henneman, E. (1968). Terminals of single Ia fibers: distribution within a pool of 300 homonymous motor neurons. *Science*,*160*(3823), 96-98.

(Merletti et al., 2010) Merletti, R., Aventaggiato, M., Botter, A., Holobar, A., Marateb, H., & Vieira, T. M. (2010). Advances in surface EMG: recent progress in detection and processing techniques. *Critical Reviews™ in Biomedical Engineering*, *38*(4).

(Micera et al., 2010) Micera, S., Citi, L., Rigosa, J., Carpaneto, J., Raspopovic, S., Di Pino, G., ... & Rossini, P. M. (2010). Decoding information from neural signals recorded using intraneural electrodes: toward the development of a neurocontrolled hand prosthesis. Proceedings of the IEEE, 98(3), 407-417.

(Micera et al., 2011) Micera, S., Rossini, P. M., Rigosa, J., Citi, L., Carpaneto, J., Raspopovic, S., ... & Dario, P. (2011). Decoding of grasping information from neural signals recorded using peripheral intrafascicular interfaces. J Neuroeng Rehabil, 8, 53.

(Mileusnic and Loeb, 2006) Mileusnic, M. P., & Loeb, G. E. (2006). Mathematical models of proprioceptors. II. Structure and function of the Golgi tendon organ. *Journal of neurophysiology*, 96(4), 1789-1802.

(Monster and Chan, 1977) Monster, A.W., Chan, H. (1977). Isometric force production by motor units of extensor digitorum communis muscle in man. *J. Neurophysiol*. 40, 1432–1443.

(Moseley et al., 2008) Moseley GL, Olthof N, Venema A, Don S, Wijers M, Gallace A, Spence C. Psychologically induced cooling of a specific body part caused by the illusory ownership of an artificial counterpart. *Proc Natl Acad Sci* USA 2008; 105: 13169–73.

(Muceli et al., 2010) Muceli, S., Jiang, N., & Farina, D. (2010). Multichannel surface EMG based estimation of bilateral hand kinematics during movements at multiple degrees of freedom. In Engineering in Medicine and Biology Society (EMBC), 2010 Annual International Conference of the IEEE (pp. 6066-6069).

(Muniak et al., 2007) Muniak, M. A., Ray, S., Hsiao, S. S., Dammann, J. F., & Bensmaia, S. J. (2007). The neural coding of stimulus intensity: linking the population response of mechanoreceptive afferents with psychophysical behavior. The Journal of Neuroscience, 27(43), 11687-11699.

(Naples et al., 1990) Naples GG, Mortimer JT, Yuen TGH (1990). Overview of peripheral nerve electrode design and implantation. In: Neural Prostheses: Fundamental Studies, Biophysics and Bioengineering Series. Agnew WF, McCreery DB (Eds). Prentice Hall, New Jersey, pp 107–144.

(Navarro et al., 2005) Navarro, X., Krueger, T. B., Lago, N., Micera, S., Stieglitz, T., & Dario, P. (2005). A critical review of interfaces with the peripheral nervous system for the control of neuroprostheses and hybrid bionic systems. *Journal of the Peripheral Nervous System*, *10*(3), 229-258.

(Nielsen et al., 2011) Nielsen, J. L., Holmgaard, S., Jiang, N., Englehart, K. B., Farina, D., & Parker, P. A. (2011). Simultaneous and proportional force estimation for multifunction myoelectric prostheses using mirrored bilateral training. Biomedical Engineering, IEEE Transactions on, 58(3), 681-688.

(Ortiz-Catalan et al., 2014) M. Ortiz-Catalan, B. Håkansson, R. Brånemark, An osseointegrated human-machine gateway for long-term sensory feedback and motor control of artifi cial limbs. *Sci.Transl. Med*. 6, 257re6 (2014).

(Pasquina et al., 2014) Pasquina, P. F., Evangelista, M., Carvalho, A. J., Lockhart, J., Griffin, S., Nanos, G., ... & Hankin, D. (2014). First-in-man demonstration of a fully implanted myoelectric sensors system to control an advanced electromechanical prosthetic hand. Journal of neuroscience methods.

(Patterson and Katz, 1992) P. E. Patterson e J. A. Katz, «Design and evaluation of a sensory feedback system that provides grasping pressure in a myoelectric hand», J. Rehabil. Res. Dev., vol. 29, n. 1, pagg. 1–8, 1992.

(Pearson, 2001) Pearson, K. G. (2001). Proprioceptive sensory feedback. eLS.

(Pei and and Bensmaia, 2014) Pei, Y. C., & Bensmaia, S. J. (2014). The neural basis of tactile motion perception. Journal of neurophysiology, 112(12), 3023-3032.

(Proske and Gandevia, 2012) Proske, U., & Gandevia, S. C. (2012). The proprioceptive senses: their roles in signaling body shape, body position and movement, and muscle force. Physiological reviews, 92(4), 1651-1697.

(Quiroga et al., 2004) Quiroga, R., Nadasdy, Z., & Ben-Shaul, Y. (2004). Unsupervised spike detection and sorting with wavelets and superparamagnetic clustering. Neural computation, 16(8), 1661-1687.

(Raspopovic et al., 2011) Raspopovic, S., Capogrosso, M., & Micera, S. (2011). A computational model for the stimulation of rat sciatic nerve using a transverse intrafascicular multichannel electrode. Neural Systems and Rehabilitation Engineering, IEEE Transactions on, 19(4), 333-344.

(Raspopovic et al., 2014) Raspopovic, S., Capogrosso, M., Petrini,... & Micera, S. (2014). Restoring natural sensory feedback in real-time bidirectional hand prostheses. Science translational medicine.

(Rattay, 1986) Rattay, F. (Oct. 1986). Analysis of models for external stimulation of axons. Biomedical Engineering, IEEE Transactions on, BME-33(10):974–977.

(Reilly et al., 2006) Reilly, K. T., Mercier, C., Schieber, M. H., & Sirigu, A. (2006). Persistent hand motor commands in the amputees' brain. Brain, 129(8), 2211-2223.

(Ribot et al., 1986) Ribot, E., Roll, J. P., & Vedel, J. P. (1986). Efferent discharges recorded from single skeletomotor and fusimotor fibres in man. The Journal of physiology, 375(1), 251-268.

(Rossini et al., 2010) Rossini, P. M., Micera, S., Benvenuto, A., Carpaneto, J., Cavallo, G., Citi, L., ... & Dario, P. (2010). Double nerve intraneural interface implant on a human amputee for robotic hand control. Clinical neurophysiology, 121(5), 777-783.

(Schady et al., 1983) W. Schady, J. L. Ochoa, H. E. Torebjörk, L. S. Chen, Peripheral projections of fascicles in the human median nerve. *Brain* **106**, 745–760 (1983).

(Schady et al., 1994) W. Schady, S. Braune, S. Watson, H. E. Torebjörk, R. Schmidt, Responsiveness of the somatosensory system after nerve injury and amputation in the human hand. *Ann. Neurol*. **36**, 68-75 (1994).

(Scheme et al., 2010) Scheme, E., Fougner, A., Stavdahl, Ø., Chan, A. D. C., & Englehart, K. (2010, August). Examining the adverse effects of limb position on pattern recognition based myoelectric control. In Engineering in Medicine and Biology Society (EMBC), 2010, Annual International Conference of the IEEE (pp. 6337-6340).

(Scott, A.C., 1975.) The electrophysics of a nerve fiber. Reviews of Modern Physics 47: 487.

(Schlesinger, 1919) G. Schlesinger (1919). Der Mechanische aufbau der kunstlichen glieder, M. Borchardt, Ed. Berlin, Germany: Springer, vol. Ersatzglieder und Arbeitshilfen.

(Shultz and Kuiken, 2011) Shultz AE, Kuiken TA (2011). "Neural Interfaces for Control of Upper Limb Prostheses: The State of the Art and Future Possibilities", PM R.

(Sierra González and Castellini, 2013) Sierra González D., Castellini C. (2013). A realistic implementation of ultrasound imaging as a human–machine interface for upper-limb amputees. Front. Neurorobot. 7:17 10.3389/fnbot.2013.00017

(Srinivasan et al., 1995) M. A Srinivasan, R.H. LaMotte, Tactual discrimination of softness. *J. Neurophysiol.* **73**, 88-101 (1995).

(Sripati et al., 2006) Sripati AP, Bensmaia SJ , Johnson KO (2006). "A Continuum Mechanical Model of Mechanoreceptive Afferent Responses to Indented Spatial Patterns, J Neurophysiol 95: 3852–3864.

(Stein, 1974) Stein, R. B. (1974). Peripheral control of movement. *Physiol. Rev*, *54*(2), 15-243.

(Sunderland, 1945) Sunderland, S. (1945). The intraneural topography of the radial, median and ulnar nerves. Brain, 68(4), 243-298.

(Sunderland, 1978) Sunderland, S. S. (1978). Nerves and nerve injuries.

(Szeto and Saunders, 1982) Szeto, A. Y., & Saunders, F. A. (1982). Electrocutaneous stimulation for sensory communication in rehabilitation engineering. Biomedical Engineering, IEEE Transactions on, (4), 300-308.

(Taffoni et al., 2013) Taffoni, F., Tamilia, E., Palminteri, M., Schena, E., Formica, D., Delafield-Butt, J., ... & Guglielmelli, E. (2013). Ecological Sucking monitoring of newborns. *Sensors Journal, IEEE*, 13(11).

(Tan et al., 2014) D. Tan, M. Schiefer, M. Keith, J. R. Anderson, J. Tyler, D. J. Tyler, A neural interface provides long-term stable natural touch perception. Sci. Transl. Med. 6, 257ra138 (2014).

(Tasaki 1939) I. Tasaki, I. The electro-saltatory transmission of the nerve impulse and the effect of narcosis upon the nerve fiber. Am J Physiol 127: 211-227, 1939.

(Tsakiris and Haggard, 2005) Tsakiris M, Haggard P. The rubber hand illusion revisited: visuotactile integration and self-attribution. *J Exp Psychol Hum Percept Perform* 2005; 31: 80–91.

(Tyler and Durand, 2002) Tyler DJ, Durand DM (2002). Functionally selective peripheral nerve stimulation with a flat interface nerve electrode. IEEE Trans Neural Syst Rehabil Eng 10:294–303.

(Vallbo et al., 2004) Vallbo, A. B., Hagbarth, K. E. & Wallin, B. G. (2004). Microneurography: how the technique developed and its role in the investigation of the sympathetic nervous system. *Journal of applied physiology* **96**, 1262-1269.

(Yao et al., 2015) Yao, J., Chen, A., Kuiken, T., Carmona, C., & Dewald, J. (2015). Sensory cortical re-mapping following upper-limb amputation and subsequent targeted reinnervation: a case report. NeuroImage: Clinical.

(Young et al., 2011) Young, A. J., Hargrove, L. J., & Kuiken, T. A. (2011). The effects of electrode size and orientation on the sensitivity of myoelectric pattern recognition systems to electrode shift. Biomedical Engineering, IEEE Transactions on, 58(9), 2537-2544.

(Xu et al., 2001) Xu, Z., Xiao, S., & Chi, Z. (2001). ART2 neural network for surface EMG decomposition. Neural Computing & Applications, 10(1), 29-38.

(Weber et al., 2013) Weber, A. I., Saal, H. P., Lieber, J. D., Cheng, J. W., Manfredi, L. R., Dammann, J. F., & Bensmaia, S. J. (2013). Spatial and temporal codes mediate the tactile perception of natural textures. Proceedings of the National Academy of Sciences, 110(42), 17107-17112.

(Weir et al., 2009) Weir, R. F., Troyk, P. R., DeMichele, G. A., Kerns, D. A., Schorsch, J. F., & Maas, H. (2009). Implantable myoelectric sensors (IMESs) for intramuscular electromyogram recording. Biomedical Engineering, IEEE Transactions on, 56(1), 159-171.

(Wilkie, 1949) Wilkie, D. R. (1949). The relation between force and velocity in human muscle. The Journal of physiology, 110(3-4), 249-280.

(Zecca et al., 2002) M. Zecca, S. Micera, M. Carrozza, P. Dario, Control of multifunctional prosthetic hands by processing the electromyographic signal. *Crit. Rev. Biomed. Eng*. **30**, 459–85 (2002).

(Zhou and Zheng, 2012) Zhou G., Zheng Y. P. (2012). Human motion analysis with ultrasound and sonomyography. Conf. Proc. IEEE Med. Biol. Soc. 2012 6479–6482 10.1109/EMBC.2012.6347478

(Zhou et al., 2010) Zhou, R., Jiang, N., Englehart, K., & Parker, P. (2010). A computational model and simulation study of the efferent activity in the brachial nerves during voluntary motor intent. Medical & biological engineering & computing, 48(1), 67-77.